AN ABSTRACT OF THE DISSERTATION OF

Nicole Arianne Quist for the degree of Doctor of Philosophy in Physics presented on December 9, 2021.

Title: Photostability of Organic Semiconductors: from bulk to nanoscales

Abstract approved: _____

Oksana Ostroverkhova

Organic semiconductors have attracted considerable attention due to their applications in low-cost, solution-processable (opto)electronic devices. An important class of high-performance organic semiconductors is pentacene derivatives, which exhibit high charger carrier mobilities in field-effect transistors and ultrafast singlet fission in photovoltaic devices. These derivatives have served as benchmark materials for systematic studies of exciton and charge carrier dynamics, and they are the focus of this thesis. Photo-induced degradation of organic semiconductors is one of the bottlenecks preventing their wide-spread use in optoelectronic devices. As such, it is important to understand the underlying processes and develop strategies for their mitigation. For functionalized pentacene (Pn) two photodegradation processes are known to dominate: endoperoxide formation (EPO), which occurs in the presence of oxygen, and photodimerization, which occurs regardless of the presence of oxygen. The rate of decay is dependent on the specific Pn derivative and the

local environment. This work explores the effects of environmental factors and specific molecular characteristics that affect the photostability and photodegradation reversibility of functionalized fluorinated pentacene (Pn-R-F8) derivatives, where R is a variable side group, and their non-fluorinated counterparts (Pn-R). Experiments are done in solutions and in films, from the bulk level (typically utilized in optoelectronic devices) to the single molecule level.

In solutions, degradation of Pn molecules (monitored via changes in optical absorption under continuous illumination in air) and their partial recovery after thermolysis were quantified for various derivatives depending on the solvent, Pn concentration, side group (R), and fluorination. Fluorinated molecules (Pn-R-F8) were more stable than their non-fluorinated counterparts (Pn-R) and larger side groups (R) also protected the molecule from degradation. More concentrated solutions were considerably more stable as compared to dilute solutions. The nature of the solvent was also a factor; for example, molecules in chlorobenzene decay much faster than those in benzene under the same illumination conditions. The freshly made and photobleached solutions were analyzed using nuclear magnetic resonance (NMR) to identify the types of products formed. NMR spectra enabled identification of multiple products indicating that both EPO formation and dimerization are occurring simultaneously.

In guest-host polymer films, where Pn molecules (guests) were dispersed at various concentrations in a host polymer, the photo-degradation was measured using photoluminescene spectroscopy (PL). In agreement with the experiments from solution, the thin-films showed that polymer host had a significant impact

on photostability of Pn in films. For example, for the same concentration of Pn molecules, the films with a polymethylmethacrylate (PMMA) host exhibited considerably slower photodegradation as compared to those with the polyvinylidene fluoride (PVDF) host. Furthermore, an improvement in photostability was observed on the photodegradation and recovery rates when Pn is functionalized with the side group TCHS, than when using the side group TIPS. The effects of temperature of the samples were also measured using thin-film PL. Thermally activated behavior for the photodegradation processes was observed, with faster decay at higher temperatures as the added energy acted as a catalyst for the photo-decay reactions. However, added energy did not increase the amount of PL recovery in the samples until the temperature reached a high enough threshold, which in this case is between 350-370 K. The last parameter tested was concentration of Pn in films. At higher concentrations, the rate of photo-decay decreased, which indicates that in aggregate, the molecules are more protected from the causes of photo-degradation as compared to isolated molecules. The enhanced protection is enabled by concentration-dependent changes in the excited state dynamics and associated populations of reactive states.

In order to understand and isolate the photodegradation processes on the molecular level, studies were performed on guest-host films with ultra-low concentrations of the Pn guest molecules. The Pn molecules were imaged in a variety of polymer matrices at 633 nm excitation at room temperature in air using wide-field fluorescence microscopy. Fluorescence time trajectories were collected and statistically analyzed to quantify blinking due to reversible EPO formation depending on the

host matrix. This was also compared to single Pn donor (D) molecules that were imaged in PMMA in the presence of acceptor (A) molecules at various concentrations, which modified the local environment. Both changes to nanoenvironment affected the fluorescence of the molecules. For example, the PMMA host promoted the photostability of Pn molecules as compared to other polymer hosts studied, whereas addition of acceptor molecules reduced the photostability of the Pn donor molecules.

To understand the physical changes of the molecular system, a Monte Carlo method was used to create a multi-level simulation, which enabled us to relate the change in the molecular transition rates to the experimentally measured parameters in our single-molecule fluorescence spectroscopy experiments. These comprehensive studies provide insight into the synergistic effect of the local environment and molecular characteristics on the photodegradation and subsequent recovery of functionalized pentacene, which is important for development of next-generation materials with enhanced stability for organic electronic devices.

Photostability of Organic Semiconductors: from bulk to nanoscales

by

Nicole Arianne Quist

A DISSERTATION

submitted to

Oregon State University

in partial fulfillment of
the requirements for the
degree of

Doctor of Philosophy

Presented December 9, 2021
Commencement June 2022

Doctor of Philosophy dissertation of Nicole Arianne Quist presented on December 9, 2021.

APPROVED:

Major Professor, representing Physics

Head of the Department of Physics

Dean of the Graduate School

I understand that my dissertation will become part of the permanent collection of Oregon State University libraries. My signature below authorizes release of my dissertation to any reader upon request.

Nicole Arianne Quist, Author

ACKNOWLEDGEMENTS

First and foremost, I would like to acknowledge and thank my adviser, Dr. Oksana Ostroverkhova, for her guidance, knowledge and support. I would not have made it this far without her patience and knowledge, her belief in my success, and her contagious enthusiasm for science. I would also like to thank the rest of my graduate committee members, Dr. Matt Graham, Dr. David Roundy, Dr. Bo Sun, and Dr. Michael Lerner for their feedback, instruction and advice.

I have also been fortunate to work with many student physicists both in the Optoelectronics Lab as well as in classes and other roles within the department. In particular, I would like to thank Dr. Rebecca Grollman, as my predecessor for much of my work as she was vital in teaching and training me. I would like to thank Dr. Jonathan Van Schenck for his willingness to share ideas, provide thoughtful feedback, and for his comradery. I would like to thank the graduate students Dr. Greg Giesbers, Novela Auparay, and Robert Harrison for their assistance and knowledge that they willingly shared. A special thanks to all the undergraduates who worked in the lab with me, especially Mark Li and Ryan Tollefsen for their tireless work in data collection and experimental troubleshooting on this project. Outside the lab, I am grateful for the friendship, encouragement and endless technical discussion from all of the other physics graduate students, but in particular Dr. Bethany Matthews, Dr. Allison Gicking, Dr. Emily Smith and Dr Andrew Stickel.

Outside of the University, I would like to thank those members of my church,

who provided friendship and fellowship especially when I needed it most. Specifically, I would like to thank my roommates, Virginia Kestler, Isabel Justiniano, Aisha McKee, and Clara Stone, who supported me, encouraged me, and put up with me when life was rough. All of my friends including, Raven, Hattie, and the Super Seven. Last, but definitely not least, I would like to acknowledge and thank my parents, Doug and Claudia, and my siblings, Danielle, Kepler, Jacqueline, Nathaniel, and Alexandra for their unwavering support, constant encouragement /pestering, and laughter and fun when needed. My success in this endeavor is a testament to the support and encouragement of those in my life. Thank you.

TABLE OF CONTENTS

TABLE OF CONTENTS (Continued)

LIST OF FIGURES

LIST OF FIGURES (Continued)

LIST OF FIGURES (Continued)

LIST OF FIGURES (Continued)

LIST OF FIGURES (Continued)

LIST OF FIGURES (Continued)

LIST OF TABLES

LIST OF APPENDIX FIGURES

Chapter 1: Introduction

1.1 Introduction to Organic Semiconductors

Organic materials are of current interest for use in low-cost (opto)electronic and photonic devices[48]. Organic semiconductor materials have applications in organic light emitting diodes (OLEDs) [54, 41, 69], photovoltaics [74, 13, 86], and thin-film transistors to name a few [83, 21]. Unlike most common inorganic semiconductor materials, most of these organic materials are solution processable, allowing for more inexpensive and convenient manufacturing techniques. Many organic semiconductor are lightweight and are flexible enough to adhere to curved or bendable substrates [11]. Furthermore, small changes to these molecules can tune the properties to fit a specific need. For example, small molecular changes will drastically alter the electronic properties of the material while only weakly perturbing the optical properties.

In order for these materials to be used reliably in devices, they must be photostable, a characteristic that is strongly dependent not only on molecular structures, but also on the nanoscale morphology and local environment[52, 57, 56]. The contribution of the latter to the photophysics is difficult to quantify due to a lack of nanoscale resolution afforded by typical characterization methods. Therefore, approaches that enable direct studies of the molecular photophysics depending on

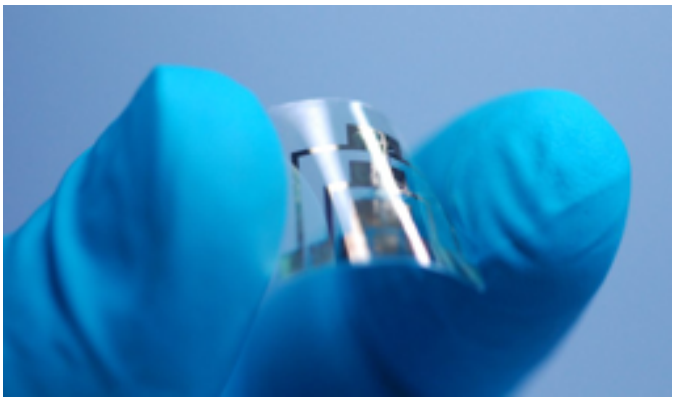

Figure 1.1: Organic Semiconductor Application Example: An organic transistor on a flexible substrate made of organic semi-conductor materials [32].

the nanoenvironment, in materials relevant for organic (opto)electronic devices, are necessary. In this thesis in addition to bulk films typically used in devices, we use single-molecule fluorescence spectroscopy to probe the effects of local environment on photophysics of functionalized acenes, which have been previously utilized in thin-film-transistors exhibiting hole mobilities of up to 11 cm^2/Vs [48, 28].

Because organic semiconductor materials can be used in thin-film applications and use solution processing, it is important to understand how various factors affect photostability for materials in both these forms. In conjunction with studying the nanoenvironment of functionalized acenes through single-molecule fluorescence spectroscopy, experiments on samples utilizing functionalized acenes in higher concentration were used to understand the dependence on molecular structure and local environment at the device scale. Specifically, optical absorption of molecules in solution was used to study the photostability of functionalized acenes in solution and how it depends on solvent and specific aspects of molecular structure.

Photoluminescence spectroscopy of thin films was used to probe the photostability in thin-films, with specific focus on the effects that host material, molecular structure, temperature, concentration of molecules, excitation wavelength, and the exposure to oxygen have on the stability.

1.2 Materials

Organic (opto)electronic and photonic materials have attracted attention due to their low cost, solution processability, and tunable properties[48]. A broad range of (opto)electronic and photonic applications, including organic light-emitting diodes (OLEDs), photovoltaics (OPVs), field-effect transistors (OFETs), sensors, photorefractive three-dimensional displays, lasers, have been demonstrated, and many of them commercialized[48, 49]. Materials that have been previously explored for (opto)electronic applications include derivatives of acenes (e.g. anthracene (Ac), tetracene (Tc), pentacene (Pn))[76, 59, 29, 60, 34]. Many of these derivatives (including Tc, and Pn) exhibit singlet fission (SF), the process of creating two triplet (T_1) excitons upon excitation of a singlet (S_1) state ($S_0 + S_1 \rightarrow TT \rightarrow T_1 + T_1$, where TT is a correlated triplet pair that serves as a precursor to the free triplets), which has generated a considerable amount of attention due to its potential to enhance the efficiency of organic solar cells[26].

One representative benchmark electronic and SF material of this class is functionalized Pn[3]. In field-effect transistors (FETs), functionalized Pn exhibits hole mobilities of > 1 cm^2/(V s) and up to 11 cm^2/(V s), depending on the crystal

polymorph and/or film crystallinity and morphology[48, 12]. These are among the highest mobilities in solution-processable OFETs, which has motivated research into mechanisms responsible for its enhanced electronic characteristics and into structure-property relationships over the past 20 years[46, 26, 47, 15, 30, 51, 4]. In terms of photophysics, TIPS–Pn films exhibit ultrafast ($<$ 100 fs) SF, depending on film morphology[27, 79, 40, 17], and this process in TIPS–Pn has been extensively studied from the fundamental photophysics standpoint[17, 78, 16, 70, 53] and towards applications in SF-based photovoltaics[84]. Although photophysical and electronic properties of functionalized Pn have been extensively studied, understanding environmental and morphological effects on photostability is not fully developed. Such understanding, however, would be important for designing materials for next-generation organic (opto)electronic devices.

Unlike inorganic materials, in which the optical and electronic properties are dependent on the properties of the conduction and valence band, the optical and electronic properties of organic materials are dependent on the molecular orbitals and the interaction between adjacent molecules. Although the average energy gap between the highest occupied molecular orbital (HOMO) and the lowest unoccupied molecular orbital (LUMO) is 1.8 eV in functionalized Pn, which is similar to the band gap in inorganic materials (ex. Si has a band gap of 1.1 eV), the charge mobility is limited by the low interaction between molecules.

This makes the geometry between organic semiconductor molecules critical in determining charger carrier mobilities and by extension viability as a device material. For example, organic molecules that form π-bonds results in energy

structures that are similar to inorganic materials. π-bonds form when C atoms form linear chain polymers and the sp^2 orbitals hybridize, so the p_z orbital can form π-bonds with the adjacent C[24]. In acenes, the bulk of the molecule, or backbone, is formed from C in aromatic rings, where the π-bonding results in bands of π orbitals that run the length of the molecule, both above and below the aromatic chain. If the geometry of the host material encourages molecular orientation such that the π-bond between neighboring acenes overlap, charge carriers will have much higher mobilities. Because of this conjugated molecular core, acenes have shown a lot of promise for use as organic semiconductor materials.

As a member of the acene family and because of its previous use in (opto)electronic applications, Pentacene was chosen as the molecule of study. Specifically, functionalized pentacene (Pn) derivatives were used, which utilized the tunable properties of Pn. Functionalized Pn was tested with both fluorinated and nonfluorinated backbone and TCHS ((tricyclohexylsilyl)ethynyl), TIPS (triisopropylsilylethinyl), and NODIPS ((n-octyldiisopropylsilyl)ethynyl) were used as side groups (see Figure 1.2). Each derivative will be referenced using the form Pn-R(-F8), for example Pn-TCHS-F8 or Pn-TIPS, for fluorinated and nonfluorinated derivatives, respectively. Since the ground state absorption and radiative decay are primarily dependent on the molecular backbone, the absorption and emission spectra of derivatives with varying side groups R are effectively identical. Thus, any differences in the experimental results, are due to the interactions of the side groups with the surrounding environment and, in concentrated samples, differences in intermolecular interactions due to side group-controlled differences in molecular

packing. The ability to tune the molecules in this way is one of the favorable properties of organic semiconductor materials and the effects of these molecular changes are discussed in Chapters 2 and 3.

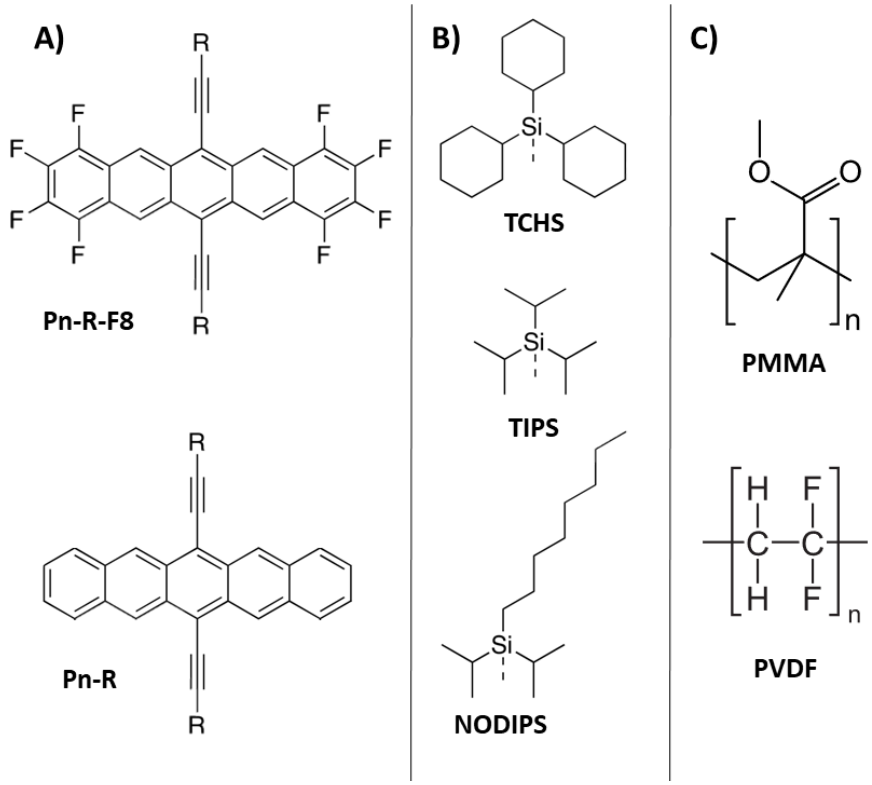

Figure 1.2: Molecules: (a) Functionalized Pentacene (Pn-R) and the fluorinated version (Pn-R-F8) are the materials of interest for these studies and (c) the two main polymers used to host Pn in thin films[22, 42]. The properties of Pn-R(-F8) can be modified by attaching side groups (TIPS, TCHS and NODIPS seen in (b)) at the places indicated by the label "R."

To use these functionalized Pn derivatives in films, a host polymer is used to create smoother more homogeneous film deposits. Such blending has been advantageous for organic electronic devices as improved film morphology results

in improved charge carrier mobility. For these experiments, two polymers were chosen poly(methyl methacrylate) (PMMA, 75,000 m.w., Polysciences, Inc.), and polyvinyliQuisdene fluoride (PVDF, 180,000 m.w., Millipore Sigma). PMMA is a amorphous clear polymer that has been used previously as a host material for functionalized Pn[18, 71]. Since it dissolves in the same solvents as Pn, it is easy to use it to make homogeneous solution processable thin-films that are optically transparent. In contrast, PVDF is a transparent semi-crystaline polymer that dissolves into very polar solvents, which are orthogonal to the non-polar solvents used for functionalized Pn. However, PVDF has low oxygen permeability and it's semi-crystalline characteristics means that properties, polarity and ferroelectric properties for example, of PVDF thin-films can be tuned based on sample preparation procedure [68, 33]. The effectiveness of both PMMA and PVDF in preventing optically induced decay of Pn guest molecules and encouraging molecular recovery is discussed in Chapters 2, 3, and 4.

1.3 Hurdles in the Use of Organic Semiconductors

Regardless of the application, successful commercialization of devices is hindered by the degradation of the organic materials due to reactions with oxygen, water, and so on. Previous studies have discovered two broadly defined mechanisms of the photo-induced decay for molecules in the acene family: endoperoxide formation (EPO) and dimerization[14, 18]. In functionalized Pn derivatives of Figure 1.2, several EPO derivatives and several types of dimers can form, as discussed in

section 3. These two processes are considered photo-bleaching processes because it is a photon induced change that stops the molecules from its original fluorescence.

Endoperoxides form when a reactive oxygen species react with an acene backbone[77]. The oxygen will replace hydrogen on one of the carbon in the aromatic rings, thus changing the molecular orbitals and either distorting or destroying the π-bond bands running across the acene backbone. Since the first order optical properties are directly dependent on the molecular orbitals formed by the aromatic rings of the acene backbone, the formation of endoperoxides through the addition of oxygen disrupts the conjugation so that the optical absorption shifts from visible for the fully conjugated Pn to the UV region for Pn-EPO and the photoluminescence also shifts or changes.

There are two photon-induced pathways for reactive oxygen to form in samples with acenes. The first pathway (denoted Type I in the literature) is through electron transfer from an optically excited acene to an inert oxygen molecule. This results in an acene cation and a superoxide (O^{2-}), which is reactive. The second pathway (Type II) is through energy transfer from an optically excited acene to a ground state oxygen ($^3O_2$), which results in a reactive singlet oxygen ($^1O_2$)[77, 45]. The preference of decay pathway is specific to each Pn derivative as discussed in section 2[14].

Once the endoperoxides form, there are two possible changes that can occur. Either the oxygen can detach, which results in the acene returning to it's original state, thus exhibiting reversibility. Alternatively, the endoperoxide can decay further turning into a secondary product which irreversibly damages the molecule

[63]. Previous work in our lab has shown that the photostability of functionalized Pn has oxygen dependence [63] and that reversibility is possible under certain conditions[18]. However, EPO formation rate is environment dependent, and can be manipulated with the changes in the environment as demonstrated in sections 2 and 4 [18].

The second important mechanism of degradation for acenes is photodimerization. This occurs at high enough concentrations that molecules are within bonding to adjacent molecules. There are two possible types of dimers: butterfly dimers and alkyen dimers. For butterfly dimers, the energy added to the high concentration samples provide enough energy to induce [4+ 4] intermolecular cycloaddition[10]. Cycloaddition is the reaction where two π-bond orbitals form a σ-bond, which in acenes occurs between four carbon atoms on two acene backbones (two atoms each)[37]. Thus two acenes form a new species which contains two acene molecules bonded together. This has been seen in functionalized Pn, where two functionalized Pn will form a bond between the rings just to the left or right of the center ring. There are two isomers of the dimer: centrosymmetric and planosymmetric, as seen in 1.3. In their study, Paolo Coppo and Stephen G. Yeates, saw the formation of photodimers in Pn-TIPS and also molecular recovery [10], indicating that is a product that we should expect in our samples.

Dimers can also form when the side groups attach to the backbone of a neighboring molecule and are named alkyne dimers. Evidence of alkyne dimers has been seen in tetracene (Tc) and hexacene, other members of the acene family, and is a step-wise reaction with a lower driving force[61]. However, alkyne dimers require

stricter molecular alignment than butterfly dimers.

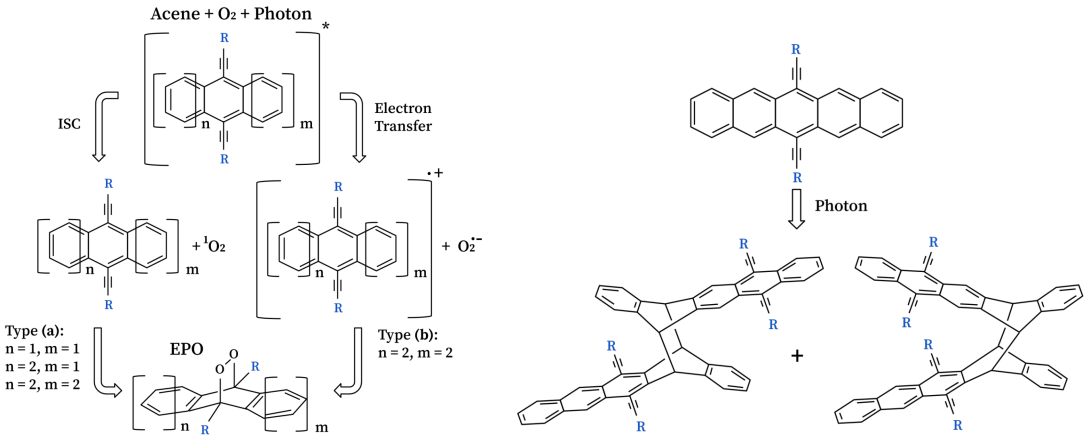

Figure 1.3: Products of Photodegradation: The chemical structure of the products of two types of photodegradation (a) endoperoxide formation product from Pn-R, with the oxygen bonded at the center (left) and the side (right). (b) The two isomers, centrosymmetric (left) and planosymmetric (right), of the butterfly dimer formed from Pn-R [10, 14].

Work done in our lab has shown that the stability of functionalized Pn is dependent on oxygen exposure[18]. However, this does not eliminate the possibility that dimerization is also occurring simultaneously, nor does it indicate which molecular and environmental factors discourage this process. The following chapters will explain the work done to determine the factors that discourage photodegradation, the products that result from this process and if and how the degradation can be reversed. The final chapter explores the photophysical processes occurring during photo-bleaching through a Monte Carlo model used to understand experimental data from single-molecule fluorescence microscopy in section 5.

Chapter 2: Probing Environmental Effects on Photostability of Functionalized Pentacene.

2.1 Introduction

One of the draws of using organic materials in semiconductor applications is that they can be used in thin film applications which can be manufactured using solution processing. Since these are key attributes, it is important to understand the stability of these materials in both solution and thin films. In particular, we want to understand the stability of functionalized Pn while in solution and in polymer blended films.

Using optical absorption, we have investigated the environmental factors that affect functionalized Pn in solution. Specifically, we looked at how the host material, side group, concentration and the addition of fluorine atoms to the molecule (fluorination) affects the photostability of functionalized Pn. For thin films, we used photoluminescence spectroscopy (PL) to measure the stability in relation to the host material, concentration, side group, wavelength and temperature.

2.2 Experimental Design

2.2.1 Optical Absorption

To study the photostability of organic materials in solution, two solvents were chosen as host: benzene and chlorobenzene. Benzene is nonpolar and chlorobenzene is only slightly polar, thus they are different enough to provide significant information, but similar enough that functionalized fluorinated Pn will dissolve into them. Both fluorinated and unfluorinated Pn was used and NODIPS, TIPS, and TCHS were used as side groups (see Chapter 1.2 for more details).

Pn-R-F8 molecules were dissolved either in benzene or in chlorobenzene at a concentration of $10^{-4} - 10^{-5}$ M, and sonicated for 30 minutes to ensure homogeneity. The starting absorption spectra was taken using either a xenon lamp or a halogen lamp, which illuminated the solution through a 200 μm optical fiber. The signal of the transmitted light was collected through a 50 μm optical fiber which was processed by the Ocean Optics USB2000 spectrometer. Spectrum of the solvent without Pn-R-F8 molecules served as reference.

After the starting data was collected, Pn-R(-F8) solution was irradiated by a UV lamp (300-400 nm) at 0.5 mW/cm^2 in air for up to 100 hours, depending on the solvent. Periodically, the absorption of the solution was taken using the set-up described above, to monitor its optical stability. The collected spectra was processed by subtracting the reference signal, and then transformed from transmittance percentage (T) to absorption (A) using $A = -\mathrm{Log}_{10}(T/100)$. The trends can be seen by overlaying the spectra or by integrating the region of interest, $\sim 550 - 650$nm

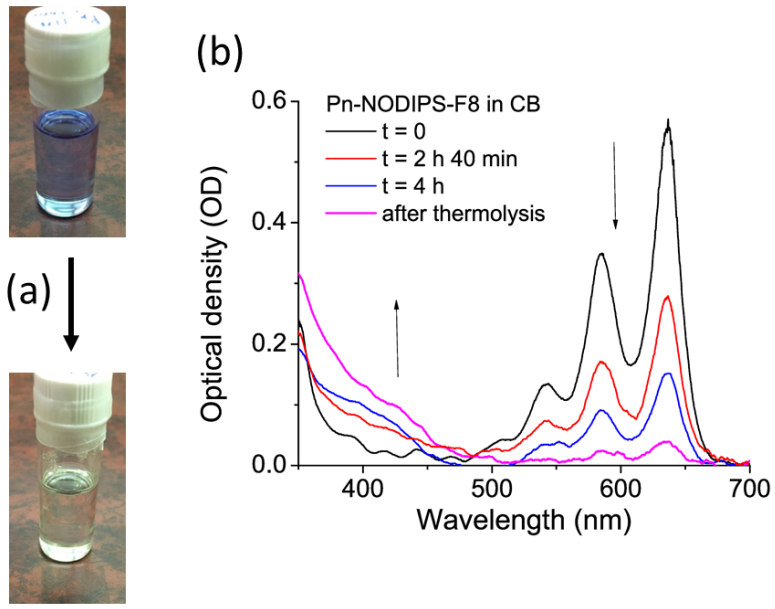

Figure 2.1: (a) Pictures of the Pn-TIPS solution before (top, blue) and after (bottom, clear) photobleaching under UV exposure. The change in color is an indication that photodegradation has occured. (b) An example of the solution absorption data of Pn-NoDIPS-F8 in chlorobenzene. As the sample sits under constant UV illumination the absorption decreases.

to see the trend of the absorption. Due to the linear shape of the integrated absorption as a function of time, the trends were scaled to 1 and then fit, using a non-linear least square's method, to the equation $A(t) = -m * t + 1$, where m is the rate of decay and 1 is the vertical offset since that is the value the trends were scaled to.

2.2.2 Photoluminescence Spectroscopy

Common application for organic semiconductor materials require the form of thin films, thus we tested the photostability of functionalized Pn in this state. The films were a Pn-polymer blend and used PMMA and PVDF as the host polymer and Pn-TIPS-F8, Pn-TIPS, and Pn-TCHS-F8 were the molecules used. Stock solutions of PMMA and PVDF were dissolved at a 13% wt into toluene and dimethylformamide (DMF), respectively. Stock solutions were also prepared with the functionalized fluorinated Pn (Pn-R-F8) dissolved in toluene at concentrations of 30 mM. For each sample, the solutions were mixed such that the intermolecular spacing could be specifically chosen from the range of $3-11$ nm[72, 73, 18]. The spacing between molecules, r, is caluclated as follows

$$r = \left(\frac{M}{N_A \rho_m c}\right)^{1/3} \tag{2.1}$$

where ρ_m is the mass density, M is the molar mass of the host material, N_A is Avogadros number, and c is the molar fraction of guest to host [67, 2, 9]. For all of the samples, except for the samples in which concentration was varied, a molecular spacing of 5 nm was chosen. This was chosen to minimize photodimerization as molecules are too far apart to form dimers. Thus the focus was on collecting EPO formation data.

The Pn-polymer solution was sonicated for 20 minutes, and then the films (either Pn-R(-F8):PMMA or Pn-R(-F8):PVDF) were deposited onto glass coverslips by spin-casting at 3000 rpm for 50 seconds from 60 μL of solution.

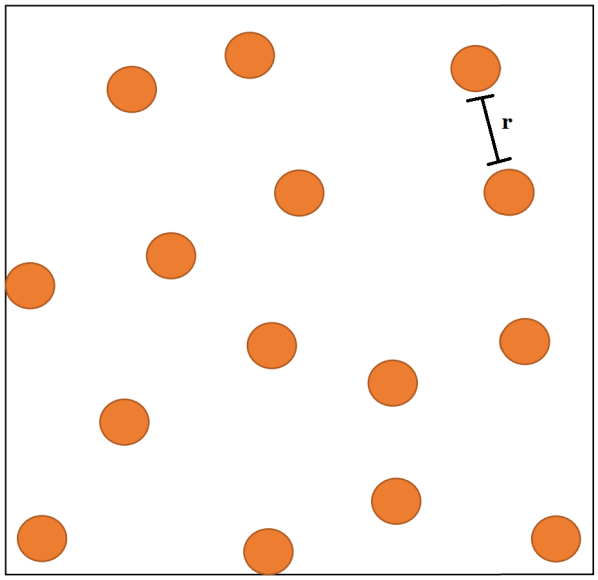

Figure 2.2: Graphic representing the molecules in the film with intermolecular spacing r.

The PL decay of the samples was collected using an Olympus IX-71 inverted microscope with a 10x magnification objective lens. This focused a 633 nm HeNe laser, the illuminating laser, with power ranging between 300 and 700 μW onto a prepared sample. A dichroic mirror was used to direct the laser to the sample and direct the photoluminescence from the sample, through an emissions filter to remove excess laser light, then to the optical fiber. The signal was collected through a 600 μm optical fiber and processed by an Ocean Optics USB2000-FLG spectrometer. Six hundred consecutive spectra were collected with an integration time of 100 milliseconds and 5 scans to average. A dark spectrum was also taken as a background reference.

For studies of photobleaching reversibility, after the first experimental run, the sample was kept in the dark for 5-20 minutes at room temperature in air, after which the experiment was repeated (run 2 and/or 3) on the same sample area. This was either done by hand, or managed with a computer program using a robotic shutter.

For temperature, wavelength, and low-oxygen exposure experiments, the sample was mounted inside a Janis ST-500 cryostat. The cryostat, mounted on top of the inverted Olympus microscope, has a window on each side so that light could pass to and from the sample. The mount inside the cryostat had a heating element and thermostat which were controlled by Lakeshore Model 335 temperature controller. Ryan Tolleffsen created a labview program to monitor and run the spectrometer, robotic shutter and the temperature controls, and used this to collect a majority of the data.

As seen in Figure 2.3, the resulting data was a series of consecutive spectra with the corresponding time and a dark reference spectrum. The data was processed by subtracting the reference spectrum from each spectrum and then each spectrum was processed by integrating over the 500-700 nm region of interest, which provided a value for each respective time. The combination of the time and integrated spectra was the integrated PL with respect to time. For runs that included shutter time, this dead time was removed from the integrated PL (see Figure 2.3). This was done using a graphical user interface written in python, which made this processing easy to do on the fly while taking data (see appendix A). To numerically quantify the decay, the integrated PL was fit, using a non-linear least square's method, to

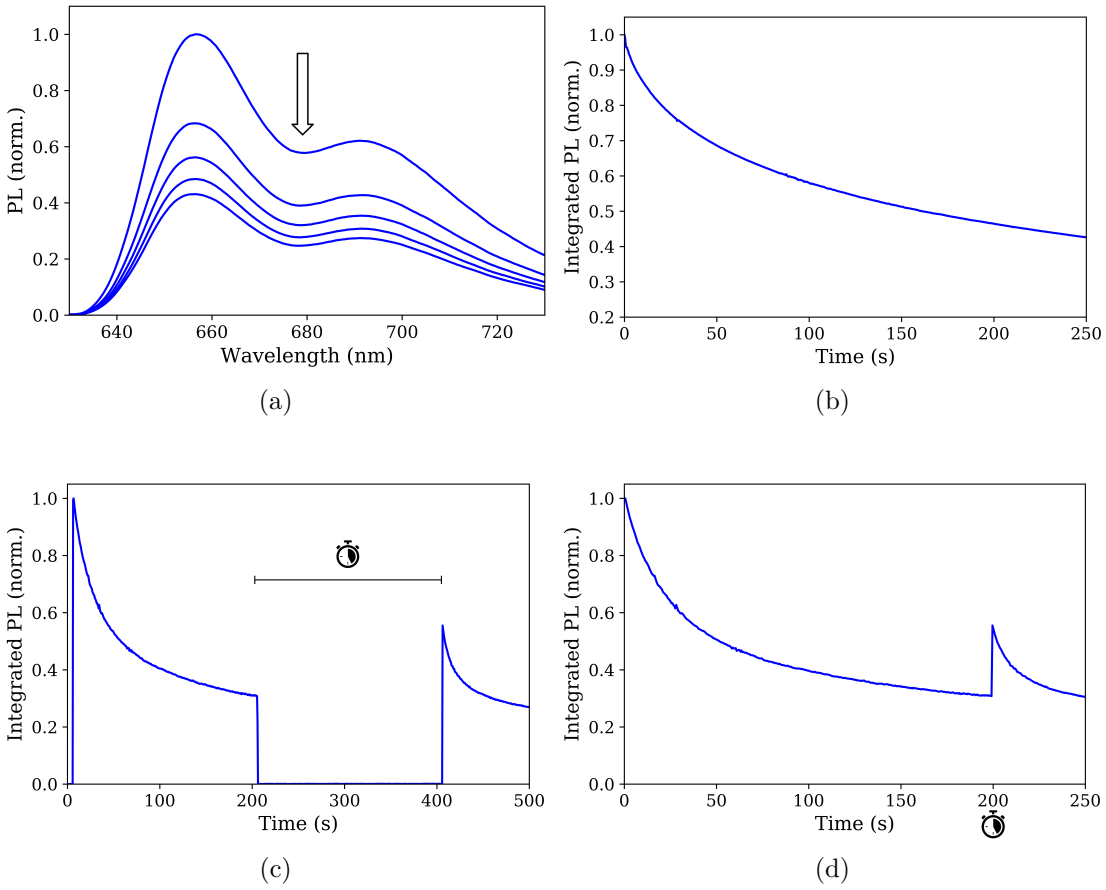

Figure 2.3: Example of Semi-Bulk Data. The transformation of the PL data of Pn-TCHS-F8:PMMA, from a collection of spectra at different periods of time (a), to a relationship between PL vs time (b). For runs which tested reversibility, the dead time, where the shutter is closed, as seen in (c), is removed after processing (d).

a bi-exponential equation $F(t)$ that follows

$$F(t) = A_1 \exp(-t/\tau_1) + A_2 \exp(-t/\tau_2) + A_3 \tag{2.2}$$

where A_1 and A_2 are the scaling coefficients for each exponential and τ_1 and τ_2 are the corresponding decay rates. From these fit values the half-life corresponding to each decay rate can be calculated using $t_{half,1 \text{ or } 2} = \tau_{1 \text{ or } 2} \ln(2)$. The half-life estimates how long it will take for the sample to lose 50% of its original value and in this case, it is a way to classify how quickly the two competing reactions occur. To find the half-life of the combined rates, the fit equation numerically solved for t, when $F(t)$ is equal to one half.

2.3 Results and Discussion

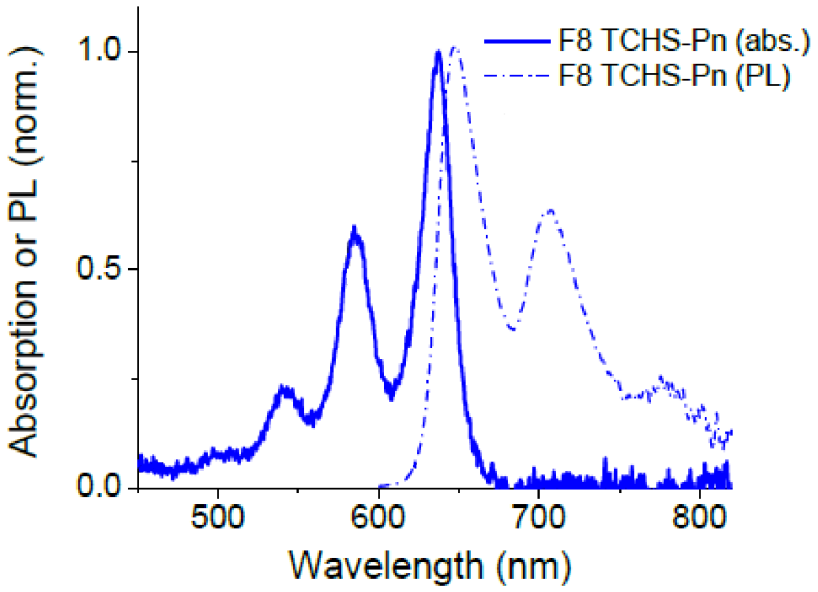

Figure 2.4: The absorption spectrum and the photoluminescence spectrum of Pn-TCHS-F8 (also notated as F8 TCHS-Pn). The two spectra are mirror images of each other and show vibronic progression with the distinct peaks.

The optical absorption and photoluminescence spectra are mirror images of each other and are characterized by ascending (or descending for PL) peaks, as seen in Figure 2.4. The defined peaks correspond to the vibronic split of the first excited state, which correlate to a slightly different energy difference between each vibronic level and the ground state. The well defined peaks are a characteristic of a sample with few aggregates. The definition of the peaks disappears at high concentrations as the intermolecular interaction provide more energetic states to transition between. The three distinct peaks and the relative heights remain the same as the spectra shrink due to photodegradation. When degradation products form, the molecular backbone, which is made up of optically significant π-bonds, is changed, which shifts the absorption and photoluminescence spectra to lower wavelengths. The signal for these products is mostly outside the range of the spectrometer being used and therefore won't be distinctly observed.

Both the optical absorption and the photoluminescence spectroscopy experiments show the photodegradation of functionalized Pn. Both experiments very clearly show how host material, fluorination, and concentration affect the photostability of Pn. Evidence that changes in side group, temperature and oxygen exposure was also found from the thin film experiment.

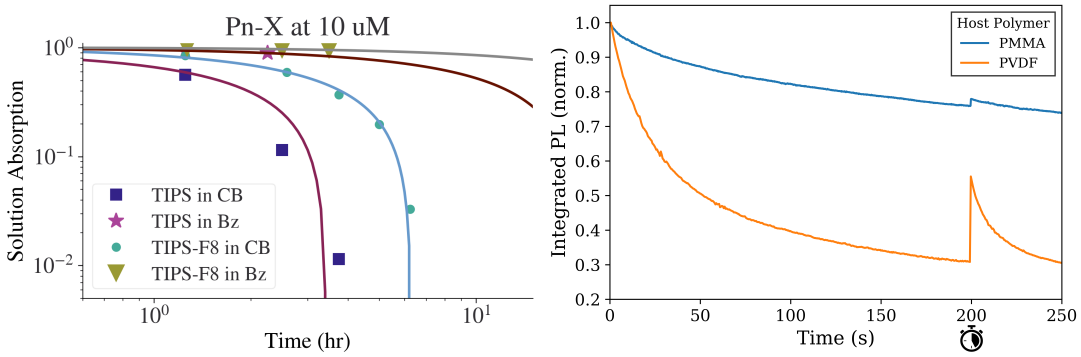

(a) (b)

Figure 2.5: Host Dependence. (a) The decay of Pn-TIPS and Pn-TIPS-F8 in both chlorobenzene and benzene. Both of the samples in benzene decay much slower than those in chlorobenzene. Pn-TIPS-F8 decays slower than Pn-TIPS in both solvents. (b) The decay of Pn-TCHS-F8 in PMMA and PVDF films. The PVDF film has a much faster decay, but also a much larger spontaneous recovery.

2.3.1 Sample Specific Factors

2.3.1.1 Effects of the Host Material

Absorption in Solution

The choice of host has significant impact on how quickly Pn decays and forms product. The most significant display of this is seen in the absorption data. Figure 2.5, shows the decay times of Pn-NoDIPS-F8 and Pn-TIPS in both benzene in chlorobenzene. All the decays were scaled to one and fit to a line and the rates of decay can be seen in table 2.1 and the corresponding half-life's were derived from this rate. For example, the rate of decrease is 0.171 hr^{-1} for Pn-TIPS in chlorobenzene, which corresponds to a half-life of $\sim$ 3 hrs. In contrast, the rate

of decrease for Pn-TIPS in benzene is 0.062 hr^{-1}, with a half-life of $\sim$ 8 hrs. For all the samples that were run in both solvents, decay was faster in chlorobenzene than in benzene.

Molecule Type	**Solvent Type**	**Decay Rate** ($\times 10^{-2}$ hr^{-1})	**Half-life** (hrs)
Pn-NODIPS-F8	Benzene	1.55	32.35
Pn-NODIPS-F8	Chlorobenzene	15.78	3.17
Pn-TIPS-F8	Benzene	18.29	2.73
Pn-TIPS-F8	Chlorobenzene	23.21	2.15
Pn-TIPS	Benzene	6.21	8.05
Pn-TIPS	Chlorobenzene	17.07	2.93

Table 2.1: Half-life and decay rates for Pn-TCHS-F8 in PMMA and PVDF at 5 nm intermolecular spacing.

Photoluminescence in thin-films

The effects of host on photostability can also been seen in the thin film samples of Pn-TCHS-F8 in PMMA vs PVDF at a 5 nm spacing, (see Figure 2.5 (b)). When scaled to one and fit to a bi-exponential, the fit parameters and half-lives were extracted. A brief look at the total half-life, seen in table 2.2, shows how quickly samples in PVDF decay. While PMMA has an average half-life of about 730 seconds, PVDF has a half-life that ranges from 13 seconds to 51 seconds, depending on the specific spot. While this is quite a large range, it is still a small difference when compared to the half-life of PMMA, which is at least twenty times longer. The fit values show that this decrease in half-life is due to the shortening of both the initial fast decay rate (τ_2) and the longer decay rate (τ_1).

Although the rates in PVDF are faster than PMMA, it is also the ratio of contributions that decreases the average on time. In PMMA, the slow decay rate has a coefficient of $A_1 \sim 0.9$, while the faster decay rate has a coefficent of $A_2 \sim 0.1$, which is a ratio of roughly $9:1$. This means that the slow decay rate is the more dominant part of the equation and the effects of this can be seen in Figure 2.5 (b), as the PMMA decay is much slower and the faster decay only presents slightly at the early times in the plot.

In comparison, the ratio of decay rate contributions for PVDF is heavily shifted the other direction. The coefficient A_1 is, at it's largest, 0.5 in comparison to the 0.48 for A_2 on that decay. This is the largest A_1 value as most of them sit around $0.2-0.3$ which means that A_2 is around $0.7-0.8$. This means that the slow decay process is, at best, contributing 50%, but more realistically 25% to the decay, which the faster decay process is dominating. This is also illustrated in Figure 2.5 (b), where the PVDF loses roughly 50% in the early time region where the short decay rate is most active.

An early conclusion from this data is that PMMA is a much more stable host than PVDF. This is an unexpected conclusion given that both PMMA and PVDF have very similar oxygen permeability rates (4.8 and 5.4 cc.-mm/m^2-25 hr.-bar, respectively), and previous studies have shown that there is a correlation between oxygen permeability and photostability[55]. The fit values also indicate that there are either two processes happening at different time scales or there is one process that has multiple mechanisms at play. Both of these conclusions will be further discussed in the discussion section of this chapter.

Host Polymer	A_1	τ_1(s^{-1})	A_2	τ_2(s^{-1})	$t_{half,1}$ (s)	$t_{half,2}$ (s)	$t_{half,tot}$ (s)
PMMA	0.877	1317.29	0.101	31.01	913.08	21.50	739.73
	0.886	1259.11	0.101	29.96	872.75	20.77	720.76
PVDF	0.417	1156.33	0.510	19.11	801.50	13.25	32.33
	0.198	450.01	0.741	21.05	311.92	14.59	18.36
	0.177	424.76	0.786	16.72	294.42	11.59	14.54
	0.507	382.58	0.484	23.40	265.19	16.22	50.57
	0.328	281.95	0.644	20.22	195.43	14.01	23.77
	0.203	164.67	0.756	14.37	114.14	9.96	12.72
	0.273	213.53	0.699	18.19	148.01	12.61	18.70
	0.273	212.42	0.699	18.15	147.24	12.58	18.69

Table 2.2: Half-life and decay rates for Pn-TCHS-F8 in PMMA and PVDF at 5 nm intermolecular spacing. The samples were fit to a biexponential using least squares fit, and the fit parameters are included here along with the corresponding half-life.

2.3.1.2 Effects of Molecular Structure: Side-groups and Fluorination

The ability to tune the properties of organic semiconductor materials is one of the reasons they show so much promise for device applications. The addition of side groups to functionalized Pn provides two functions: it increases solubility, which means functionalized and fluorinated derivatives are easier to process in solution, and it changes the molecular packing in solid state. The ability to tune molecular packing through the use of side groups dramatically affects the electronic properties and singlet fission, which are important for device development. Because of the importance these characteristics play in device development, it is critical to understand the side group and fluorination dependence of functionalized Pn in solution and thin film environments.

Absorption in Solution

For solution absorption experiments, the side groups that were used were TCHS and TIPS. As seen in Figure 2.6, at low concentrations, Pn functionalized with TIPS is more stable then Pn functionalized with TCHS. However, the difference between them effectively disappears and they decay at the same rate once the concentration reaches 120 μM.

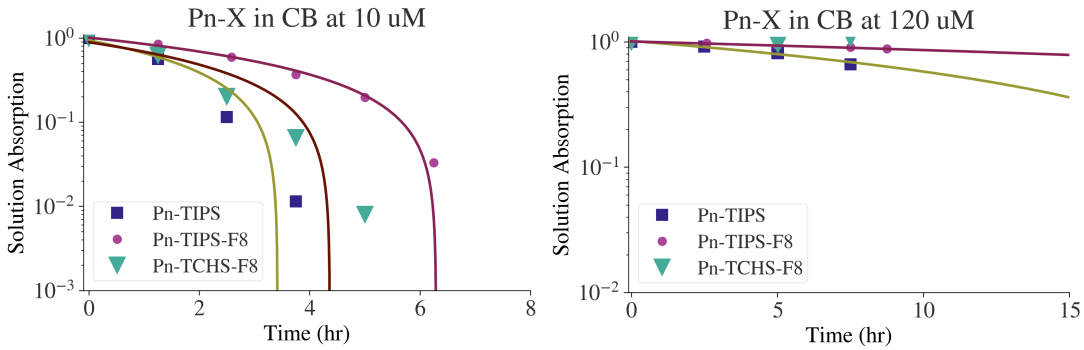

(a) (b)

Figure 2.6: Side Group and Fluorine Dependance in Solution. Solution decay for Pn-TIPS, Pn-TIPS-F8, and Pn-TCHS-F8 in (a) 10 μM solution and (b) 120 μM solution. Both pentacene derivatives with fluorine, Pn-TCHS-F8 and Pn-TIPS-F8, decay slower than the derivative without, Pn-TIPS, although the decay at the lower concentration is less pronounced. At high concentration, Pn-TCHS-F8 and Pn-TIPS-F8 have overlapping decay curves, which indicates that at this concentration, the side groups don't have a strong effect.

The effect of side groups R on the photobleaching of Pn-R-F8 in solution was more pronounced in chlorobenzene as compared to benzene (Figure 2.6(b)), with TCHS and NODIPS derivatives exhibiting about a factor of 2 longer half-lifetimes than the TIPS derivative. This is consistent with our previous observations of higher stability of NODIPS and TCHS derivatives as compared to TIPS, in Pn-

R-F8:PMMA films,[71] indicative of a protective role of large side groups against photo-induced degradation.

A second way that the molecular structure of functionalized Pn can be changed is through fluorination, which consists of replacing the eight hydrogen on the outer sides of the last aromatic rings (four per ring) with fluorine. The difference in stability between fluorinated and nonfluorinated Pn can also been seen from the solution data. Figure 2.6 shows the decay of solution absorption of both Pn-TIPS and Pn-TIPS-F8 at two different concentrations. For both concentrations, the fluorinated Pn is much more stable.

Photoluminescence in thin-films

Thin-film experiments also investigated the effects that side groups had on stability. Figure 2.7 shows the comparison of Pn-TIPS-F8:PMMA versus Pn-TCHS-F8:PMMA. In this case, the molecules with TCHS as the side group are much more stable than molecules with TIPS. This agrees with the results found in the paper by Shepherd, et. al., in which they also found the PL decay of Pn-TCHS-F8 and Pn-TIPS-F8 but the host material was t-bu-BTBTB instead[71]. However, this does not agree with the data from solution as discussed above.

The differences between the results found for the side groups in solution in comparison to thin-film are not wholly surprising. In solution, a molecule has full range of motion and will be constantly changing position. This means that the orientation of the side groups with the backbone will be in flux. Therefore, the molecular configuration that is optimal for photodegration will be a position that

the molecule can move through as it is suspended in solution. In contrast, the molecules in film are not free to move. Therefore, if the molecule is folded in such a way that it would discourage EPO formation or dimerization, it will not change from that position. Therefore larger side groups have a greater capacity to shield access of oxygen or other dimers to the bonding sites along the backbone. Since TCHS has a volume of 469.2 Å, NoDIPS has a volume of 402.5 Å and TIPS has a volume of 278.5 Å, both TCHS and NoDIPS are more protective of the backbone than TIPS [28]. In contrast, functionalized Pn in solution does not have the same level of protection from the side groups, unless sufficiently high concentration has been reached and either mobility of each molecule is more constrained or other excited state processes, such as singlet fission or excimer formation, deplete the reactive states.

Just as side groups offer protection against photodegradation, so does fluorination of the molecule. As seen in the solution experiments, molecules with fluorine on the ends of the Pn backbone are significantly more photostable. Because fluorine is much more electronegative than hydrogen, when the hydrogen are exchanged for fluorine the π-bonds adjust and the electron cloud shifts to have higher probability closer to the fluorine. The drop in electron density probability closer to the center means that the bonding sites for both EPO formation and dimerization are less favorable. This is in agreement with the data that we have collected from optical absorption.

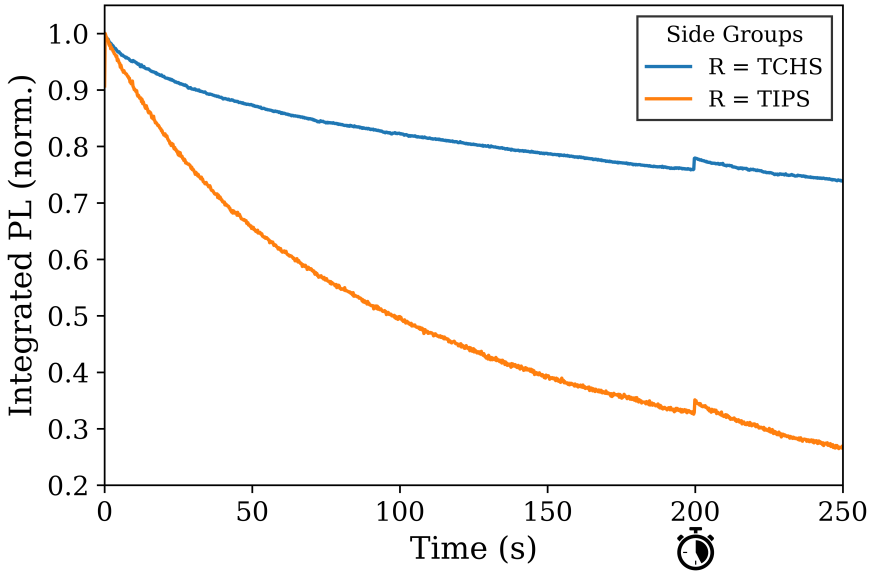

Figure 2.7: Thin Film Side Group Dependence of Pn-R-F8 in PMMA at 5 nm spacing. Pn-TIPS-F8 decays at a significantly faster rate.

2.3.1.3 Concentration

Another sample property that affects the photostability is the molecular concentration. In solution, the optical absorption shows that at higher concentrations, the decay is much slower (see Figure 2.8a). For both Pn-TIPS and Pn-TIPS-F8, the decay rate decreased by an order of magnitude with the increase of the concentration of the solution from 10 μM to 120 μM. This agrees with the data from PL.

In the photoluminescence spectroscopy of thin-films, there was also a decrease in decay rates as the concentration increased as seen in Figure 2.8(b). In fact, the

concentration increased so high, that the PL would rise for a while before starting to decay. This is a very unusual and unexpected effect, but agrees with the physics of the situation. At higher concentrations, the molecules in the sample are spaced closer and closer together. When functionalized Pn are close enough together, they can interact. Specifically, at high concentration, singlet fission becomes an active intermolecular interaction, which is a nonfluorescent process and therefore quenches the photoluminescence. This means that although all the molecules in the sample are actively absorbing the incident photons, there is no emission from these molecules to contribute to the PL that is being collected. As molecules form endoperoxides or dimers, they no longer absorb the emitted photons of their neighbors and the PL increases.

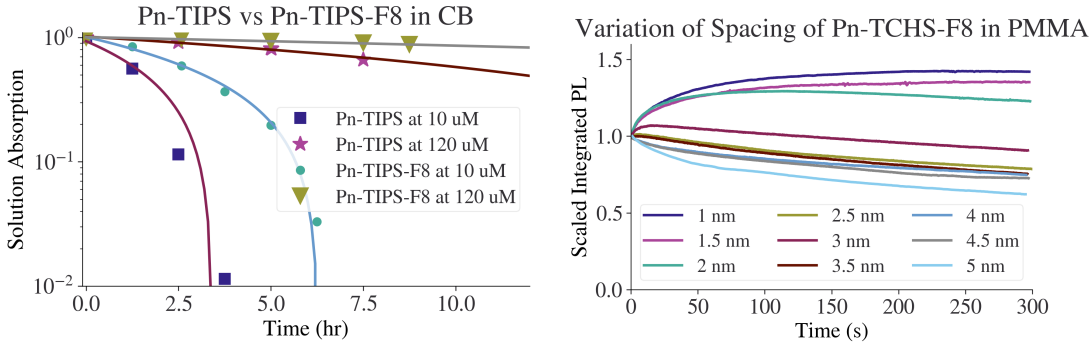

Figure 2.8: Concentration dependence in solution and thin-film. (a) Pn-TIPS and Pn-TIPS-F8 in 10 μ M and 120 μ M concentrations. For both derivatives the higher concentration is more stable than the lower concentration samples. (b) Pn-TCHS-F8 in PMMA at concentrations between 1 nm to 5 nm with data taken at every 0.5 nm. At really close spacing, the "decay" actually rises before decaying, due to the break in the aggregation. Once the aggregates are broken up, the sample starts decaying in the same way as the lower concentration samples.

For both solution and thin films, when the higher concentration samples decay, they have slower decay rates. This enhanced photostability is most likely due to formation of nanoaggregates with reduced free volume, which decreased the oxygen permeability resulting in inhibited reactions of Pn-TCHS-F8 molecules with oxygen. Thus, for more photostable samples, higher concentrations should be used even with the addition of competing photodimerization, as it is not as significant a decay process as photo-oxidation.

2.3.2 Effects of External Factors

2.3.2.1 Temperature

As seen in the previous section, choices in sample preparation affects its photostability. Likewise, external factors can also have an effect. Temperature is an external factor that is often changing. Understanding the effects of temperature change on organic electronic materials is critical for device development. Using PL, we tested the Pn-TCHS-F8:PMMA at a variety of different temperatures, as seen in Figure 2.11. As expected, the films decayed faster at higher temperature. This is due to the additional energy that is added to the system as heat, which acts as a catalyst for either dimerization or EPO formation.

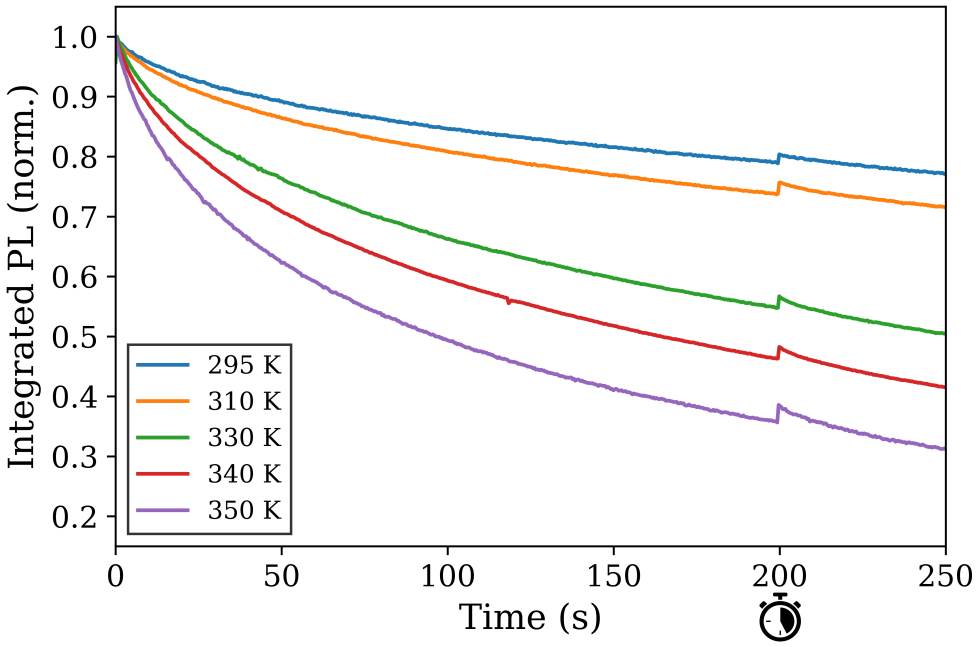

Figure 2.9: Thin film temperature dependence. As the temperature increases, the decay rate increases because the added energy aids in the decay chemical reactions.

2.3.2.2 Oxygen and wavelength exposure

Previous work has shown that without exposure to oxygen, functionalized Pn is considerably more optically stable. The data collected through PL confirmed this. In Figure 2.10, the PL for Pn-TCHS-F8:PMMA in vacuum under 633 nm excitation is almost completely flat. When fit to a biexponetial, it has decay rates that are on the order of 10^{-6} s^{-1}. However, this is so flat, that it can also be fit to a line that has a slope of -1.56×10^{-5} s^{-1}. At that rate, this sample would decay to zero in roughly 18 hours. This is orders of magnitude longer than seen in the

samples in air (at standard room conditions), which have half-lives ranging from a few seconds to a few minutes.

However, this very slow decay in vacuum is only true when the excitation wavelength is 633 nm. When the UV laser was used instead, the PL decayed at a rate that was comparable to the decay rates in air. This indicates that the dimerization is occurring, but requires more energy than is available from 633 nm photons. This indicates that at room temperature and under 633 nm, dimerization is not a favorable reaction. This also indicates some molecular clustering in the sample as photodimerization should not be occurring at 5 nm molecular separation.

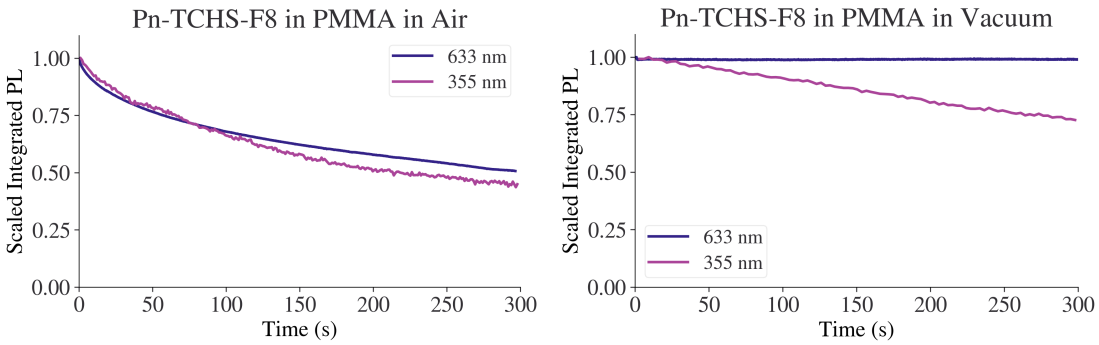

Figure 2.10: Thin Film Wavelength Exposure Dependence of Pn-TCHS-F8 at 5 nm spacing. When excited using a UV laser the decay is similar to 633 nm laser excitation in air. However, this changes when the sample is in vacuum. In vacuum, the 633 nm excitation is very stable, but the uv excitation causes the sample to decay.

2.3.3 Molecular Recovery

For both experiments, molecular recovery was attempted. For the solution samples, $3-6$ hour thermolysis at 80°C was used, followed by taking absorption spectrum. For films, the recovery was spontaneous as the film was allowed to rest in the dark between data collection runs.

Absorption in Solution

In both solvents, and for all derivatives, the 3-6 hour thermolysis recovered about 6% of the original 500-700 nm absorption strength observed in fresh solutions. This recovery is most likely due to the EPO converting to the parent Pn molecules, as reversal of photodimerization would not be expected under low-temperature thermolysis conditions used in our experiments. The percentage of recovery did not considerably change between 3 and 6 hours of thermolysis; however, the absorption spectra obtained after 6 hours of thermolysis had an increased 350-450 nm spectral component as compared to those after 3 hours, which indicates that degradation processes continue during thermolysis.

Photoluminescence Spectroscopy

In PL, the spontaneous recovery was seen in all experimental conditions. However, it was only temperature and host polymer that saw any variation. As seen in Figure 2.11, the recovery of functionalized Pn remains constant or decreases until the temperature reaches somewhere between 350 K and 370 K when it increases

dramatically. Since there is some recovery without the addition of heat, this indicates that there is a product formed that requires additional energy to reverse and that is activated once the film is heated to a high enough temperature.

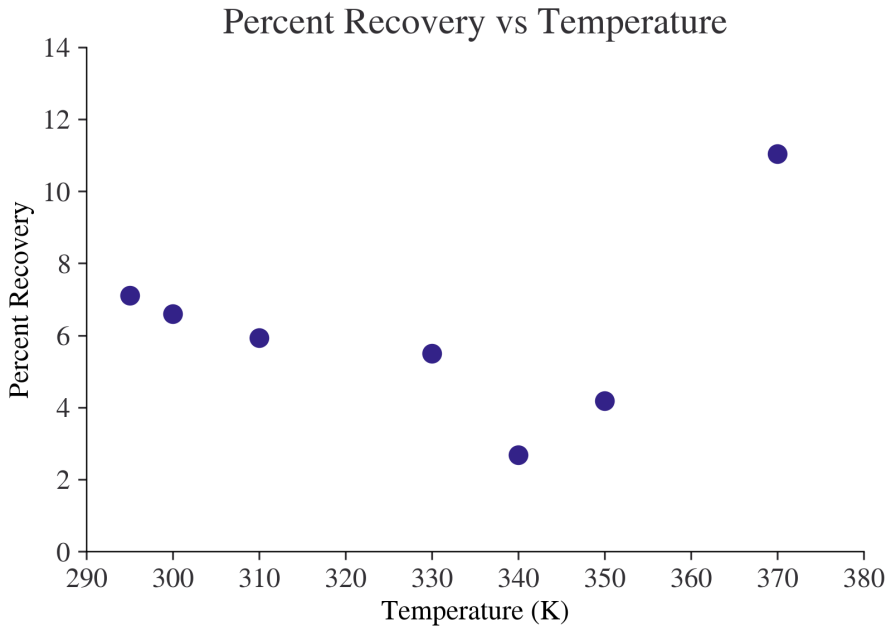

Figure 2.11: Temperature Dependance of Recovery. The percent recovery starts to slowly decrease as the temperature increases until the temperature reaches a threshold somewhere between 350 K to 370 K. This agrees with the literature as most heat aided recovery is performed at somewhere between 350 K to 370 K.

This could be the reversal of photodimerization, as that has been shown to reverse at temperatures of around 100°C [10] and the threshold for the recovery process could be lower. However, these samples were at 5 nm spacing, which should have very limited dimerization, which is supported by the low decay rates of Pn-TCHS-F8 in vacuum as discussed in the previous section. The decay of Pn-TCHS-F8 in PMMA at 5 nm spacing in vacuum is so slow that there couldn't

be a large enough population of dimers to increase recovery from an average of 5% to 12%.

Instead this is an indication of EPO formation. Because EPO formation is a two step process, first the oxygen and functionalized Pn interact to form reactive oxygen and then the reactive oxygen and functionalized Pn bond, there are effectively two states in which functionalized Pn is not emissive. As will be discussed further in Chapter 4, after the first step in EPO formation, functionalized Pn can return from being non-emissive to being emissive again. When the sample rests at room temperature the functionalized Pn in this non-emissive state can revert, but the competing process of molecules entering this state disappears without the photons present. Thus, the room temperature recovery is recovery of the first step EPO formation. However, with the addition of heat, functionalized Pn-EPO can make the transition back to their original structure.

Host polymer also had an effect on recovery, as seen in Figure 2.12. PVDF has significantly higher decay rates and corresponding half-lives, however the percent recovery is much larger. This suggests that both steps of the EPO process are faster in PVDF because the half-life is short. This indicates that EPO formation is occuring rapidly, but the large percent recovery also indicates that a larger portion of the functionalized Pn is in the dark non-emissive state. This is likely due to the clustering that functionalize Pn experiences in PVDF due to polarization, which will be discussed in Chapter 4. The wide spread of recovery percentages and half-lifes is due to the non-uniform nature of PVDF, which will also be further discussed in Chapter 4.

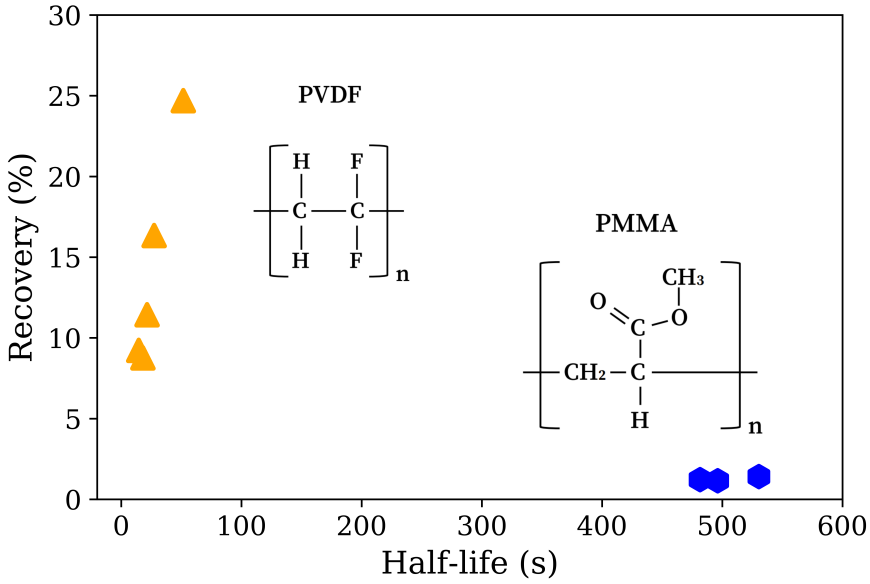

Figure 2.12: Host Dependence of Recovery. Although the molecules decay much faster in PVDF, the percent recovery is much higher than in PMMA.

2.3.4 Discussion

The Pn-R-F8 derivatives exhibit more than an order of magnitude (a factor of 15-40, depending on the derivative) higher stability in benzene as compared to chlorobenzene (Figure 2.6(b)). A strong dependence of photodegradation on the solvent polarity, and the case of benzene versus chlorobenzene in particular, was also observed for Pn-TIPS[10] and attributed to the $\pi - \pi$ interactions of the Pn molecule with the surrounding benzene molecules which prevented Pn-Pn dimerization. Similar considerations can be applicable to the case of fluorinated Pn derivatives in polymer hosts.

As seen in the data, in polar host materials, PVDF and chlorobenzene, func-

tionalized Pn photodegrades much more quickly than in the non-polar host materials, PMMA and benzene. This suggests that intermolecular interactions between the non-polar hosts and functionalized Pn protect the molecule from both EPO formation and dimerization. The polar nature of PVDF and chlorobenzene also encourages aggregation of functionalized Pn, which increases the probability of dimerization and the rate at which reactive oxygen can bond with a fluorinated Pn molecule. When the sample is heated the added energy increases the rate of these products, specifically it increase the rate at which oxygen can move through the material.

The very small decay of functionalized Pn in vacuum indicates that the primary decay pathway is EPO formation and that dimerization is a much smaller contributor to photodegradation. The spontaneous recovery in the PL experiments at room temperature also supports this conclusion as dimers require added energy in order to return to the original molecular state[10].

2.4 Conclusions

Both the optical absorption of solution and the photoluminescence spectroscopy of thin-films illustrate the significance of photodegradation and the impact that small adjustments to the sample can make in photostability. Some of the adjustments can be made when preparing the sample, like concentration, choice of Pn derivative, or choice of host material. Other adjustments are external, such as temperature, oxygen exposure, or the choice of what wavelength of light to use. All of these

parameters affect the stability of the organic material used.

For sample preparation, the shift from one solvent or polymer host to another solvent or polymer can change the half-life of the sample by an order of magnitude. Likewise, molecules that have large side groups, like NoDIPS or TCHS, and are fluorinated are more stable than molecules with smaller side groups, like TIPS, and that are unfluorinated. Although, in this regard, the fluorine have a much stronger effect on the stability of the material than the side groups do. The choice of molecular concentration also has a huge bearing as high concentration samples have much slower decays than low concentration samples.

Just as the sample design choices affect the stability of the materials, so do the external factors. The photoluminescence spectroscopy experiments showed that external conditions have strong effects on the stability. Of the three external factors studied, it was the wavelength dependence that had the least impact as the decays for the UV light were very similar to those from the red laser. Temperature had a more significant impact as the added temperature increased the decay rate, leading to the hypothesis that lower temperatures would lead to higher stability in Pn films. However, lower temperatures leading to higher stability would be less helpful in device development. Of the three, the most significant environmental adjustment was limiting the oxygen exposure, which plays a huge contribution in the stability of functionalized Pn. While ideally, organic semiconductor materials could be kept in vacuum, it is not the most practical approach for large scale manufacturing.

The data from these two experiments confirms that photodegradation is a sig-

nificant hurdle to device development, but careful choices in environmental factors and sample composition can mitigate some of the decay. Photoluminescence spectroscopy also illustrated the oxygen dependence of photodegradation, which indicates that EPO formation is occurring as part of the degradation process.

Chapter 3: Experimental Probe into Product Formation in Functionalized Pentacene

3.1 Introduction

To understand the causes for the photodegradation of the functionalized pentacene (Pn) that were observed in optical absorption and photoluminescence experiments, the products that were created through the reactions were studied. Since there are two competing methods of photodegradation, it would be helpful to characterize the products formed in these processes. To do this, the solution samples that were used for optical absorption were tested using Nuclear Magnetic Resonance Spectroscopy (NMR) to isolate the types of products that formed.

3.2 Nuclear Magnetic Resonance Spectroscopy

To understand the photodegradation pathways of the Pn molecules, Nuclear Magnetic Resonance Spectroscopy (NMR) was used to analyze the products of various Pn derivatives in solution. Because NMR probes the magnetic dipole moment of a selected atomic isotope, the responding signal provides information about the local nanoenvironment for each nuclei probed. The signal response of each isotope provides information about the local nanoenvironment, with emphasis on the

neighboring atoms with which the probed atom shares bonds. Because this process only probes the magnetic moment of the nuclei in a given sample, this is a noninvasive way to determine molecular structure. Because of this property, NMR has a wide variety of uses including applications in medicine, chemistry and petroleum research [1, 20]. It is very frequently used by biologists and chemists to determine the molecular structure of newly synthesized proteins or other materials [1].

3.2.1 The Physics of Nuclear Magnetic Resonance Spectroscopy

Nuclear Magnetic Resonance Spectroscopy (NMR) utilizes the magnetic moment of atomic isotopes, to noninvasively probe the molecular structure of a sample. NMR samples are placed in a large local magnetic field $(4 - 16\text{T})$ in order to align the magnetic moments of all the atoms in the sample. In an attempt to align the magnetic moment of the nucleus with the external magnetic field, the angular momentum of the atom causes a precessional motion, which is named the Larmor precession. The frequency of this precession is unique to each of the isotopes present in the sample. A radio frequency pulse that matches the frequency of the isotope that is being probed is applied via a transmitter for a short period of time ($\sim 1\ \mu$s) perpendicular to the applied field. This deflects the magnetic moment of the atoms toward the perpendicular direction of the applied pulse. Precession of the atom in the deflected state as it returns to equilibrium yields a radio frequency field which is detected by the receiving inductor. The time dependent induced voltage is the signal of the experiment[20].

To strengthen the signal, the process of applying a radio frequency pulse and collecting the radio frequency during relaxation can be performed repeatedly, however, the isotopes being probed need to relax back to their equilibrium before another pulse can be applied. The time it takes for relaxation to occur is dependent on the isotopes and the degree of deflection from equilibrium, which is dependent on the strength and length of time the signal is applied. Heavier atoms and larger deflection angles require longer relaxation times[20].

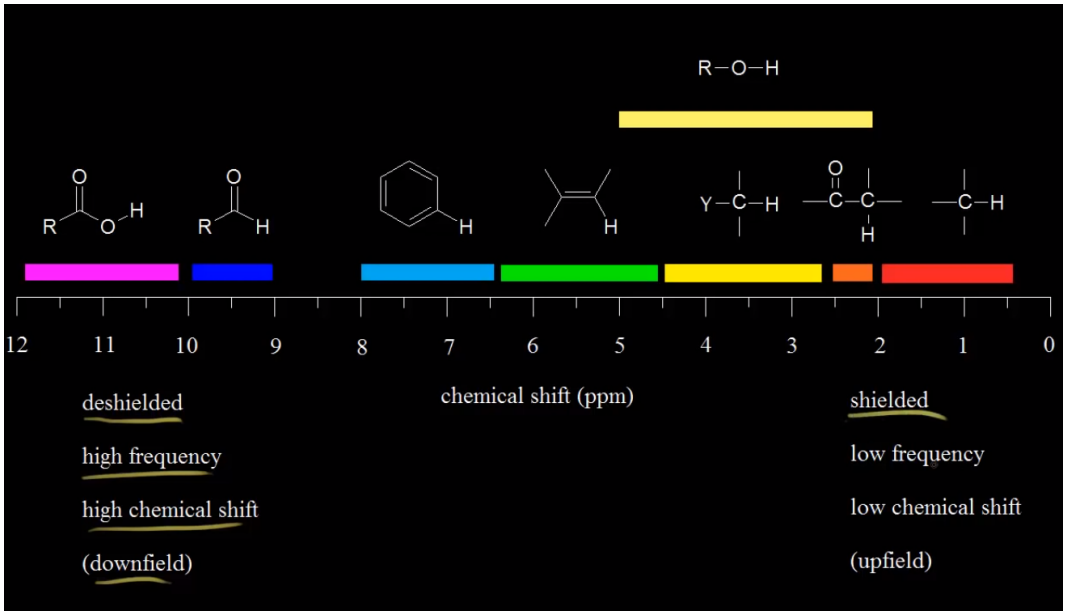

Figure 3.1: The location of common hydrogen bonds on the H^1 NMR spectrum. Hydrogen atoms that experience less magnetic shielding will be shifted downfield.[25]

To interpret time dependent induced voltage, a Fourier transform is taken of the signal. The frequencies present in the signal are correlated to the location of a specific atom in a molecule. The specific frequency of precession of an atom

is dependent not only on its nuclear make-up, but also on the interactions it has with surrounding molecules. The bonds between the atoms being probed and their neighbors results in a shift of frequency, also called the chemical shift, for the atom of interest. This is due to the electrons that are involved in the bonding process. The electrons around each atom are also affected by the magnetic field applied to the system. In response, they align with the field, creating a small magnetic field that is opposite the applied field. Thus, the effective magnetic field is slightly reduced for the nucleus. This magnetic shielding affects the frequency that the nucleus produces when relaxing[20].

The chemical shift is very small, on the order of one millionth of the applied frequency. Since it is the small shifts in frequency that contain the information about the molecular structure, NMR employs a relative spectrum which measures the shift of frequencies (in parts per million, ppm) relative to a reference frequency. In proton (H^1) NMR, tetramethylsilane (TMS) is normally used as the reference compound[20].

From the chemical shift spectrum, the molecular structure can be determined using three characteristics of NMR: the location of the signal, the shape of the signal and the integrated value of the signal. To begin, there is a relationship between the amount of shift and the types of molecular bonds connected to the atom. Figure 3.1 classifies spectral regions based on molecular structures for proton NMR. The general rule for determining where a molecular bond lies on the spectrum is that hydrogen that is shielded is “upfield” or closer to zero. Molecules that are deshielded are shifted “downfield” or further away from zero. In general,

determining the chemical shift can be done by determining the electronegativity of the bond, since the electrons are pulled away from shielding the nucleus[20].

There are of course special cases that deviate from this rule or have more complicated molecular interactions occurring. For example, hydrogen in aromatic molecules are shifted further downfield than might be expected of a chain of carbon-hydrogen bonds. The shift downfield in aromatic molecules is due to the conjugated π-bonds, which allow for electron movement across the whole length of the conjugated chain. Because of this property, the applied magnetic field will induce a much stronger magnetic field in the electrons in the band of electrons that can move freely across the top and bottom of the length of the aromatic rings. This significantly decreases the effective magnetic field felt by the hydrogen atoms bonded to the outside of aromatic rings, which shifts their signal downfield[20]. This is of significance in this study as Pn-R(-F8) has an aromatic backbone, and the photodegradation products affects the aromatic rings of Pn derivatives.

A second characteristic of an NMR spectrum is that the shape of a signal is dependent on the bonds of the nearest neighbors. For example, the signal of a specific hydrogen bonded to a carbon will be split into two peaks if the atom bonded to the carbon also has a single hydrogen. This happens because when the magnetic field is applied, an atom can either be aligned or anti-aligned. This changes the net magnetic field felt by neighboring atoms, which results in some of the neighboring atoms in the sample being shifted either slightly downfield or slightly upfield[20]. The physics of this process can lead to exceptions when it comes to signal strength, however the general rule is that the number of peaks of a

signal is the number of neighboring like atoms plus one. This spectral characteristic is very helpful in determining molecular structure.

The NMR spectrum has another characteristic that is helpful in determining the molecular structure of the material. The area of a specific peak (or group of peaks) indicates the relative abundance of that specific nanoenvironment. Therefore, by comparing the integrated values of the peaks of interest in a spectrum, the frequency of a bond in a specific molecule can be determined. This can also be used to determine the relative concentrations of two materials that have distinct spectral peaks[20].

3.2.2 Experimental Design

For Pn-R(-F8), H^1 NMR was primarily used, with C^{13} NMR done on selected samples to confirm expected structure, which probes the hydrogen-1 nuclei and the carbon-13 nuclei, respectively. In order to understand how various aspects of molecular structure contribute to the signal of hydrogen with distinct nanoenvironment, I took NMR spectra of two Pn derivatives: fluorinated (Pn-TCHS-F8) and non-fluorinated (Pn-TIPS) and featuring different side groups (TCHS and TIPS, respectively) separately in deuterated benzene and correlated the known molecular structure with the spectra. Figure 3.2, shows the two molecules labeled with colored symbols to indicate locations of the different hydrogen groups.

For example, in Pn-TIPS (Figure 3.2 (a)), there are five groupings of hydrogen with distinct molecular environments, three groups on the backbone, and two on

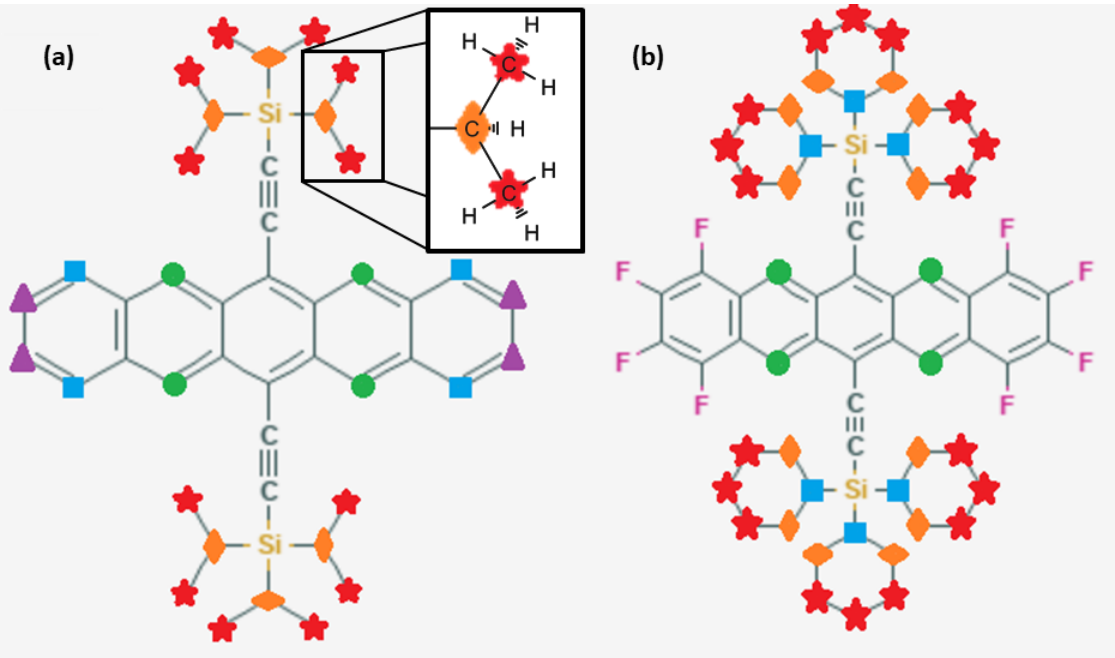

Figure 3.2: Locations of Hydrogen with Unique Bond Configurations. (a) In Pn-TIPS, there are five groups. By symmetry, the four hydrogen atoms in the molecule that are bonded to the green circle carbon have identical molecular environments. Following the same logic, there are four hydrogen at the blue square carbon, four hydrogen at the purple triangle carbon, and six hydrogen at the orange diamond carbon. The stars are unique as there are three hydrogen bonded to the carbon at each star location as seen in the inset, so there are twenty-four hydrogen at the red star carbon in the molecule. (b) For Pn-TCHS-F8, there are four hydrogen at the green circle carbon, six hydrogen at blue square carbon, twenty-four hydrogen at orange diamond carbon, and thirty-six hydrogen at red star carbon, since there are two hydrogen per carbon for both orange diamonds and red stars.

the side group. Because of the symmetry of the molecule, there are four hydrogen associated with the site labeled by the green circle, four associated with the blue square, four associated with the purple triangle, and six associated with the orange diamond. The red star is unique because it labels a site where there are three

hydrogen atoms bonded to the carbon at that location, which means there are a total of 36 hydrogen in the molecule with the same bonds and neighbors as the hydrogen atoms at the red star. Based on this classification, we can see that all 54 of the hydrogen in the Pn-TIPS chemical formula ($C_{44}H_{54}Si-2$) are accounted for and we can use the spectral reference (Figure 3.1) to estimate the location of the peaks.

Because the blue squares, purple triangles, and green circle sites are connected to aromatic rings, they would be further downfield than the hydrogen located at the orange diamonds and red stars. The blue square sites and purple triangle sites are more similar to each other than they are to the green circle sites, so it is likely that they will be close together and may even have overlapping or interacting signals. The green circles sites are closest to the center of the molecule and are surrounded by more electronegative atoms, so the hydrogen there will be deshielded more than the other hydrogen at the backbone and will therefore be shifted downfield even more.

Based on this information, predictions can be made about the expected spectra for both Pn-R-F8 and Pn-R. Since the products we are investigating affect the optical properties, which are dependent on the backbone of the molecule, the NMR signal from the side groups is not of interest. However, the NMR signal from TCHS and TIPS should look different, but will all be contained at spectral values lower than 4 ppm. However, for the backbone signal, Pn-R-F8 should have one single-peak signal around 9 ppm and Pn-R should have three significant signals, one single-peak signal around 9 ppm and two four-peak signals somewhere between 6

and 9 ppm.

Figure 3.3 shows the spectra for both the molecules depicted in Figure 3.2 and the spectra agree with our expectations. As indicated in the figure, the furthest peak (9.31 ppm) correlates to the hydrogen atoms on the aromatic rings closest to the center of the molecule. The other downfield signals (centered at 7.98 ppm and 7.12 ppm) correspond to the hydrogen on the aromatic rings at the end of the rings and the signals overlap. The hydrogen corresponding to the side groups (TIPS or TCHS) has signals that are located upfield (between 1.3 ppm to 1.4 ppm) as expected. These results are confirmed by comparing the ratio of the area under each signal, which show that the peaks have a ratio of 4:4:4:6:36, which is what we expect from the hydrogen groups discussed above (Figure 3.3) and the Pn-TIPS spectrum agrees with the published NMR data for Pn-TIPS in the paper by Fudickar and Linker[14].

3.3 NMR Simulation

To help identify the NMR signals originating from products of photodegradation of Pn derivatives, the simulation feature of the Bruker TopSpin 4.0.8 software was used. The built in Pulse Program (nmrsim) was used in combination with the NMR Wizard. Functionalized Pn has between 100-150 atoms, depending on the derivative (e.g.100 in Pn-TIPS) that make up each molecule, which is too many for TopSpin to simulate all together. To combat this, I ran simulations to determine the difference between the parent molecule and the potential products.

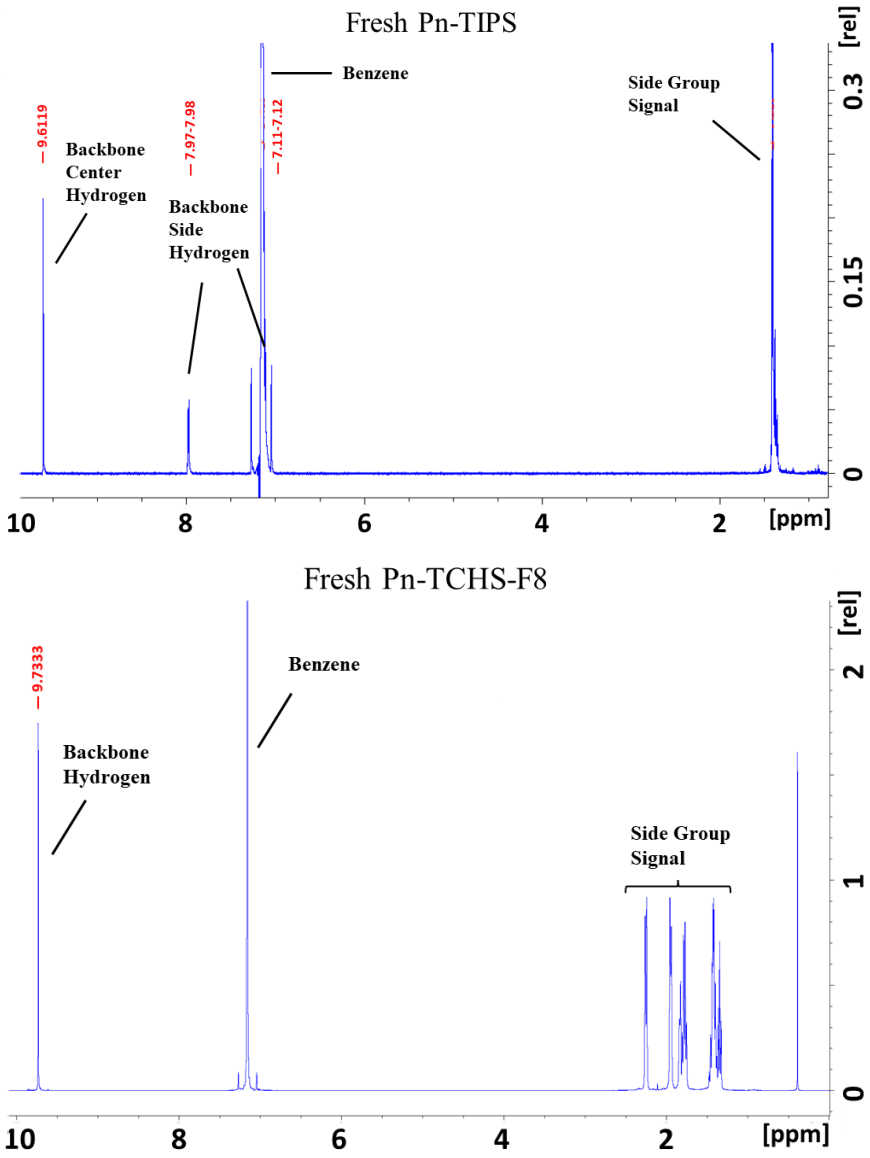

Figure 3.3: Functionalized Pentacene NMR H^1 Spectrum. The full NMR spectrum of Pn-TIPS (top) and Pn-TCHS-F8 (bottom) in deuterated benzene. As expected, Pn-TCHS-F8 has only one single-peak signal that is downfield and Pn-TIPS has one single-peak signal and two four-peak signals downfield.

Each molecule could be roughly broken up into two pieces of interest, the backbone and the side group, since these are the unique substructures in the molecule.

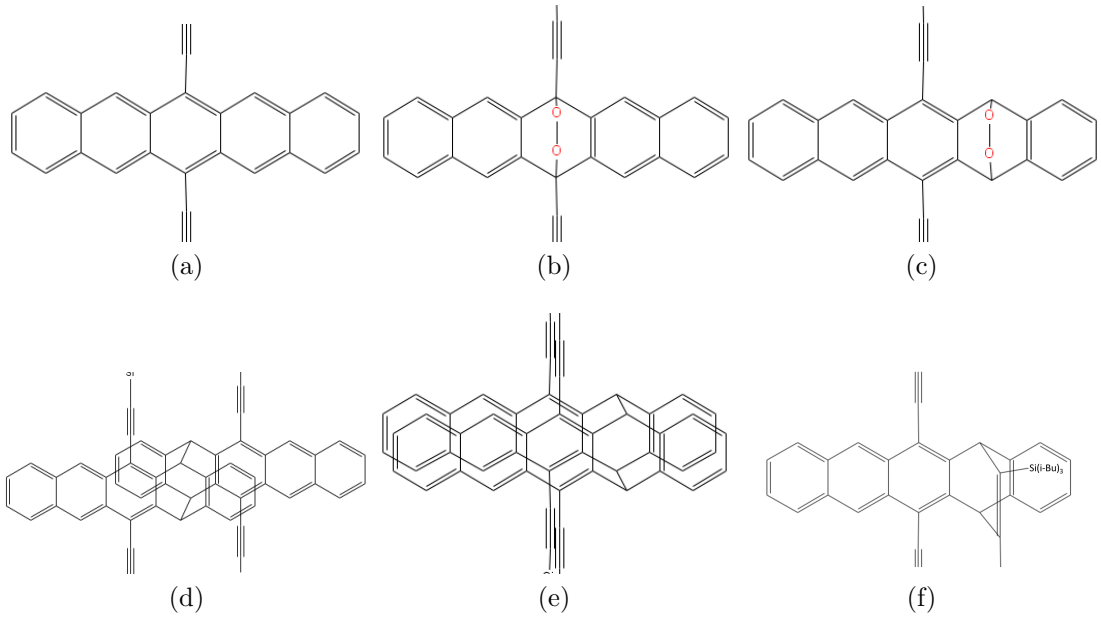

Figure 3.4: Functionalized Pentacene Simulation backbone structure. (a) the original structure of non-fluorinated Pn. The oxygen bonding sites for both center EPO (b) and side EPO (c). The two types of butterfly dimers: centrosymmetric (d) and planosymmetric (e). The alkyne dimer structure (d).

Based on the research done by other groups[14, 10], there are five different photodegradation products that can form, as seen in the Figure 3.4. EPO can form with the double oxygen bonded either across the center aromatic ring (which will be referred to as "center EPO"), or across the ring to either side of the center ring (which will be referred to as "side EPO")[14]. Dimers, on the other hand, have a few orientations. Butterfly dimers form with bonds between the aromatic rings on either side of the center ring, either exactly mirroring each other, centrosymmetric,

or with the backbone off-set, planosymmetric[10]. It is also possible for dimers to form between the backbone and the side groups in an alkyne dimer.

The simulated data (see Figure 3.5) for these configurations show that for all of the configurations, except center EPO, the original three NMR group peaks, which are downfield, get split into six. This follows intuition as the bonds of either a dimer or an O_2 molecule on the aromatic ring adjacent to the center ring would only affect the hydrogen atoms on that side while the signal of the hydrogen on the other side of the molecular backbone would remain unchanged. There is a slight difference between the EPO formation and the dimer as the lower single peaked signal is further downfield. This is due to the stronger deshielding that comes from the oxygen atoms. The simulated data provides a reference point for understanding the spectrum of the solutions from our experiments.

3.4 NMR Results

In order to investigate products formed as a result of photobleaching, samples of Pn-TIPS, Pn-TIPS-F8, Pn-TCHS-F8 were prepared in benzene or chlorobenzene, at 1 mM concentrations. Solutions were illuminated with a continuous wave light source, for which either a UV lamp ($360 - 370$ nm with a 365 nm peak) or ambient florescent light were used, which will be referred to as "UV" and "Vis" in the discussions below. Once the measured optical absorption of the solution samples was below 10%, the solvents were evaporated off and the molecules were dissolved in deuterated benzene. Both proton (^1H) and carbon (^{13}C) NMR were run on

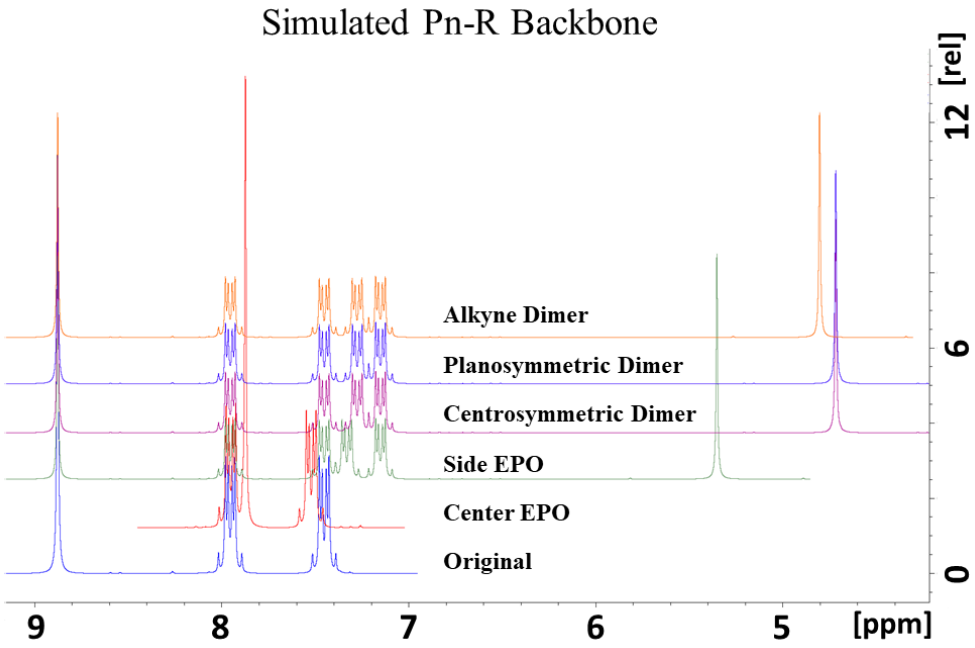

Figure 3.5: Simulated NMR Data: The simulated data for the original backbone of unflorinated pentacene. The simulated data for each product in order (from top to bottom) alkyne dimer, planosymmetric dimer, centrosymmetric dimer, side EPO, center EPO and then the parent signal at the bottom. The signals for both the butterfly dimers align and are almost aligned with the alkyne dimer, indicating that the orientation of the dimerization does not matter. The side EPO has a similar alignment for the middle signals, but the lower peak is not as far shifted upfield.

the samples using the Brucker 700 MHz NMR Spectrometer with the BBO Probe in the NMR Facility at Oregon State University. The data was processed using Bruker TopSpin 4.0.8, which applied a Fourier transform on the raw data. The resulting frequency spectrum was leveled and smoothed using the phase and baseline adjustment tools and the peaks of interest were integrated.

Using the simulation information, the four signals in the NMR spectra as high-

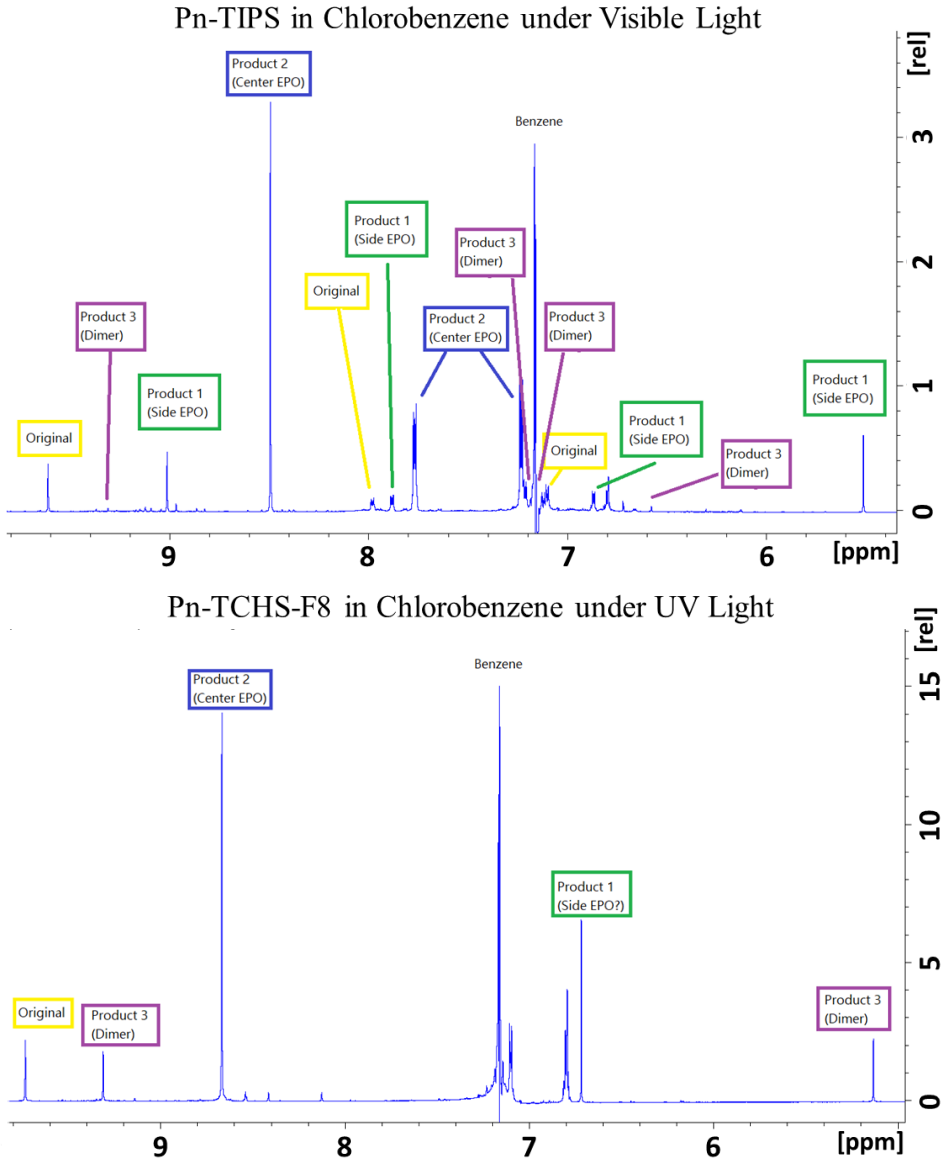

Figure 3.6: NMR H^1 Spectrum of Pentacene Products. The full NMR spectrum of Pn-TIPS (a) and Pn-TCHS-F8 (b) in deuterated benzene after bleaching in chlorobenzene under visible light and UV light (respectively), with the signal for each group labeled.

lighted in Figure 3.6 were classified. The peaks were grouped based on integrated area and then used the integrated values to find relative concentrations. Figure 3.7 (b) shows the ratio of the decay species that are identified by the signals downfield. There are three signals identified besides the original spectral signal as notated in Figure 3.6. Based on the relative concentration, the primary product type is EPO. Both side EPO and center EPO were present, as well as a small population of dimer.

With the products identified and the relative concentrations determined, conclusions about the degradation products can be drawn based on the comparisons between the different samples. To check that our ratios are accurate, the percentage of the original product that is still in the solution found in NMR was compared to the percentage of original product as obtained using absorption data. These values can be seen in the table below. Although the values are not exactly the same, they are close enough to give us confidence that the trends we find are accurate.

The first conclusion that can be drawn is that the most prominent signal comes from three peaks which are shifted up-field from the original signal. The single peak signal and the two double peak signals have the same area, so it can be concluded that they all originate from the same product. Because there are only three peaks with this area, this is the signal for center EPO. When comparing the integrated value of this signal with the integrated values of the other signals, it is clear that this product is the most prominent for all the sample types.

The other two signals that appear all have six corresponding peaks. Based on the location of the peaks, we can conclude that the signal with peaks at 5.15 ppm

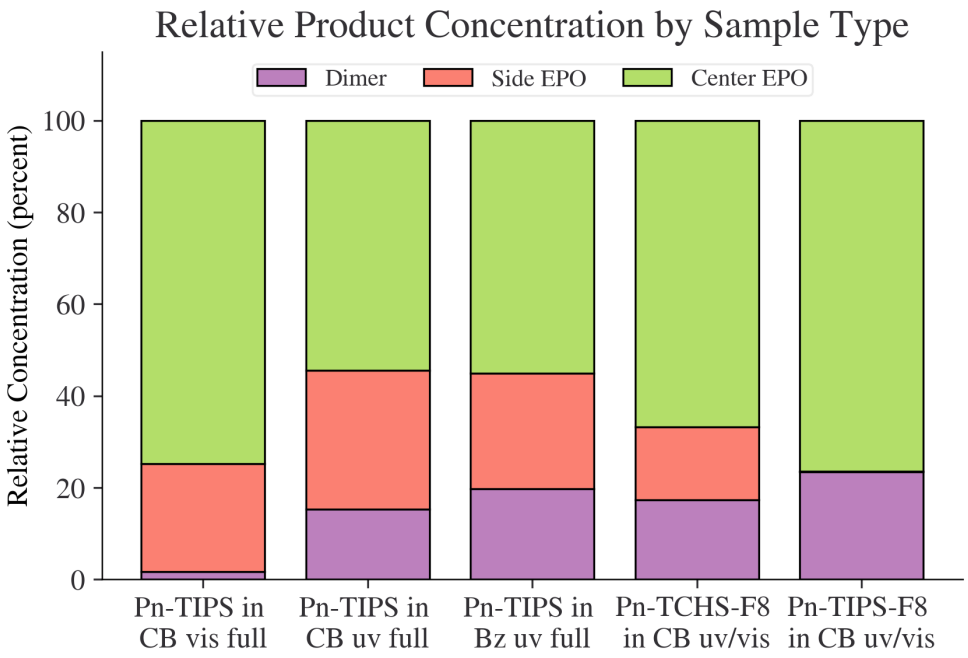

Figure 3.7: Histograms of NMR Product and Decay Ratios. Three downfield signals appear, aside from the original signal, which correspond to both types of EPO formation and dimerization. For all the samples, EPO is the biggest product. It is also of note that dimerization is virtually not present for the sample that was only exposed to visible light.

Sample Type	Decay Ratio	NMR Ratio
Pn-TIPS in CB vis full	0.030	0.044
Pn-TIPS in CB uv full	0.024	0.033
Pn-TIPS in CB uv full+rec	0.111	0.071
Pn-TIPS in Bz uv full+rec	0.078	0.056
Pn-TIPS in Bz uv full	0.067	0.080
Pn-TIPS in Bz uv half	0.361	0.701
Pn-TIPS in Bz uv half+rec	0.361	0.710
Pn-TCHS-F8 in CB uv/vis	0.079	0.061
Pn-TIPS-F8 in CB uv/vis	0.044	0.064

Table 3.1: Table of Absorption Decay Ratios to NMR Decay Ratios for functionalized pentacene. The samples are labeled with the molecule type, solvent used during bleaching (bz for benzene and cb for chlorobenzene), if they were fully bleached (to less than 10% of original absorption) or only half bleached (to about 50% of original absorption), and if recovery was attempted using thermolysis (indecated by a +rec). The last two samples were bleached in a combination of UV and Vis and are labeled uv/vis due to very slow decay under vis.

and 9 ppm in the Pn-TIPS sample is side EPO and the other signal indicated in Figure 3.6 is dimer. Converting the integrals into ratios, we can see the ratio of products depending on product types as seen in Figure 3.7.

A few conclusions can be made from these ratios. The first is that EPO formation is the most prominent product. The second is that dimers are more likely to form when exposed to UV in comparison to only visible light. Finally, fluorinated derivatives are less likely to form side EPO.

3.5 Conclusions

Due to its ability to non-invasively probe the molecular structure of materials, NMR spectrocopy was a useful tool in identifying the products of photodegradation of functionalized Pn. Using the simulation tools, predictions for peak locations were predicted, and the predictions were used to identify the products in the samples. Though there was some variation in the samples, EPO formation was the primary product found, with center EPO being the more prominent of the two. This is in agreement with the data in Chapter 2, which indicated that EPO formation was the primary decay pathway.

NMR data also shows that dimers formation is not a prominent decay pathway, especially under visible illumination. This supports the experimental data which shows slow photodegradation of functionalized Pn in vacuum, but only under UV illumination. Therefore the most significant decay pathway for functionalized Pn is photo-oxidation.

Chapter 4: Examining Photostability of Isolated Molecules Using Single Molecule Fluorescence Spectroscopy

4.1 Introduction

The previous chapters have indicated that the photostability of functionalized Pn is affected by environmental factors and that when photodegradation occurs, it can produce a variety of products (see Chapter 3). The optical absorption experiments were conducted using functionalized Pn in solution, where their freedom of movement allowed for both endoperoxide formation (EPO) as well as dimerization. Likewise, the fluorescent spectroscopy experiments were conducted using $1-5$ nm average spacing between Pn molecules dispersed in polymer matrix films, and it was found that even in most dilute films some molecules were close enough to form both EPO and dimers. While it would be expected in more concentrated (e.g. $1-2$ nm average spacing) films, the evidence of dimer formation observed even in dilute films (5 nm average spacing, Fig 2.10) suggests non-uniform guest molecule distribution. Such non-uniform distribution can also lead to changes in photophysics due to differences in intermolecular interactions in various domains. In order to understand the differences between these two types of photodegradation as well as rule out effects of intermolecular interactions, it is useful to experimentally isolate one of these processes and prevent the other. This is done by using

single molecule fluorescence spectroscopy (SMFS), which uses samples with such low concentration that photoluminescence from individual molecules can be optically resolved and therefore the molecules are too far apart to form dimers or participate in any short-range interactions which would modify the photophysics (e.g. via singlet fission).

SMFS is an experimental technique which is used to probe the nanoenvironment of individual molecules and determine the influence of local atoms, functional groups, polarity, viscosity, and electrostatic charges [23, 35, 39, 48, 82]. Because it can probe multiple individual molecules simultaneously, it is possible to measure orientation of a molecular transition dipole, probe intermediate states, and study dynamics, energy transfer, and charge transfer processes in molecules at the nanoscale[39].

Materials that can be used in SMFS must have high optical absorption cross section and high quantum yield[31] so that the optical signal is high compared to the background noise. The molecules must be optically stable, such that the molecule emits a sufficiently large number of photons before it photobleaches. The materials must also be able to form low concentration ($\sim 10^{-10}$ M) samples, so that the intermolecular spacing is much greater than the diffraction limit. Functionalized Pn satisfies these requirements because it has a high quantum yield of $\Phi \sim 0.7 - 0.8$ and a low photobleaching quantum yield of Φ_B of $\sim 10^{-6}$, since the quantum yield is measured from zero to one and measures the ratio of emitted photons to absorbed photons, which should be high for high fluorescent molecules. The photobleaching quantum yield measures the probability that a molecule will

photobleach when it absorbs a photon and therefore should be low for optically stable materials. Because of these characteristics, SMFS is a good choice as an experiment to probe photophysical and photochemical processes in isolated molecules of functionalized Pn.

Since the purpose of this work is to understand the environmental factors that play a roll in the photostability of functionalized Pn and associated decay, single molecule experiments focused on testing the effects of host materials, the effects of functionalized side groups, and the effects of adding acceptor molecules. Due to the experimental design, testing temperature dependence is not possible to investigate with SMFS.

4.2 Experimental Design

4.2.1 Sample Preparation

Pn-TIPS-F8 and Pn-TCHS-F8 molecules were used for single molecule fluorescence spectroscopy (SMFS) as well as the previously discussed polymers, PMMA and PVDF. In addition to these materials, three other polymers were used: polystyrene (PS, Mw 280,000 g/mol), poly(9-vinyl)carbazole (PVK, Mw 1,100,000 g/mol) and functionalized benzothiophene (6,12-bis[2-(t-butyl)ethynyl]- Benzo[1,2-b:4,5-b]bis(1)benzothiophene, t-bu BTBTB). Since the end goal of these molecular characterization experiments is to use these materials in electronic devices, the host materials were chosen with properties that would be beneficial to this goal. PS is a

useful host polymer for development of thin film blends, where two or more molecular types, usually a donor molecule and an acceptor molecule, are mixed together to increase electron transfer efficiency. Because PS is an amorphous polymer, it improves the film morphology of blended films and is often used for this purpose [44]. Although similar in being amorphous polymers, PS and PVK differ in their conductivity. PVK is a photoconductive polymer making it extremely useful in photonic devices[50]. T-bu BTBTB is unique because it is a small-molecule crystalline organic semiconductor with a molecular structure relatively close to that of Pn guest molecules.

Previous SMFS studies have shown that the photostability of organic materials hosted in polymers is dependent on the oxygen permeability and diffusion coefficient, with low diffusion and low permeability correlating to higher photostability [55]. Thermo Fisher Scientific has compiled a list of physical properties, including oxygen permeability, for some of their materials, including PMMA, PS and PVDF. The oxygen permeability is determined by calculating the product of the amount of gas (in cm^3) and the thickness of membrane or film (in mm) divided by the product of the area of membrane or film (in m^2), the time length of exposure (24 hrs), and the differential pressure of gas (Bar). The values of oxygen permeability are 4.8 cm^3-mm/m^2-24 hr.-Bar, $116 - 155$ cm^3-mm/m^2-24 hr.-Bar, and 5.4 cm^3-mm/m^2-24 hr.-Bar for PMMA, PS, and PVDF, respectively[68]. Based on these values, it is expected that functionalized Pn will more photostable in PMMA and PVDF than in PS.

The collected data from varying host polymers was also compared to data

taken in PMMA with the addition of acceptor molecules. Most successful organic photovoltaic devices rely on efficient charge separation at donor-acceptor bulk heterojunctions (BHJ). Nanoscale morphology of BHJs plays a critical role in promoting charge photogeneration, and yet its characterization is not possible with the required resolution using conventional techniques. Thus, our SMFS study probes the donor-acceptor interactions on the nanoscale.

Phenyl-C61-butyric acid methyl ester(PCBM) and indenofluorene functionalized with TIPS (IF-TIPS) were used as acceptor molecules. These are good choices for acceptor molecules for functionalized fluorinated Pn because the HOMO (highest occupied molecular orbital) and LUMO (lowest unoccupied molecular orbital) energy levels of PCBM and IF-TIPS are slightly lower than the HOMO and LUMO levels for functionalized fluorinated Pn, so it is energetically favorable for either energy transfer or electron transfer to the acceptor molecules. PCBM and IF-TIPS are also non-fluorescent in the optical region being probed, and therefore will not contribute to the fluorescence collected during SMFS experiments. Diagrams of the molecules can be seen in Figure 4.1.

For high confidence in the collected experimental data, a variety of controls were used in SMFS sample preparation. This process was developed to ensure that only the molecule of interest is fluorescing during the imaging process. Glass coverslips were soaked overnight in a solution of detergent and water and then sonicated for 40 minutes in the detergent/water solution to ensure their cleanliness. Each glass coverslip was rinsed thoroughly with deionized water, and dried under N_2. A subset of the glass coverslips were tested in the imaging set-up to confirm their

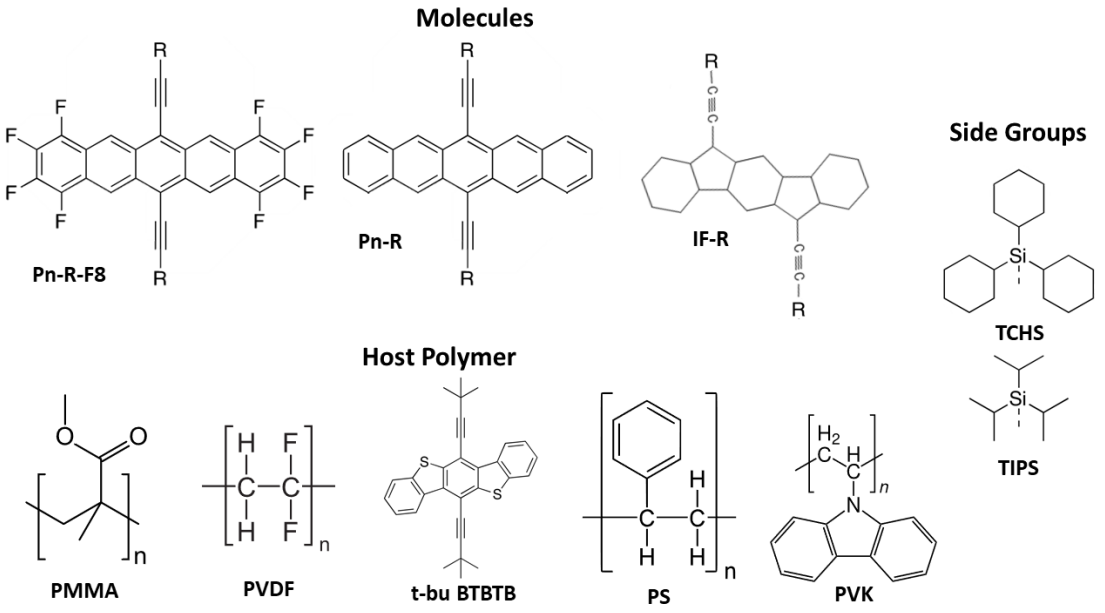

Figure 4.1: Molecular structures of the materials used in single molecule fluorescence spectroscopy experiments. The fluorinated Pn (Pn-R-F8) and non-fluorinated Pn (Pn-R) have can have either TIPS or TCHS side groups. The molecules were hosted in one of the polymer matrices, PMMA, PVDF, PS, PVK or t-bu BTBTB [58, 85, 22, 42].

cleanliness and that they were non-fluorescent under constant excitation. The solvents used for both the host polymer and the molecules were also tested on clean glass coverslips under the experimental imaging conditions to confirm their cleanliness as well before use in the experiment. The same cleanliness checking was done at every step of the sample preparation (coverslip, toluene, pristine PMMA host, and acceptor-only samples) to ensure cleanliness.

To prepare the experimental samples, the host polymers, PMMA, PS, or PVK were dissolved at a 1% wt into toluene. Stock solutions were also prepared with the functionalized florinated Pn (Pn-R-F8) dissolved in toluene at concentrations

of $10^{-9} - 10^{-11}$ M. Tetrahydrofuran (THF) was used as the solvent for both t-bu BTBTB and Pn in the samples where t-bu BTBTB was used as the host material since it made better films. The final solutions of Pn with host material were created by mixing the solution of host polymer with the solution of functionalized Pn at a ratio such that the Pn concentration was 10^{-12} M.

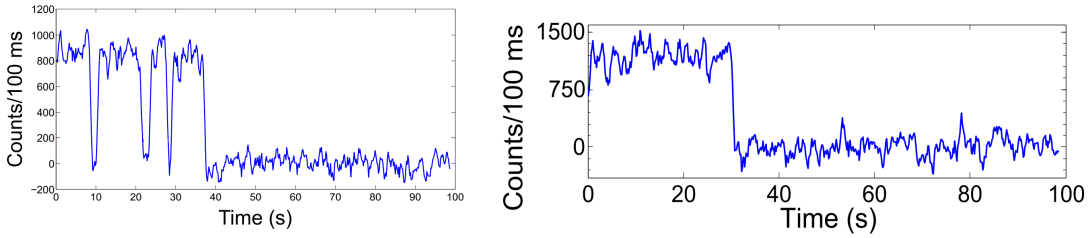

(a) (b)

Figure 4.2: An example of a blinking trace (a) and non-blinking trace (b).

When using acceptor molecules, both donor and acceptor molecules served as guest molecules in a PMMA host. A fluorophore (Pn-TCHS-F8) concentration of 3.4×10^{-10} M served as our baseline concentration ($1\times$). Based on the molar fraction of the acceptor and PMMA, the acceptor (TIPS-IF or PCBM) solution was added to achieve varied average acceptor-acceptor spacings[18]. Data was collected from donor-only samples at $1\times$ and $2\times$ donor concentrations, samples where the donor concentration was held at $1\times$ and the average acceptor-acceptor spacing varied from $6 - 20$ nm, and donor-acceptor samples where the average acceptor-acceptor separation was 5 nm and varying concentrations of the donor molecules ($6 \times -100\times$).

After sonication to ensure homogeneity, the guest-host solution was spin-cast

onto slides at 3000 rpm, or 2000 rpm for t-bu BTBTB, for 50 seconds. This spin rate and solution concentration resulted in molecular spacing of $\sim 5\mu m$ on the films, which is much larger than the $\sim$ 200 nm diffraction limit[73], with a film thickness of 19 ± 2 nm as confirmed by AFM [18].

Unlike the other polymers, PVDF is a semi-crystaline polymer that has tunable properties and low oxygen permeability, which is what makes it a promising host for functionalized Pn[33, 68]. As seen in Figure 4.1, PVDF is a polymer chain that has alternating pairs of hydrogen atoms and fluorine atoms attached to a chain of carbons. Because flourine is so electronegative, this polymer chain is highly polar. With the high stability and polarity of PVDF, there are only a few solvents it will dissolve in, including dimethyl formamide (DMF) and dimethyl sulfoxide (DMSO). After attempting to dissolve PVDF in DMSO, unsuccessfully, I finally succeeded in creating a solution of PVDF in DMF by heating the solution.

In contrast to PVDF, Pn-TIPS-F8 and Pn-TCHS-F8 are both non-polar compounds due to their high symmetry. The solutions they dissolve in are either non-polar or only slightly polar, such as toluene, benzene, chlorobenzene. In an attempt to make Pn-R-F8:PVDF films in the same way the other films were created, using the process described above, I made multiple attempts to dissolve functionalized Pn in DMF, without destroying the Pn-R-F8 molecules. Therefore sample preparation for these samples were slightly different than the other SMFS samples. PVDF was dissolved into DMF at a 1% wt. Due to the nature of PVDF and DMF, the optical noise during the cleanliness checks, and the inability to mix the solvents, higher concentrations of Pn-R-F8 solutions were needed. Pn-R-F8

was dissolved in toluene at 10^{-7} M and then the samples were made through a layering process. For both the bottom and top layer, 100 μM of DMF solution was spincast onto the coverslip using a spin sequence of 300 rpm for 10 seconds, then 600 rpm for 3 seconds, and finally 1600 rpm for 1 minute. In between a layer of Pn-R-F8 was formed by spincasting the solution at 600 rpm for 50 seconds. As a control, a sample was made following this same procedure, but with PMMA in DMF. The experiments performed on these (10^{-7} M) samples will be referred to as "quasi-SFMS" as compared to SFMS performed on $\leq 10^{-9}$ M samples. Note that the samples for quasi-SFMS are considerably more dilute than the least concentrated guest-host films used in our semi-bulk studies of Ch. 2, which had 5 nm average Pn spacing (about 10^{-2} M), whereas the single molecule spacing ranged from 0.5 μm, for 10^{-7} M concentrations, to 5 μm for 10^{-10} M concentrations.

4.2.2 Imaging Experimental Design

The schematic for the basic experimental set-up can be seen in Figure 4.3. Single molecule samples were imaged on an Olympus IX-71 inverted microscope using a 100x UPlanSApo (NA 1.4) oil objective. The sample was illuminated by a 633 nm HeNe laser or a 532 nm Nd:YVO_4 cw source in wide field. A dichroic mirror is used to direct the light to the sample and allows for the fluorescence from the sample to pass through the mirror into the camera. Prior to entering the mirror, the signal passed through an emission filter to remove any residual laser light. The fluorescence images were collected by an Electron Multiplying Charge Coupled

Device (EMCCD) camera, the Andor iXon EMCCD (DU-897). The EMCCD had adjustable gain, to boost the signal, and was set to either x20 or x40, depending on the experiment. Videos of 600 frames (with 100 milliseconds integration time) were taken of each sample and then processed following the procedure outlined below.

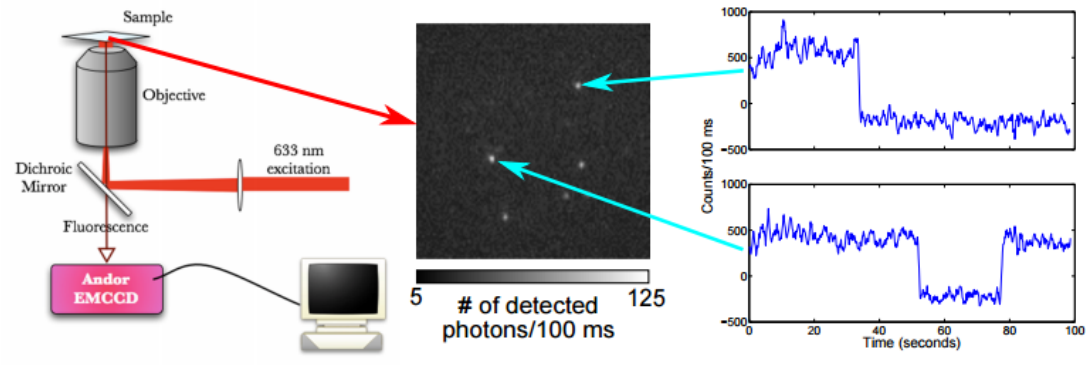

Figure 4.3: The experimental set-up for Single Molecule Spectroscopy. The sample is placed on the objective in the microscope and illuminated by a 633 nm laser. The fluorescence is collected by the Andor EMCCD and then processed by the computer to extract fluorescence time traces.

4.2.3 Data Processing

4.2.3.1 Video Analysis

To extract the fluorescence of each molecule under optical excitation, the videos needed to be processed. A set of custom MATLAB scripts, created and used previously in other SMFS experiments, were used to analyze the single molecule data in

PMMA, PS, PVK and the samples with acceptors. The MATLAB scripts located the fluorophores and created the fluorescence time trace for each fluorophore as detailed in our previous work[19]. Time traces were selected for further analysis if the trace exhibited a two-level behavior with a digital "on"-"off"/"off"-"on" switching, with a threshold of three standard deviations above the average "off" count level. The resulting traces were further sorted into two types, "non-blinkers", which are fluorophores that exhibited only one "on"-"off" event, and "blinkers", which had multiple "on"-"off" events.

Once sorted, the "on" and "off" times were extracted from the traces using another custom MATLAB script, which found the time between each transition and classified that time as either an "on" or an "off" time. The last "off" or "on" time of each trace was discarded due to an uncertainty in their actual duration. The "on" times and "off" times for "blinkers", as well as "on" times for "non-blinkers" were compiled in three separate lists.

4.2.3.2 Fitting Times to Distributions

To quantify the effects of the changes in environment, we want to analyze the distributions of these "on" and "off" times. This can be done through probability distributions, however, the probability density functions for this data is difficult to fit because the data broadens toward the end. Using complementary cumulative distribution function (CCDF) instead contained the same information as the density function, but the data is cleaner and easier to fit. The complementary

cumulative distribution function is the relationship between a given value, in this case time, and the ratio of values that are greater than the given value. This is found by finding the cumulative distribution function (CDF) first.

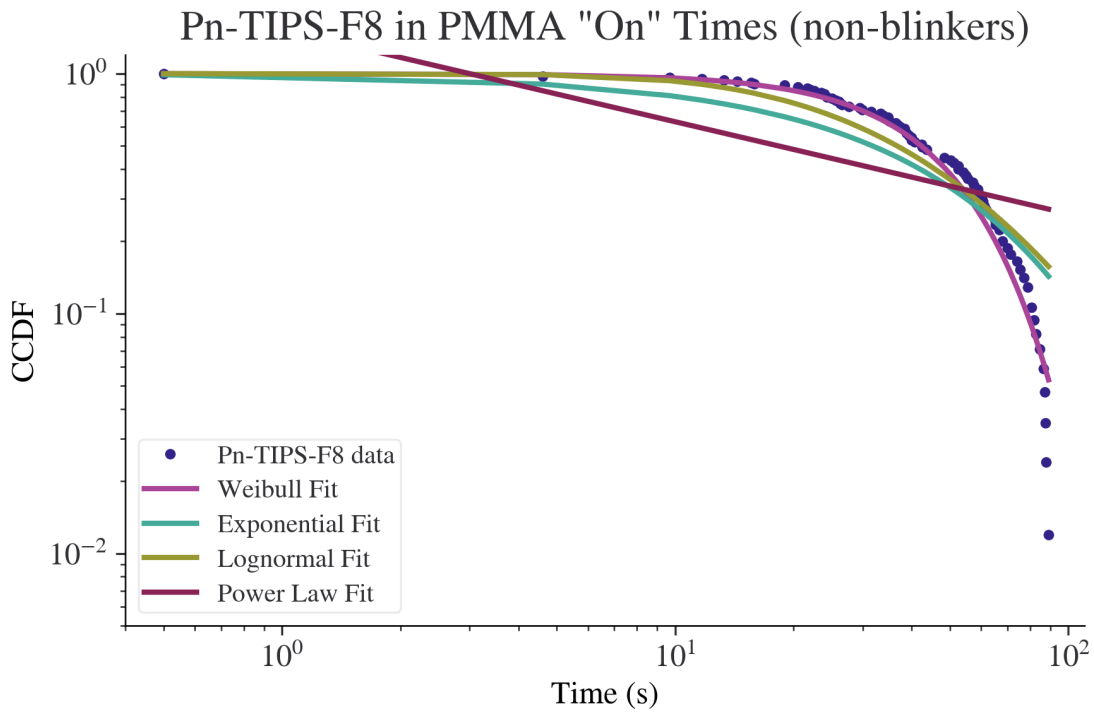

Figure 4.4: Example of CCDF and the corresponding fits. This is the "non-blinker" "on" times for Pn-TIPS-F8 in PMMA.

The CDF $S(t)$ was calculated directly from collected "on"or "off" times t_i using

$$S(t) = \frac{1}{N}\sum_i t_i \leq t \tag{4.1}$$

where N is the total number of "on"("off") events and t is a unique time in the set of collected "on"("off") times. The complementary CDF (CCDF) is $F(t) = 1 - S(t)$

and was the form used to fit the data. The CCDFs were fit using maximum likelihood estimation (MLE) and Klomogrorov-Smirnov (KS) test to various distribution functions (Figure 4.4)[65]. The KS test provides a p-value between zero and one, which indicates how closely the data matches the distribution, with closer matches having p-values closer to one.

The four CCDF distributions that were used were power-law, exponential, Weibull, and lognormal. These are distributions that are commonly used for single molecule data[19]. The CDF distributions $S(t)$ are

$$S_{PL}(t) = 1 - \left(\frac{t}{t_{min}}\right)^{-\alpha} \tag{4.2}$$

$$S_{EXP}(t) = 1 - e^{\lambda t} \tag{4.3}$$

$$S_{WB}(t) = 1 - \exp(-t/\beta)^{A} \tag{4.4}$$

$$S_{LN}(t) = \frac{1}{2}\text{erfc}\left(-\frac{\ln(t) - \mu}{\sigma\sqrt{2}}\right) \tag{4.5}$$

respectively, and the CCDF $F(t)$ is calculated by $F(t) = 1 - S(t)$. Note erfc is the complementary error function. These four distributions were chosen because they are common distributions used in other studies to quantify experimental changes. For example, exponential distributions describe populations or systems that have a single rate of increase or decrease. Power law distribution is also commonly used to describe many physical systems that have distribution of rates.

Lognormal distributions are used to describe a very diverse number of systems, particle distribution, time independent rates, and random independent variables[75, 65]. Specifically for SMFS, it has been used to describe the "off" time distribu-

tion of back charge transfer and the "on" time distribution due to proton transfer [38, 65, 80].

Weibull distributions are also used to describe a wide variety of situations, including mechanical strength of materials and chemical reactions of distributed activation energies[7, 5]. For example, the time-dependent Weibull rate $k(t)$ can be related to the activation energies by $k = k_0 \exp[-E_a/RT]$ where k_0 is a pre-exponential factor, E_a is the activation energy, R is the universal gas constant, and T is the temperature. This is also related to the Weibull parameters by $k(t) = (A/\lambda)(t/\lambda)^{A-1}$, which means the activation energy can be written as

$$E_a = -RT\left[\ln(A/(k_0\lambda)) + (A-1)\ln(t/\lambda)\right]. \tag{4.6}$$

Using this relationship, the distribution of energies for a given transition can be found using

$$D(E_a) = \mathrm{PDF}(t)|dt/dE_a|. \tag{4.7}$$

Combing equation 4.6 and the probability distribution function, $\mathrm{PDF}(t)$, which is

$$\mathrm{PDF}(t) = (A/\lambda)(t/\lambda)^{A-1}\exp[(-t/\lambda)^A]. \tag{4.8}$$

gives the equation of activation energy distribution of

$$D(E_a) = \frac{1}{RT}\frac{A}{A-1}\left(\frac{t}{\lambda}\right)^A e^{(t/\lambda)^A}. \tag{4.9}$$

Thus, Weibull distribution fit parameters can be used to describe the shift in activation energies.

As seen in equations 4.3 and 4.4, a Weibull distribution is a modified version of a single exponential, where the rate of change is time dependent except in the special case where $A = 1$. This has been used to describe the distribution of "on" times of perylenediimide single molecules in PMMA, when SMFS was used to measure the probability of radical ion pair intersystem crossing[65].

Using the fit parameters, the average "on" and "off" times ($\langle\tau\rangle_{on/off}$) were calculated using the following formulas

$$\text{Exponential} \qquad \langle\tau\rangle_{on/off} = \frac{1}{\lambda} \tag{4.10}$$

$$\text{Weibull} \qquad \langle\tau\rangle_{on/off} = \beta\Gamma(1 + 1/A) \tag{4.11}$$

$$\text{Lognormal} \qquad \langle\tau\rangle_{on/off} = \exp(\mu + \frac{\sigma^2}{2}) \tag{4.12}$$

Where Γ is the Gamma function and λ, β, A, μ, and σ are the corresponding fit parameters.

4.2.3.3 Quasi-SMFS processing

Due to the unique way that PVDF samples were created, the quasi-SMFS data was slightly different than SMFS data collected from the previous samples. The bright diffraction-limited spots in the video were not necessarily due to the emission of a single fluorophore, but rather a mix of typical single molecule fluorophores, multi-

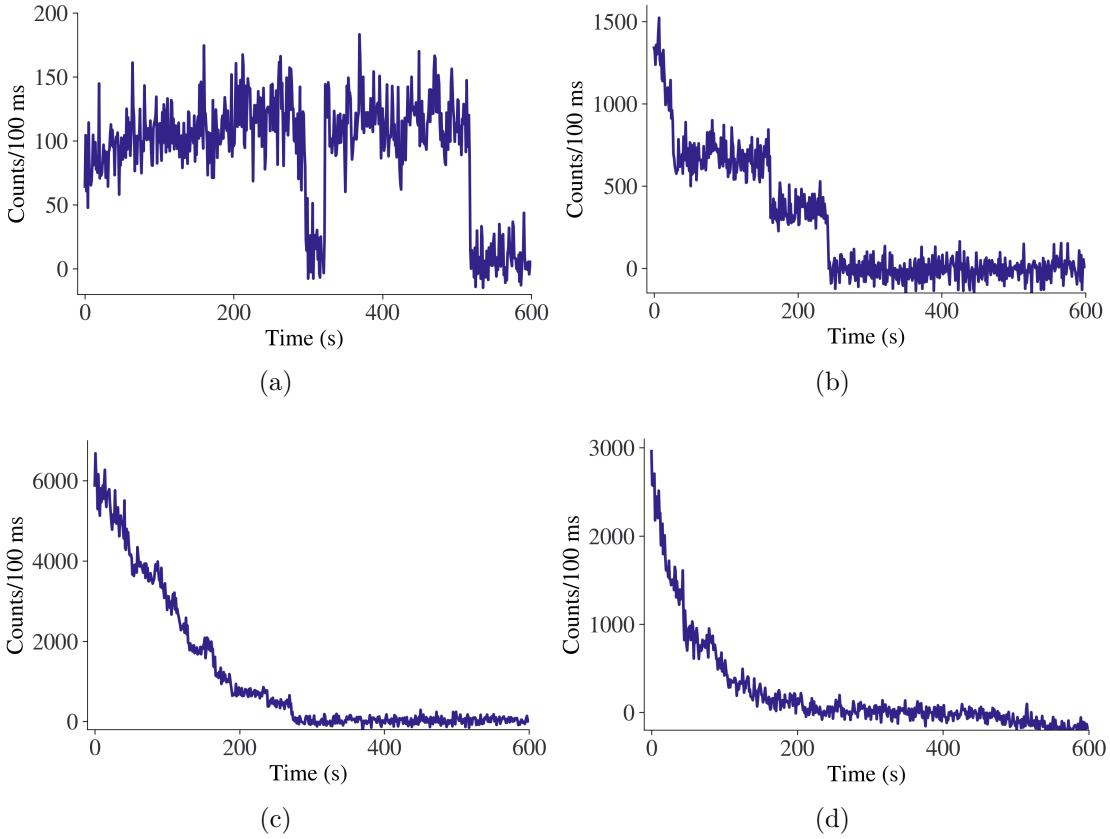

Figure 4.5: Example of Single Molecule Data and Quasi-Single Molecule Data. (a) The two level time traces that are looked for in single molecule data. In traditional single molecule experiments, only these types of traces are analyzed. For the layered single molecule samples, three other time traces are also analyzed. They are multi-level discrete step traces (b), decay traces (d), and hybrid decay and multi-step traces (c).

step fluorophores which had discreet transitions but multiple fluorescent levels, traces that looked like exponential decay curves, and traces that were a mix between decay curves and multi-step fluorophores (see Figure 4.5). Because the ratio between these types of "fluorophores" varied from spot to spot in the sample, all

of the traces had to be analyzed and quantified. This was done with a custom python script that I developed for this data (for more details see appendix B). The script processed the data in a similar way to the Matlab script, as it took the videos and located the fluorescent spots. It then found the time trajectory of each spot by integrating counts of the grouped pixels for each spot and subtracting the background.

Like the Matlab scripts, the traces were reviewed and either sorted into the groups defined above or discarded if they contained noise that could not be analyzed. The analysis of the remaining traces consisted of fitting exponential decays to the decay traces and finding the transition times and discrete fluorescence levels for the traces that had steps. The decay traces were scaled to one and then fit to e^{-kt}, where k is the rate of decay. A modified version of change point detection was used to find the "on" and "off" times for the traces with discrete steps. The transition times were sorted into "on" and "off" time lists, converted to CCDFs and then fit to distribution functions.

4.3 Results and Discussion

In order to understand the environmental dependance of the molecular photophysics, it is necessary to understand the causes of the blinking that is seen from our molecules on the order of a few seconds to tens of seconds. Since the integration time of the EMCCD is 100 ms, the blinking that would be seen due to intersystem crossing, which is on the order of microseconds, is not observed. Thus,

the longer blinking that is observed must be due to other factors such as charge transfer reactions, where the molecule is dark when in a charge-separated state, or during photo-oxidation reactions, the reaction of the molecule with oxygen creates a dark state, as seen in the literature [38, 8, 87]. In the case of our materials, photo-oxidation is a prominent reaction and therefore the cause of blinking in functionalized Pn SMFS experiments.

As mentioned in the sample preparation section, both Weibull and lognormal distributions indicate that there is a distribution to the activation energies of the processes that result in the molecule turning "on" or "off". Since the measured "on" and "off" times are on the order of tens of seconds, the processes that result in transitions between "on" and "off" times are not internal to the molecule. Therefore, the processes can be visualized using Figure 4.6. In this model, the detected emission occurs when there is a transition from the excited state (2) to the ground state (1). The transition to the state 3 corresponds to the molecule turning "off", which designates state 3 is a "dark" state. The transition rates between these states (labeled $k_{\text{"original state" "new state"}}$ in the figure) depends on the molecule and the nature of the "dark" state. Since the average "on" times for "blinkers" and "non-blinkers" were similar, the pathway for turning "off" is also similar, which agrees with other reports of organic molecules in polymer matrices[87, 28].

Once in the "dark" state, a "blinker" can return back to the ground state at a rate k_{31} which determines the "off" time. If the molecule does not return to the ground state within 10 minutes, it is considered "photobleached", meaning that the probability of the molecule spontaneously returning to the original ground state to

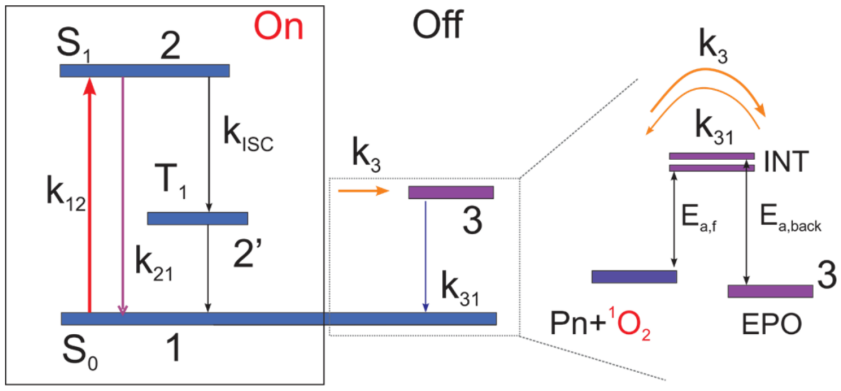

Figure 4.6: Model of the states of molecules with intermittent fluorescence on the order of 10 seconds.

resume it's absorption and emission cycle is low. This could correspond to charge transfer or product formation, or other processes which would significantly change the molecule such that it has new optical properties. In this case, the process is product formation, specifically EPO formation.

The photostability can also be quantified by measuring the number of photons emitted over a molecule's lifetime, which is named N_{tot}. The total number of photons detected for a single molecule is calculated by integrating the time trace without the background over the lifetime. This is augmented to find the N_{tot} for multi-step spots by integrating for only a specific photon level. The change in the histogram of N_{tot} provides insight into the photostability of the molecules.

The rate at which the molecules blink and photobleach changes with changes in the environment and with the molecular structure as explained in the following sections.

4.3.1 SMFS Host and Side Group Dependence

In the single molecule experiments, fluorinated Pn derivatives with two side groups in various hosts were measured. Both Pn-TIPS-F8 and Pn-TCHS-F8 were measured in PVK and PMMA, but only Pn-TCHS-F8 was measured in PS and t-bu BTBTB. The data taken from the samples of Pn-TCHS-F8 and Pn-TIPS-F8 in the various hosts shows the effects of side groups on photostability. In Figure 4.7 (b) the CCDFs of Pn-TIPS-F8 and Pn-TCHS-F8 in PVK and PMMA are plotted. The difference in side group is very noticeable in PVK. Pn-TIPS-F8 has much shorter "on" times than Pn-TCHS-F8 in PVK. This is more clearly seen in the average "on" times calculated from the fit parameters, since the average "on" time for Pn-TIPS-F8 is 31.7 seconds and the average "on" time for Pn-TCHS-F8 is 35.5 seconds. Although not a huge difference, it is large enough to be outside the error of these calculations. This difference from the side groups agrees with the data from high concentration experiments, as the larger Pn-TCHS-F8 side groups are more protective of the backbone of the molecule.

Figure 4.7 (a) also shows the effects that the host polymer makes on the average "on" times and "off" times of Pn-TCHS-F8. PS is the least stable of the four polymers, followed by PVK, t-bu BTBTB and finally PMMA. This agrees with the average "on" ("off") times that were calculated with the distribution fit parameters (see table 4.2). Since $80-90\%$ of the molecules don't blink, most of the analysis will focus on the "on" times of the non-blinking molecules, however when discussed, the "on" and "off" times of blinking molecules only represent a small

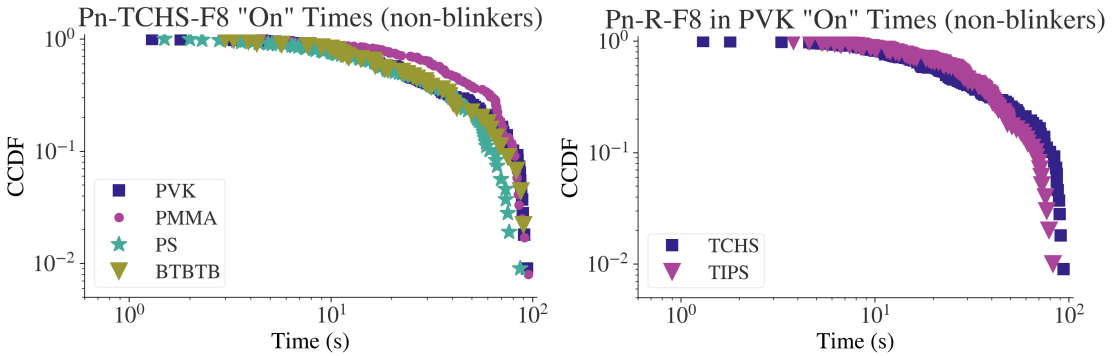

Figure 4.7: Polymer and Side Group Effects. The complimentary cumulative distribution (CCDF) of Single Molecule Fluorescence Spectroscopy (SMFS) of "non-blinking" "on" times for (a) Pn-TCHS-F8 in four different polymers: Polystyrene (PS), Poly(9-vinylcarbazole) (PVK), Poly(methyl methacrylate)(PMMA), and functionalized benzothiophene (t-bu BTBTB). Molecules in PS has smaller "on" times, followed by t-bu BTBTB, PVK and then PMMA. Although different, the distributions are quite close. Plot (b) shows the CCDF of "non-blinking" "on" times of Pn-TCHS-F8 and Pn-TIPS-F8 in PVK. The distributions are very similar, however, the slight difference is enough to see it expressed in the fit paremeters. As expected the "on" times are shorter for Pn-TIPS-F8 in PVK.

population of the data. When looking at the calculated average "on" times for "non-blinker", PMMA has the longest with an average time of $\sim$ 43.8 seconds followed by PVK (35.3 seconds), t-bu BTBTB (35.3 seconds), and PS (28.7 seconds). The "blinking" "on" times also agree with this order, except that t-bu BTBTB has the shortest of the average "on" times at only 13.8 seconds. The short average "on" time and the more even distribution of data points across all three classifications indicates that t-bu BTBTB encourages more blinking in Pn-TCHS-F8 than the other host polymers.

To gain insight into the physics for each data set, the data sets were fit to

the four distributions and table 4.1 shows the p-values for those fits. Most of the data has p-values that are quite low, which does not indicate a strong correlation. However, the highest p-value for the majority of the samples was for the Weibull distribution. Two of them had higher p-values for exponential: "blinker" "on" times for Pn-TCHS-F8 in PVK and "non-blinker" "on" times for Pn-TCHS-F8:PS. For these two cases, the p-value is quite low, and not that much larger than the p-value for the Weibull fit. It is also worthwhile to note that for the Weibull fits, the A value is around 1.2, which is close to 1, which is the special case when a Weibull distribution becomes an exponential distribution. The combination of these parameters is an indication that the data is not described completely by a single decay rate.

Besides the exponential fits, three of the data sets had higher p-values for log-normal distributions: "blinker" "on" times for Pn-TIPS-F8:PVK, "non-blinker" "on" times for Pn-TCHS-F8:PVK and "blinker" "on" times for Pn-TCHS-F8 in t-bu BTBTB. There is not a strong pattern to the data sets which fit the non-Weibull distributions. Fortunately, both Weibull and Lognormal distributions are used to describe a distribution of activation energies for chemical processes. From these fit values we can calculate the average "on" or "off" time for each trace type using equations 4.10, 4.11, and 4.12, as seen in table 4.2. It is of note that the calculated "on" or "off" times are roughly the same value regardless of which distribution's fit parameters are used as seen in table 4.2 for the "Blinker" "off" times of Pn-TCHS-F8 in PMMA. This can be seen for the "Blinker" "on" times of Pn-TCHS-F8 in PMMA, where the p-values are all very close, so the fit values

and average "on" times are included in the chart. The calculated values are within one second of each other. Thus, regardless of the best fit, all of the distributions agree on the average "on" or "off" times for each distribution.

Using the average "on" and "off" times, we can draw conclusions about the effects of the polymer on the stability. The average "on" times for "non-blinkers" are then 42 seconds for PMMA, 32 seconds for PVK, 30 seconds for t-bu BTBTB and 29 seconds for PS. This is in agreement with the relationship between oxygen permeability and diffusion coefficients in these matrices and the average "on" times for molecules in these polymers which were discussed in Chapter 2 [55].

Additionally, the percentage of molecules that exhibit blinking increased from 13% in PMMA to 20% in PS. This suggests that on average even though the reaction of the Pn-TCHS-F8 molecule with singlet oxygen is more probable in PS (as manifested through shorter average "on" times) as compared to PMMA, the EPO conversion back to the parent Pn-TCHS-F8 molecule (shorter "off" times) is also more probable in PS, possibly due to enhanced oxygen diffusion in PS that could promote singlet oxygen quenching.

This is in agreement with the ratio of "blinking" and "non-blinking" fluorophores that are found in the data set. In all of the polymers except t-bu BTBTB, the data heavily favors "non-blinker" molecules. For example, 88.5% of fluorophores in the Pn-TIPS-F8:PVK samples were "non-blinkers" and 84% of the fluorophores were "non-blinkers" for Pn-TCHS-F8:PVK samples (see statistics in table 4.1. Since the average "on" times for both "blinkers" and "non-blinkers" in all the polymers except for t-bu BTBTB is somewhere between a

quarter ($\sim$ 24 seconds) to almost half ($\sim$ 43 seconds) of the video recording time of 100 seconds, the probability of a molecule turning back "on" during the rest of the video is small. Pn molecules in the t-bu BTBTB host on the other hand had shorter "on" times, with the average "blinker" time being 13.8 seconds and the average "non-blinker" time being 30.3 seconds.

4.3.2 Acceptor Dependence

As expected, adding acceptors decreased the number of fluorophores found in the samples. Pn-TCHS-F8 experiences Förster Resonance Energy Transfer (FRET), when a Pn-TCHS-F8 molecule is within the transfer radius of an acceptor and when the absorption spectra of the acceptor and the emission spectra of Pn-TCHS-F8 overlap, which is true for the acceptors used. When this is the case, the energy from the excited Pn-TCHS-F8 can transfer to the acceptor instead of being emitted as a photon, thus quenching the fluorescence of the molecule. Therefore, in the experiment, these molecules would not show up as they would not be emitting any photons. Because FRET decreases the number of visible Pn-TCHS-F8, the addition of acceptors allows optically resolved samples of higher concentrations of Pn-TCHS-F8 since the acceptors decrease the number of active fluorophores while changing in the sample's molecular landscape. For this to work correctly, the acceptors must have a large enough spacing to not interact with each other, but still be frequent enough that many Pn-TCHS-F8 are within the FRET radius. The closest this spacing can be is $\sim 3 - 3.5$ nm between each acceptor molecule.

Host	Molecule Type		Number of Times	Weibull	Exponential	Log-normal	Power Law
PVK	Pn-TIPS-F8	"Blinker" "on" times	9	0.335	0.234	0.933	0.037
		"Blinker" Off Times	8	0.9	0.182	0.574	0.0475
		"Non-blinker" "on" times	99	0.821	0	0.0185	0
	Pn-TCHS-F8	"Blinker" "on" times	19	0.283	0.441	0.0835	0.003
		"Blinker" Off Times	15	0.728	0.486	0.675	0.068
		"Non-blinker" "on" times	109	0.0545	0.022	0.172	0
PMMA	Pn-TIPS-F8	"Blinker" "on" times	3	0.6145	0.0625	0.245	0.017
		"Blinker" Off Times	4	0.8025	0.19	0.7645	0.0155
		"Non-blinker" "on" times	85	0.387	0	0	0
	Pn-TCHS-F8	"Blinker" "on" times	10	0.5185	0.0865	0.1165	0.004
		"Blinker" Off Times	121	0.6485	0.6295	0.686	0.0115
		"Non-blinker" "on" times	85	0.001	0	0.001	0
PS	Pn-TCHS-F8	"Blinker" "on" times	15	0.814	0.143	0.647	0.0295
		"Blinker" Off Times	25	0.594	0.305	0.352	0.052
		"Non-blinker" "on" times	108	0.154	0.251	0.038	0
BTBTB	Pn-TCHS-F8	"Blinker" "on" times	31	0.088	0.009	0.627	0.013
		"Blinker" Off Times	39	0.872	0.423	0.56	0
		"Non-blinker" "on" times	45	0.679	0.355	0.556	0

Table 4.1: p-values for "non-blinker" "on" times. The values of significance are highlighted in yellow. Notice that most of the data sets fit well to a Weibull distribution and none of them fit to a Power Law distribution.

Host	Molecule Type		Fit Type	Fit Parameters		Average Time
				$\lambda_{Exp}, \beta_{Weib}, \mu_{LN}$	A_{Weib}, σ_{LN}	$\langle\tau\rangle_{on/off}$
PVK	Pn-TIPS-F8	"Blinker" "on" times	Lognormal	2.5	0.73	15.9
		"Blinker" Off Times	Weibull	18.2	1.81	16.2
		"Non-blinker" "on" times	Weibull	35.4	1.61	31.7
	Pn-TCHS-F8	"Blinker" "on" times	Exponential	0.0412		24.3
		"Blinker" Off Times	Weibull	21.8	1.24	20.3
		"Non-blinker" "on" times	Lognormal	3.14	0.92	35.3
PMMA	Pn-TIPS-F8	"Blinker" "on" times	Weibull	31.8	6.42	29.6
		"Blinker" Off Times	Weibull	37.4	2.49	33.2
		"Non-blinker" "on" times	Weibull	51.1	1.94	45.3
	Pn-TCHS-F8	"Blinker" "on" times	Weibull	27.3	1.59	24.5
		"Blinker" Off Times	Weibull	39.8	1.32	36.6
			Exponential	0.0274		36.5
			Lognormal	3.26	0.85	37.4
		"Non-blinker" "on" times	Weibull	47.2	1.67	42.2
			Lognormal	3.49	0.81	45.5
PS	Pn-TCHS-F8	"Blinker" "on" times	Weibull	24.1	1.49	21.8
		"Blinker" Off Times	Weibull	27.3	1.18	25.8
		"Non-blinker" "on" times	Exponential	0.0348		28.7
BTBTB	Pn-TCHS-F8	"Blinker" "on" times	Lognormal	2.36	0.73	13.8
		"Blinker" Off Times	Weibull	35.1	1.27	32.6
		"Non-blinker" "on" times	Weibull	32.5	1.25	30.3

Table 4.2: The fit parameters for the largest p-value distribution for each sample type. The parameters were used to calculate the average "on" or "off" time based on the equations 4.10, 4.11, and 4.12

Another noticeable difference with the addition of acceptors was a consistent increase in blinking. In Pn-TCHS-F8 1× donor-only concentration samples only $\sim 10-14\%$ of molecules are "blinkers". This number increases to over 50% when acceptors are added to the sample at a spacing of less than 8 nm apart from other acceptor molecules. This indicates that the addition of acceptors changes the immediate environment of Pn-TCHS-F8 molecules, which affects their photophysics.

Once the data was collected of Pn-TCHS-F8 and acceptor molecules at a variety of spacings, the fluorescence time trajectories for "nonblinkers" and "blinkers" were analyzed. The long integration time of 100 milliseconds used in data collection processes like microsecond time-scale blinking (e.g., due to the intersystem crossing (ISC)) is not detected. This means that the molecule appears to be "on" even after the ISC from S_1 to T_1 occurred, provided it is then followed by a cyclic process of relaxation, re-excitation, and emission. This means that "blinking" events seen in the fluorescence time traces are related to longer time-scale processes. The "on" and "off" time durations are at least 3 seconds and are $\sim 20-40$ seconds on average, as seen in Figure 4.2. Processes involving long "off" times, which correspond to long-lived dark states, have been previously attributed to either charge transfer reactions or to photo-oxidation reactions[38, 8, 87]. Charge transfer reactions are when a fluorescent molecule temporarily becomes a non-fluorescent ion, which means that the dark state is charge-separated. In contrast, photo-oxidation reactions are when a fluorescent molecule reacts with oxygen, which creates the dark state.

From the observed "on" (for "blinkers" and "nonblinkers") and "off" (for "blink-

ers") time durations, the complementary cumulative distribution functions (CCDFs) were calculated directly from the experimental data. The data were compiled for ensembles of 150-350 fluorophores, depending on the acceptor concentration. Figure 4.8 shows examples of CCDFs of "on" and "off" time intervals, exhibiting shorter average "on" and longer average "off" time durations with the addition of acceptors.

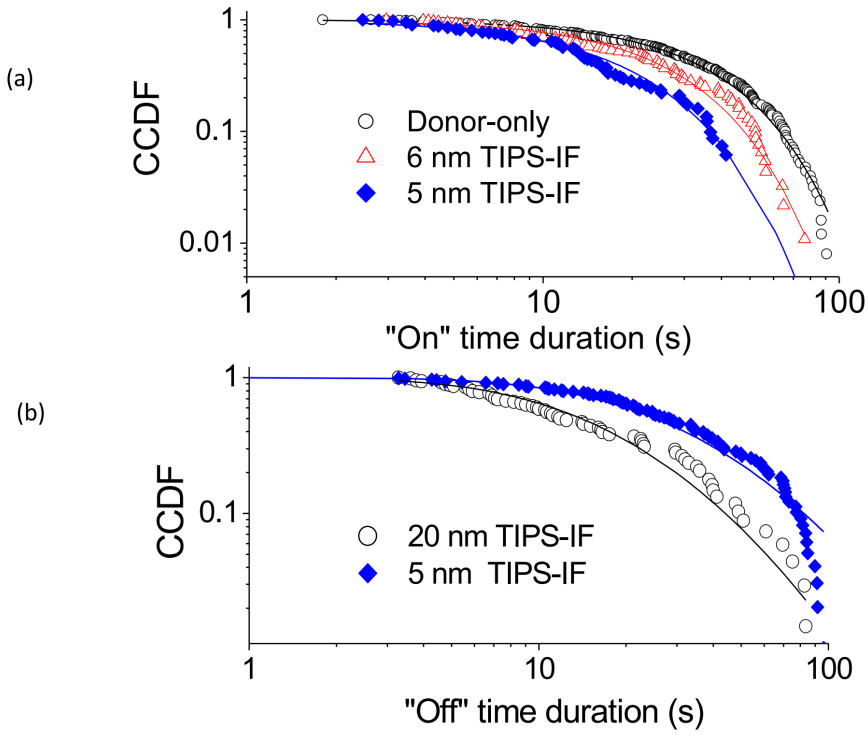

Figure 4.8: Example of CCDFs when acceptors are added, with the average "on" times shifting lower and the average "off" times shifting higher with the addition of acceptors.

Statistical p-tests were used to identify the most probable distribution which describes the CCDF data. In most samples, the CCDFs for the "on" time durations

in "nonblinkers" were best described by the Weibull function. For example, the "on" time CCDFs in a donor-only sample had a p-value of 0.93 and the p-value for a donor-acceptor sample with 5 nm spaced acceptors was 0.48, with the p-values of all other distributions tested yielding $p \leq 0.03$. The Weibull fit parameters were used to find the average "on" times, which showed a decrease from 32 ± 1 seconds in donor-only samples to 14 ± 1 seconds in donor-acceptor samples at average acceptor-acceptor separation of 5 nm. As seen in table 4.3 it is the Weibull scaling parameter β that changes with the addition of acceptor, while the parameter A had slight variation, but remained close to ~ 1.4. The "on" times in "blinkers" were similar to those in "nonblinkers" in most samples but fit parameters A and β were slightly different, with both parameters having a larger range. Just as in "nonblinkers", the average "on" time for "blinkers" decreased upon acceptor addition.

The last fluorophore group, "off" times for "blinkers", had the best fits to Weibull distribution, as indicated by the p-tests, though a few of the samples fit better to lognormal distributions. The average "off" times calculated from fit parameters (as seen in table 4.3) demonstrates an increase in the average "off" time as acceptor is added from 22 seconds in donor-only samples to 38 seconds in donor-acceptor samples with an acceptor spacing of 5 nm. In contrast to the "on" times, the A fit parameter increases with added acceptor as does the Weibull scaling parameter β.

As mentioned in the beginning of this chapter, the change in the "on" and "off" times is related to effects of the molecular structure and environmental factors on

CCDF Type	Sample Type	Fit Parameters		Average Time
		$\beta_{Weib}, (\mu_{LN})$	$A_{Weib}, (\sigma_{LN})$	$\langle\tau\rangle_{on/off}$
Non-blinkers "on"	Donor-only	1.34	34.3	31.5
		1.3	35.2	32.5
		1.47	34.8	31.5
		1.48	31.3	28.3
		1.52	39.4	35.3
	20 nm IF-TIPS	1.47	29.8	27
	10 nm IF-TIPS	1.44	33.1	30
	9 nm IF-TIPS	1.55	40.2	36.1
	8 nm IF-TIPS	1.57	39.7	35.6
	6 nm IF-TIPS	1.39	26.2	23.9
	5 nm IF-TIPS	1.3	21.4	19.8
		1.54	10.1	9.1
		1.4	14.8	13.5
		1.27	15.8	17.6
Blinkers "on"	Donor-only	1.79	37.8	33.6
		1.56	36.9	33.1
		1.62	31.7	28.4
		1.91	41.2	36.6
		1.88	34.1	30.3
	20 nm IF-TIPS	1.93	36.2	32.1
	10 nm IF-TIPS	1.8	41.7	37.1
	9 nm IF-TIPS	1.59	37.7	33.8
	5 nm IF-TIPS	1.19	15.7	14.8
		1.46	15.3	13.9
		1.34	14.7	13.5
		1.31	13.7	12.7
Blinkers "off"	Donor-only	1.09	25.8	25
		1.2	22.7	21.3
		1.11	23.4	22.5
		1.09	15	14.5
		1.02	24.5	24.3
		-0.89	-2.67	-21.5
	20 nm IF-TIPS	1.15	22.1	21.1
		-0.89	-2.64	-20.9
	8 nm IF-TIPS	1.26	31.2	29
	7 nm IF-TIPS	1.2	29	27.3
	5 nm IF-TIPS	1.52	42	37.9

Table 4.3: The fit parameters for the largest p-value distribution for each sample type. The parameters were used to calculate the average "on" or "off" time based on the equations 4.10, 4.11, and 4.12

photo-oxidation and product formation, specifically EPO formation. Since the "on" and "off" times fit either a Weibull or lognormal distribution, this indicates that the transition rates between the "on" and "off" states are not fixed. If these rates were fixed, then the distribution of times would fit a single exponential. This indicates that there is a distribution of activation energy for the molecule to interact with oxygen and both form EPO and return to the ground state from EPO formation. With the addition of acceptors, the activation energy distribution decreases for transitions into EPO, but it increases for the return to the ground state. The distribution of the energy is due to the way the molecule sits in the sample. As mentioned in previous chapters, how the side groups sit with respect to the backbone of the molecule determines how well protected the molecule is from degradation. In single molecule sample, each molecule will have a slightly different orientation, which affects how well the side groups are protecting the molecule. The addition of the acceptors changes the film morphology, and encourages molecular orientations which are more vulnerable to EPO formation.

4.3.3 Quasi-SMFS

Because of the unique sample preparation for the quasi-SMFS samples, the data collected was different than the data that is traditionally collected in SMFS. Fluorescence time traces were analyzed for the bright spots on the film that either had a fluorescence decay curve, transitions between quantized fluorescence levels (where the fluorescence time traces have distinct "steps" when the spot decreases

in fluorescence), or hybrid, which have both a decay aspect as well as quantized fluorescence levels (see Figure 4.5 for examples). The samples of Pn-TCHS-F8 in PVDF had 72 traces with 22 of them being traces with quantized fluorescence levels, 21 traces are decays, and 29 are hybrid traces. The sample of Pn-TIPS-F8 in PMMA that was made using the same process had 112 traces with 60 quantized fluorescence levels, 31 decay traces, and 21 hybrid traces. Once these traces were classified, the progressing program collected data from each trace either by fitting the data to a single exponential function Ae^{-b*t}, which was done for both decay traces and hybrid traces, or by extracting the "on" or "off" times for each transition between quantized fluorescence levels, which was done for both the hybrid traces and the ones that only had these quantized levels. The "on" and "off" times were sorted based on what type of trace they originated from. Times from traces that had more than two fluorescence levels (one "on" and one "off" level), were classified as multi-step times. Whereas, the times that originated from a two level system were considered traditional SMFS times.

Just as was done in the previous SMFS experiments, the "on" and "off" times for both the multi-step traces and the traditional SMFS traces were sorted into "blinkers" and "non-blinkers". Unfortunately, the number of "blinkers" for both multi-step and traditional SMFS were less than five out of the 184 fluorescence trajectories analyzed. This means that there is not enough "off" times for any analysis and that all the "on" times are effectively "non-blinker" "on" times. Thus, all the analysis of this data will exclusively discuss the "non-blinker" "on" times, which we will call "on" times.

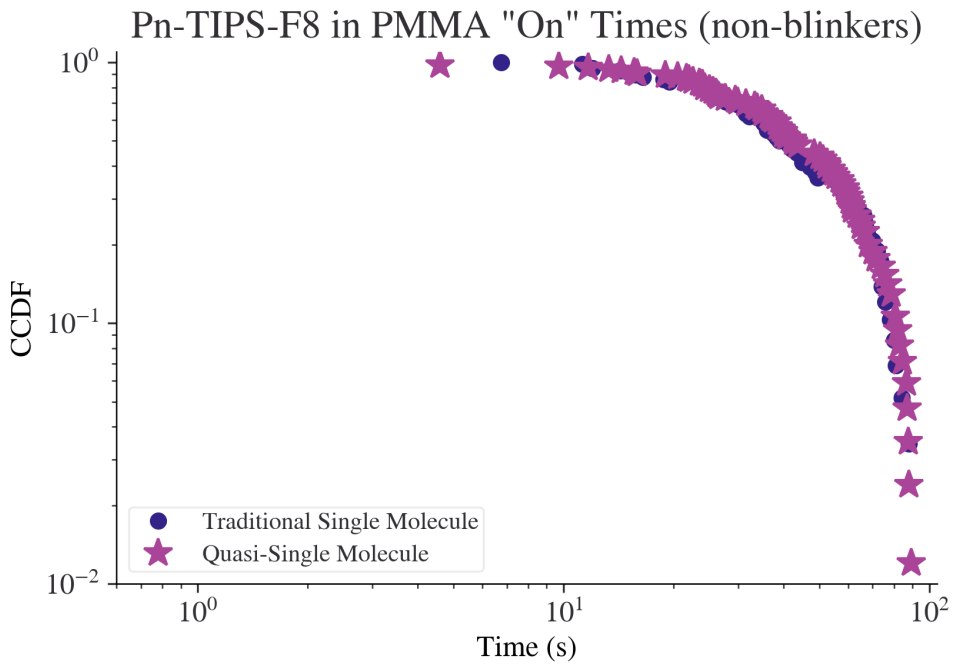

Figure 4.9: "Non-blinker" "on" times for Pn-TIPS-F8 in PMMA in both the layered sample and the non-layered sample, which was created using solution which included polymer and molecule. The distribution is nearly identical, with slight variation likely due to the size of the data sets (58 points for layered vs 85 for non-layered). This indicates that this variation in sample preparation does not significantly affect the molecular stability.

Once the data was sorted, the traditional SMFS step size was compared to the step size of the "multi-step" traces. The step size is the amount of fluorescence lost in one of the quantized steps. Figure 4.10 shows a comparison of the step sizes of the data collected from PMMA and PVDF. The histograms, (a) and (c), show the population of "on" times depending on their corresponding step-size. The distributions look fairly similar with none of the sample types or trace types favoring either smaller or larger steps.

The scatter plots in Figure 4.10, (b) and (d), were used to find the correlation between "on" time and step size. A trend on this plot would indicate that there was a correlation between how long the fluorescence lasted and the brightness of the fluorescence. The lack of trend is a sign that the data encompasses a wide population of molecules.

Before any further analysis is done, the sample of Pn-TIPS-F8:PMMA using the layered sample preparation is compared to the "non-blinker" "on" times of Pn-TIPS-F8:PMMA using the original sample preparation that was discussed in the Host Dependence section of this chapter. Figure 4.9 shows the CCDF of these two data sets. The data sets appear almost identical, with the slight variation likely due to the difference in the number of data points used to create the CCDF (58 points for layered vs 85 for non-layered). This is further supported by the fits to the distributions. While neither of them have high p-values for the fits, they both have the highest p-values for the Weibull distribution. The Weibull fit values are very close ($\beta = 51.1$ and $A = 1.92$ for non-layered and $\beta = 49.9$ and $A = 2$ for layered), which means that the calculated average "on" time is 45.3 seconds for non-layered and 44.1 seconds for layered. The close alignment of these data sets indicates that the original SMFS traces found in the layered samples are in fact, single molecules. This also indicates that the different methods of sample preparation used here are not a significant factor in the molecular performance.

This data set of Pn-TIPS-F8 in layered PMMA acts as a reference for the rest of the data sets in this experiment. In particular, it is a reference point for the other "on" times collected. Looking at the data for the multi-step traces of Pn-

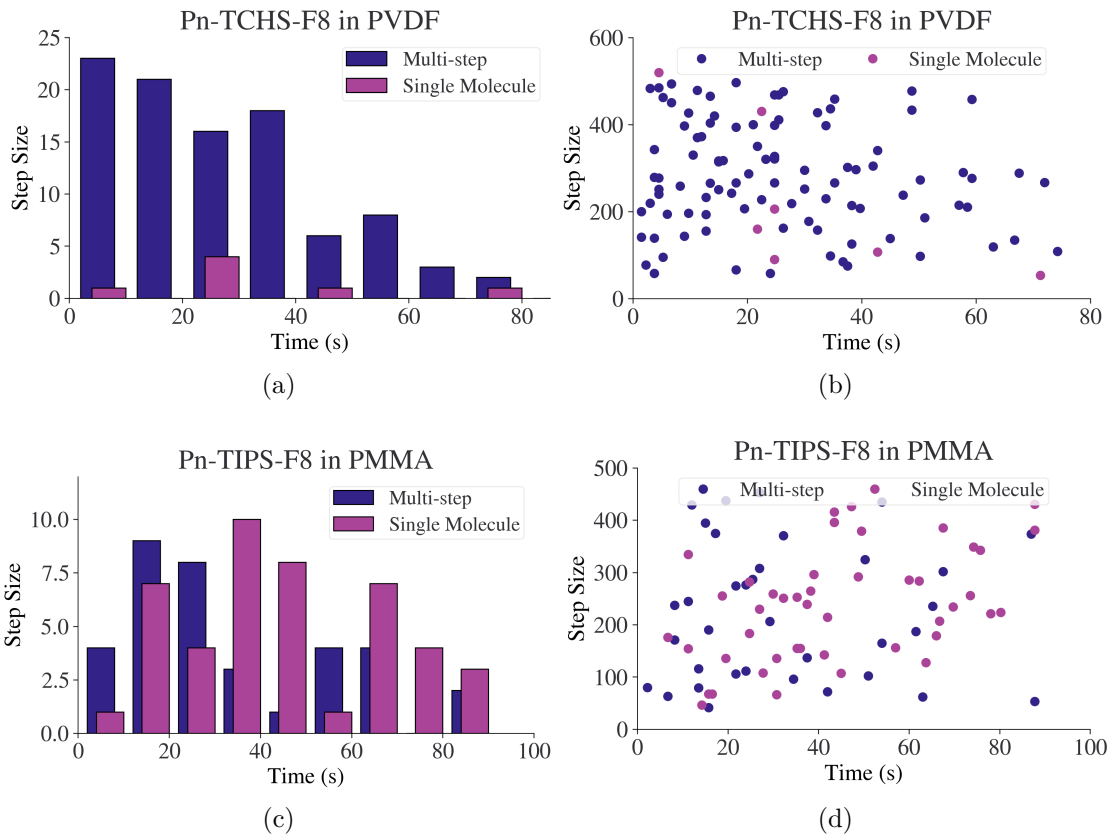

Figure 4.10: Comparison of step-size for traditional SMFS and "multi–step" in Pn-TCHS-F8 in PVDF ((a) and (b)) and in Pn-TIPS-F8 in PMMA ((c) and (d)). The histograms, (a) and (c), shows the number of "on" times with heights in a given range. The scatter plots, (b) and (d), shows the "on" times with their corresponding step size. This plot was used to determine if there was a relationship between how much fluorescence was lost and the length of time the fluorescence was active.

TIPS-F8 layered in PMMA, shows that the "on" times are slightly smaller than the traditional SMFS "on" times (see Figure 4.11). It also fits best to a Weibull distribution, with fit parameters $\beta = 40.3$ and $A = 1.56$, which has an average "on" time of 36.2 seconds. This is 17% smalller than the layered Pn-TIPS-F8 in PMMA

and the traditional non-layered Pn-TCHS-F8 in PMMA, which makes sense when comparing the fluorescence time traces. In order for there to be multiple steps in a single trace, the transitions between levels must be spread out far enough that they can be distinguished, which leads to a higher probability that the transitions will occur closer to the beginning of the trace.

Both the Weibull fit and the shorter average "on" times for the multi-step traces have interesting physical implications. Weibull distributions have been used to describe chemical reactions when there is a distribution in the activation energy. This is seen in equation 4.4 as the traditional transition rate β is now affected by the exponential term A. Since the multi-step traces indicate that there are multiple molecules at that spot, having multiple molecules increases the chance of decay and decreases the fluorescence lifetime for the molecules. In terms of EPO formation, multiple molecules clustered together would decrease the fluorescence lifetime. The first step in EPO formation is the creation of a reactive oxygen, followed by that oxygen diffusing until it finds a molecule to react with and form EPO. When molecules are clustered, the amount of time needed for reactive oxygen to find a molecule to react with decreases because there are more molecules nearby. This decreases the lifetimes of the molecules. There is also the increase in probability of photodimerization. Since multiple molecules sit inside the diffraction limit, it is possible that some of the molecules inside the clusters will form dimers. With these clusters, a second degradation pathway is available, which would increase how quickly the molecules turn off. The blinking statistics of the small aggregates could also be affected by singlet fission, from a correlated triplet pair of adjacent

molecules, if the molecules are close enough. However, it has not been determined if this happens at the single molecule level.

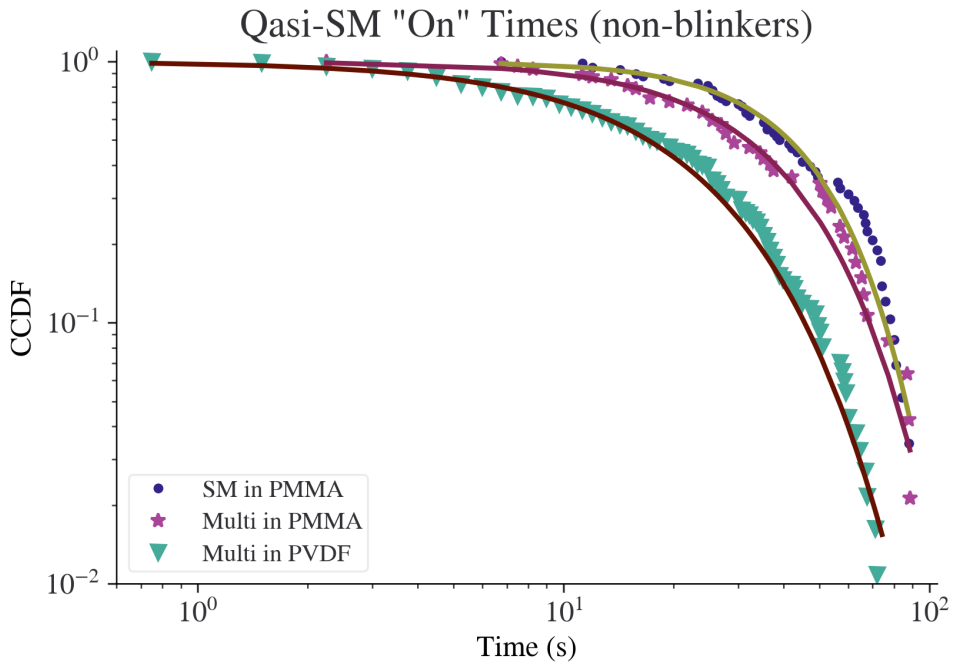

Figure 4.11: CCDFs for Quasi-single molecules in PMMA and PVDF with the corresponding Weibull fits. There was not enough single molecule data for a significant CCDF in PVDF.

This same trend of multi-step traces having shorter "on" times than traditional SMFS is found in Pn-TCHS-F8 in PVDF. Both of the data sets fit to Weibull distributions with their fit values being $\beta = 33.8$ and $A = 1.59$ with an average time of 30.3 seconds for traditional SMFS and $\beta = 23.4$ and $A = 1.22$ with an average time of 21.6 seconds for multi-step. Not only is multi-step faster in it's degradation rates, but the rates for both multi-step and traditional SMFS in PVDF are faster than in PMMA. It is also worth noting that the number of traditional

SMFS traces was very small, with a sample size of 7. This indicates that in PVDF almost all of the molecules are clustered and that PVDF is not as protective as PMMA.

This is supported by the decay traces. When fit to an exponential function, the decay rate ranges from $b = 0.031$ s^{-1} to $b = 0.307$ s^{-1} with a mean of $b = 0.106$ s^{-1} for decays in PVDF. From these fit parameters, we can find the half-life of the decay by using $\ln(2)/b$, wich means the average half-life for PVDF is 8.74 seconds. In contrast, the fit values for PMMA range from $b = 0.0023$ s^{-1} to $b = 0.233$ s^{-1} with a mean of $b = 0.063$ s^{-1}, which results in a average half-life of 15.64 seconds. So all three types of traces have smaller average "on" times in PVDF than the traces of Pn in PMMA. This is in agreement with the higher concentration thin-film experiments discussed in Chapter 2.

The SMSF experiment provides some physical insight into the reasoning behind this faster decay. As mentioned in Chapter 2, the relationship between the oxygen permeability and the stability of a host polymer is correlated [55]. Since PMMA has an oxygen permeability of 4.8 cm^3-mm/m^2-24 hr.-Bar and PVDF has a permeability of 5.4 cm^3-mm/m^2-24 hr.-Bar [68], values which are close enough to each other that is reasonable to expect similar behavior from the molecules they would host. However, this is not what is seen experimentally. This strong discrepancy is likely due to the huge difference in polarity between PMMA and PVDF. Specifically, the non-polar functionalized Pn is going to behave differently in polar PVDF than it would in non-polar PMMA. This was seen when attempting to make PVDF samples using the same process as PMMA samples – the functionalized Pn would

not dissolve into the same solvents and therefore a new process had to be created. Despite this new process, the data shows that it was not statistically favorable for the functionalized Pn to mix evenly throughout the PVDF, since almost all the bright spots were not single molecules, but rather aggregates.

This is likely due to the nonuniform nature of PVDF. PVDF films also has four different forms which are either more crystalline or more amorphous depending on the sample preparation [66]. Based on the method of our sample preparation, the PVDF films have a combination of phases, specifically the γ and α phase. The α phase has chain conformation that alternates between two molecular conformations, whereas the γ has chains with more of the molecules in one particular conformation[66]. The results of these phases is that the PVDF film is nonuniform.

The nonuniformity of PVDF is seen in our data as there is high spot-to-spot variation in our single molecule traces. This is also seen in our higher concentration thin film data where each of the film spots had a slightly different decay time (see Chapter 2). The effects of multiple phases present in the thin film leads to variations in other properties, for example, in PVDF, there is a wide range of dielectric constants within a film due to the multiple phases present [23]. As seen in the donor-acceptor SMFS studies, small changes in morphology can have a large effect on the stability of functionalized Pn.

Despite having a low oxygen permeability, PVDF as a host polymer is a less photostable environment for functionalized Pn. A major reason for this is the high polarity of PVDF. Since functionalized Pn is nonpolar, the two materials do not mix well. This leads to higher aggregates and low bonding and interaction between

the polymer and functionalized Pn, unlike PMMA, which can form protective bonds with functionalized Pn. This also causes the functionalized Pn to aggregate, which leads to higher probabilities of both dimerization, as the probability of dimerization increases with the increase in concentration, and EPO formation. Because EPO formation is a two step reaction, the first to create the reactive oxygen and the second to bond with the reactive oxygen, film regions with higher concentrations decrease the amount of time the diffusion driven reactive oxygen takes to find a functionalized Pn molecule to bond with. This is similar to what happens in solution with Chlorobenzene as the polarity of the solution increases the photodegradation.

4.4 Conclusions

Single Molecule Fluorescence Spectroscopy experiments provide insight into the environmental and molecular factors that affect EPO formation in Pn-R-F8. The only non-environmental parameter that was tested was the effect of side groups on EPO formation. In agreement with the higher concentration studies, Pn-TCHS-F8 has much higher "on" times in comparison to Pn-TIPS-F8, when hosted by the same polymer. This shows that larger side groups are better at protecting the molecular backbone from binding with reactive oxygen.

The effects of two environmental factors were tested: host polymer and acceptor addition. In agreement with the study done by Hubert Piwoński, et. al. the stability of Pn-TCHS-F8 is related to the oxygen permeability of the host

polymer[55]. This was seen in the samples of PMMA, PVK and PS. PMMA has the lowest oxygen permeability, followed by PVK and PS and the average "on" time for Pn-TCHS-F8 in these hosts followed the exact opposite ranking. However, the relationship between oxygen permeability and "on" times was not seen in quasi-SMFS experiments with PVDF, as Pn-TCHS-F8 degraded quickly despite the low oxygen permeability. This is due to the low mixing of Pn-TCHS-F8 in the PVDF films due to the difference in polarity. Since PVDF and Pn-TCHS-F8 do not mix well, Pn-TCHS-F8 clusters when hosted in PVDF, which results in higher photo-oxidation, since the diffusion lengths are shorter, and higher dimerization, since the molecules are closer together. The difference in polarity also eliminates the protective polymer-molecule interactions that occur with same polarity hosts and molecules.

Adding acceptor molecules to the polymer also affected EPO formation. Adding acceptor molecules naturally decreased the number of fluorophores fluorescing, as some of them were close enough to acceptor molecules and were therefore transferring their energy via FRET. However, the addition of acceptors also changed the blinking dynamics of the fluorescing molecules because the change in the film morphology affected how much free volume was available for the Pn molecule and the reactive oxygen it produced. Higher density films cause the Pn-TCHS-F8 to sit in the film in orientations that were more conducive to oxygen interaction and EPO formation. This means that for donor-acceptor film development, care must be taken to optimize the morphology to prevent rapid degradation of Pn-TCHS-F8.

The SMFS experiments showed that EPO formation was occurring and that

the effects we were seeing in the higher concentration films also appear on the single molecule level.

Chapter 5: Molecular State Modeling of Photodegradation Using Monte Carlo Modeling Simulations

5.1 Introduction

While the experimental data characterizes the environmental factors that affect the photostability of functionalized Pn, it does not completely illuminate the physics of the interaction. In order to better understand the photophysical processes that are incorporated in the experimentally measured fluorescence time trajectories as discussed in Chapter 4, I computationally modeled the physical process occurring in each molecule. The simulation used a multi-state model and ran using a Monte Carlo process to simulate the excited state dynamics of individual molecules. The simulation incorporated the experimental parameters, and produced data similar to the experimental data so that both experimental and simulated data sets could be processed the same way. Modeling the system in this way allowed us to connect parameters extracted from experimental data with the physical interactions that were occurring.

5.2 Previous Models

In 2004, Shinya Maenosono published a study which used Monte Carlo simulations to model the luminescence properties of quantum dots. The model consisted of three electron states: the ground state, the excited state, and a "dark" third state. The "dark" state represented all the potential trapped states for the quantum dot. The model used rates between states to determine when transitions between states was to happen as the simulation moved forward in time. Since the transition between the excited state and the ground state is radiative, the emission intensity is collected during the simulation and compared to the emission of the quantum dots. The emission over time from the simulation has fluctuations, where the intensity shifts from bright to dark and it looks like it is "blinking"[36].

Emission spectra with slow "blinking" ($\sim$ 10 seconds) is a characteristic of single molecule fluorescence spectroscopy. Other research groups began using this three level Monte Carlo simulation to model "blinking" materials or systems[81, 80, 6]. In particular, through Monte Carlo modeling, correlations could be drawn between the changes in the statistical distributions of the times that molecules were emissive ("on") or nonemissive ("off") and the changes in transition rates between states, which correlated with physical properties. For example, in the paper by Natalie Z. Wong, et al, the lognormal distribution of "on" times in Rhodamine G6 and Rhodamine B, was correlated with a distribution of activation energies between the excited state and the dark triplet state of these materials[80].

The similarity between the data seen in the literature and the data collected

from single molecule fluorescence spectroscopy (SMFS) experiments discussed in Chapter 4, motivated the development of a Monte Carlo simulation for functionalized Pn. The three level system and tradition rates found in these studies was the foundation for the model, and modifications were made to align the model with experimentally determined parameters and through iterations of data simulation.

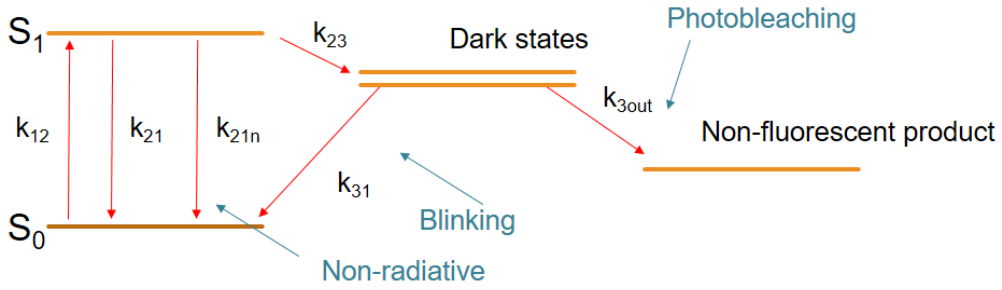

Figure 5.1: The Finalized Model. This diagrams the four states that exist within the final model, including the ground state S_0 or state 1, the excited state S_1 or state 2, the dark state or state 3, and the photobleached state or state "out". The associated rates of transitioning between states is also indicated, with the subscript on each rate corresponding to the state of origin followed by the destination state.

5.3 Model Development and Simulation Procedure

The model was written in Python and was written to simulate one molecule at a time. To collect a batch of data ($\sim$ 100 traces), the physics department computer lab was used as a computational cluster. During evenings and weekends, when the lab had little to no use, a Bash script was initiated to run the Python code on each computer in the lab with the chosen parameters and the resulting data was

stored on the main server computer. After completion, the code was run a second or third time on a given computer until the predetermined number of total runs was reached.

The model represents the possible electronic states that contribute to fluorescence time trajectories measured in our experiments. In order to determine the electron states that are preferred and the relationship between the transitions to those states and what is seen experimentally, we can simulate the electron transitions to created data similar to what is seen experimentally. To model this, the simulation had to move through time and allow the electron to transition between states.

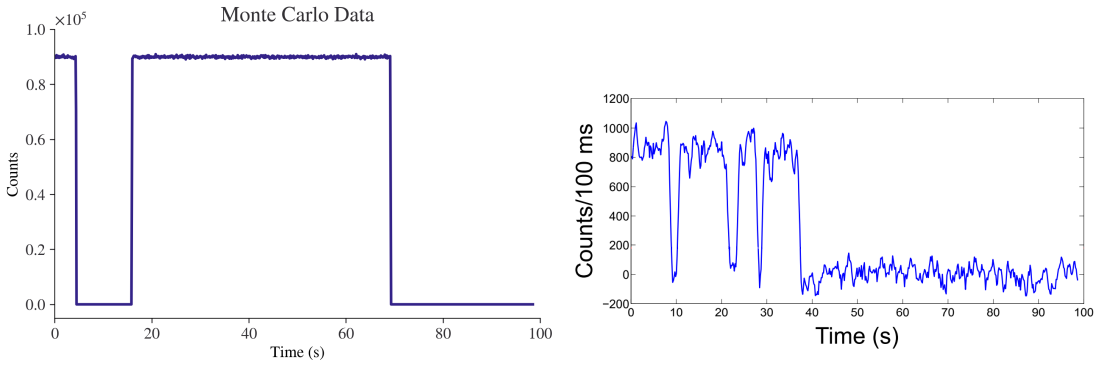

Figure 5.2: Comparison of Simulated Data to Experimental Data. The experimental data (a) was taken of single molecule Pn-TCHS-F8 in PMMA from the acceptor data set as discussed in Chapter 4. The simulation data was taken from a data set with transition rates of $k_{12} = 1.1 \times 10^6$, $k_{23} = 5 \times 10^4$, $k_{21} = 9.1 \times 10^7$, $k_{31} = 0.01$, $k_{34} = 0.01$.

Since the single molecule experiments are run for 100 seconds, the simulation also runs until 100 seconds of data was produced. Because many of the transitions happen at very short time scales, the simulation uses a one nanosecond time step.

Choosing the correct time step is critical to the success of this simulation, since it is used to calculate the probability of transition between states. If the time step is too big, the probability will always be larger than one, which means the transition will always occur, and the fine details of the simulation are lost. A time step that is too small, will take significantly more computation time without providing any new information. To find the balance, I used the time step that was the same size as the fastest transition. In this case, previous studies have shown that the lifetime of the excited state for functionalized Pn is on the order of nanoseconds, with all the other transitions taking much longer. Therefore, I chose a nanosecond time step. This is in agreement with other single molecule Monte Carlo models[81].

Each nanosecond, the simulation checks to see if the electron transitions from its current state to another available state. To determine if a transition can occur, the simulation calculates the product of the transition rate (k_{ij}) with the time step (Δt). This calculated value is the probability that the transition will occur and, for this simulation, should be between zero and one when using a nanosecond time step.

With the probability of transition lower than one, the simulation uses a Monte Carlo process to determine the success of the transition. A random number is chosen between zero and one. If $k_{ij}\Delta t$ is larger than the random number then the electron transitions to the new state. Otherwise, the electron remains in the same state. If a given state has more than one available state to transition into, this transition process is divided into two steps. First, the simulation determines if the electron leaves the current state. This can be found by calculating the

product of the time step (Δt) with the sum of all available transition rates from the current state ($k_{ij} + k_{im} + k_{in} + ...$). As outlined previously, the product is compared to a randomly chosen number between zero and one to determine if the electron leaves the state. Once the electron has successfully 'left' the state, the simulation determines which state it moves to by calculating the probability of the molecule entering each state and comparing that to a random number. Since the first transition to pass the test is the chosen new state, the testing is done in ascending probability.

As the simulation steps through each nanosecond time, it tracks the current molecular state as well as the florescence events. The transition from S_1 to S_0 can be both radiative and non-radiative. If during the simulation the radiative transition succeeds, a photon is added to the emission count. As described in Chapter 4, in the Single Molecule Fluorescence experiments, the integration time for data collection is 0.1 seconds. Therefore, this was the time used to bin the collected photons for the simulated data. Every 0.1 seconds the photon count was added to the fluorescence list and then the counter was reset to zero for the next bin period. After the simulation was run, the plotted list of binned data, which was the florescence time trace of the molecule, looks similar to the experimental data that was collected (see Figure 5.3).

Once the code was written to model the time traces, it was important to use the correct transition rates. Some of the transition rates can be determined using experimental information, while others are much more difficult to determine. Other studies that used this approached, used a combination of experimentally

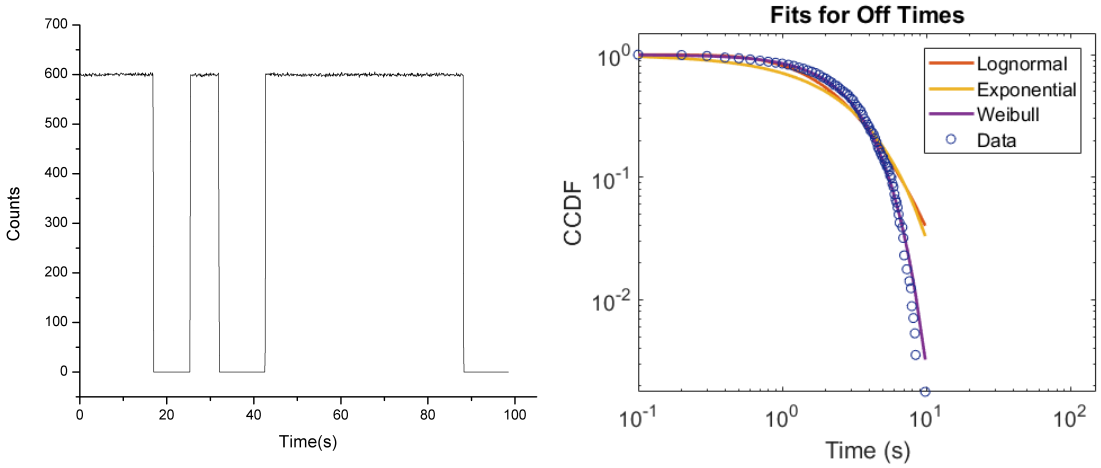

Figure 5.3: Simulation Data. The simulation creates fluorescent time traces (left) that look similar to the experimental data from the single molecule fluorescence spectroscopy experiments. The "on" and "off" times are extracted from the set of time traces and are converted into complementary cumulative distribution functions (CCDF) and fit to common distributions (right).

determined transition rates and computationally determined transition rates[81]. For example, the transition from the ground state to the excited state is dependent on the molecule absorbing a photon, and therefore this is dependent on the laser power. The rate at which the molecule returned to the ground state after turning off k_{31} was not information that we had experimentally probed and therefore was determined using computational testing.

It is also worthwhile to note that some of the transition rates were, by nature, variable while other transition rates were fixed. Since this computational model was specifically used to understand how the statistics of the ensemble changed as the environment changed, some of the rates were varied to determine the correlation between the changes of transitions between states and the changes in the

experiment. For example, both the transitions k_{12} and k_{21} are fixed transition rates. The rate k_{21} is dependent on the fluorescence quantum yield and fluorescence lifetimes, which are fixed characteristics. Likewise, the k_{12} rate is dependent on variables that are constant to either the molecule itself, like absorption cross-section, or are fixed for the experiment, like laser power.

The model was developed while data was being collected for the single molecule fluorescence spectroscopy experiments where acceptor was added (see Chapter 4), so those experimental values were used. The experimentally determined transition rates were determined as follows. Transition k_{12} was calculated using the laser power, wavelength, molecular absorption cross section, and laser spot size on sample. The power for the $\lambda = 633$ nm laser was $P = 850$ μW measured at the sample, with a spot with radius of $r_{\text{spot}} = 50$ μm. The molecular absorption cross section for functionalized Pn is $a_{\text{mol}} = 8.49 \times 10^{-20}$. Therefore, the amount of rate at which the photons interact with the molecule is calculated by taking the product of the photon rate from the laser (Power/Energy or Power/(h*c/wavelength)) and multiplying it by the ratio of molecular absorption cross section to the laser spot area.

$$t_{\text{photon}} = \frac{\lambda P}{hc} \frac{a_{\text{mol}}}{\pi r_{\text{spot}}^2} = 2.92 \times 10^4 \text{ photons/s} \tag{5.1}$$

Since the molecule of study, functionalized Pn, cannot transition into the excited state without absorbing a photon in this experiment, this is the transition rate k_{12}. It is worthwhile to note that while this was the rate I used for my later simulations,

originally I started with the rate of 1.1×10^6 s^{-1} since that was the value being used in some of the literature, and it was an easy value to use to test the simulation functionality during development.

Similarly, the transition for k_{21} can be calculated using fluorescence lifetime of high concentration Pn-TCHS-F8 in PMMA, which is 11.7 ns and the fluorescence lifetime of Pn-TCHS-F8 in toluene, which is 11.7 ns [71]. The fluorescence lifetime is the time between the excitation and the emission of a photon for a given molecule, which is the inverse of the k_{21} transition rate[71]. Since both the fluorescence lifetime values were found for high concentration Pn-TCHS-F8 films and not single molecule films, these values provide a baseline for what rates to start with, which was 9.1×10^8 s^{-1}. As the simulation progressed, the k_{21} rate was refined based on the data produced.

The fluorescence quantum yield is the ratio of number of emitted photons to number of absorbed photons and was also used to calculate rates. Since it is the ratio of the number of emitted photons to the number of absorbed photons, this ratio can be rewritten in terms of transition rates. Since the quantum yield is 0.82, this means that for every 100 photons that are absorbed, 82 of them are emitted as fluorescence and the remaining 18 decay through one or more alternative paths. Since the number of photons emitted in a given time, ΔT, is equal to $k_{21}\Delta T$, the fluorescence quantum yield can be written as

$$\Phi_{\mathrm{F}} = \frac{k_{21}\Delta T}{\sum_i k_{2i}\Delta T} = \frac{k_{21}}{\sum_i k_{2i}} \tag{5.2}$$

This provides a relationship between the k_{21} rate and any other decay rates. Based on the model that is being used, there are a minimum of two pathways of decay from the excited state S_1 to S_0 is two: one for the fluorescent path and one for the dark state. This dark state is a longer lifetime state and is the cause of the dark "off" times in fluorescence time traces. However, based on the experimental data, if the transition to the dark state happened 18%, then on average the transition to the dark state should occur for every six absorbed photons, or every $6/k_{12} = 0.205$ ms. Since the experimental data exhibits transitions to the dark state on the order of 10's of seconds, there must be a third decay pathway available. The third pathway is a non-radiative pathway that is labeled k_{21n} and is a direct transition between the excited state S_1 to the ground state S_0.

Using a similar methodology and the average amount of time before the Pn-TCHS-F8 molecules transition into the dark state from the experimental data, the approximate k_{23} can be calculated. Experimentally, the average amount of time before Pn-TCHS-F8 transitions to the dark state (also known as the "on" time) is 43.8 seconds. Since each molecule is interacting with photons at a rate of 2.92×10^4 photos/s, then on average, there are 1.279×10^6 photons that interact with a molecule before the transition to the dark state. This means that the transition between S_1 and the dark states happens 7.82×10^{-5}% of the time. The rate of transition between the excited state S_1 to the dark states can be found by recognizing that the ratio of k_{21} to it's percentage of probability, 82%, must equal the ratio of k_{23} to it's percentage of probability, 7.82×10^{-5}%. Thus, the initial k_{23} rate is 868 s^{-1}.

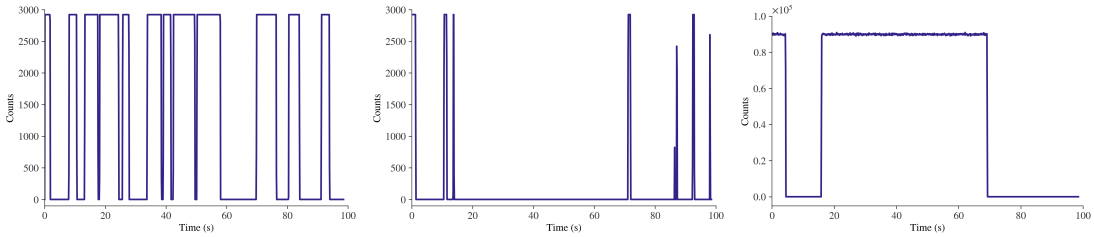

(a) (b) (c)

Figure 5.4: Different types of simulation fluorescence time traces based on changes in transition rates. The rates are $k_{12} = 1.1 \times 10^6$, $k_{23} = 1 \times 10^5$, $k_{21} = 9.1 \times 10^7$, $k_{31} = 0.01$, $k_{34} = 0.01$ for the first trace (a), which has "off" times that are too short. The second trace (b) has rates of $k_{12} = 1.1 \times 10^6$, $k_{23} = 1 \times 10^5$, $k_{21} = 9.1 \times 10^7$, $k_{31} = 0.05$, $k_{34} = 0.01$, which has "on" times that are too short. The last trace has a better balance of "on" and "off" times, with rates of $k_{12} = 1.1 \times 10^6$, $k_{23} = 5 \times 10^4$, $k_{21} = 9.1 \times 10^7$, $k_{31} = 0.05$, $k_{34} = 0.01$.

Once two of the three initial transition rates were determined, the third transition rate k_{21n} can be calculated through the fluorescence quantum yield equation. The equation can be rearranged to solve for k_{21n} as follows

$$QY = \frac{k_{21}}{k_{21} + k_{21n} + k_{23}} \rightarrow k_{21n} = \frac{k_{21}}{QY} - k_{21} - k_{23} \tag{5.3}$$

Thus, the initial transition rate for k_{01n} is 2.0×10^0.

Once the initial rates were selected, the simulation was run and the rates were finessed to find the region with data most similar to experimental data. Some of the data collected had fluorescence time traces that did not visually resemble the experimental data (see Figure 5.4). However, other data sets looked similar enough that it was difficult to determine how similar the experimental data was to the simulated data. These visually similar traces were more accurately compared

by processing them following the SMFS trace processing method as explained in Chapter 4. This involved extracting the "on" and "off" times for the whole data set of traces and then converting the probability distribution into the complementary cumulative distribution function (CCDF), which is much easier to accurately fit than the probability distribution. The CCDFs for the simulated data was fit to lognormal, exponential and Weibull distributions, as seen in Figure 5.5, and the fit parameters were extracted.

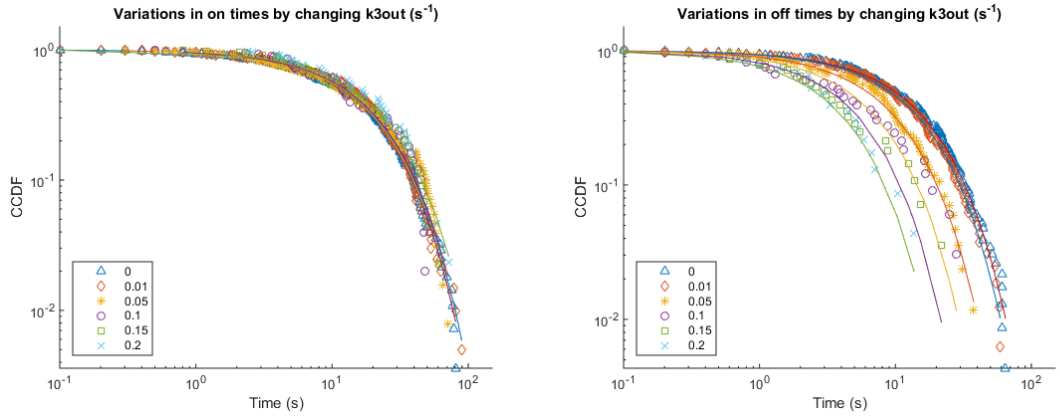

Figure 5.5: Testing. Testing the model included holding specific sets of variables constant and then varying the others. In this case, $k_{d,out}$ was changed while the other transition rates were held constant. The "on" times were unaffected by the change (right), but the "off" times changed significantly (left).

Rigorous testing was carried out to determine the validity of the simulation as well as the ways in which each parameter affects the time traces and the resulting CCDFs. Each parameter was varied while the other parameters remained fixed. For example, as the transition rate between the dark state and the irreversible (photobleached) state ($k_{3,out}$ in Figure 5.5) increased, the CCDF of the "off" times exhibited decays at earlier times, whereas the "on" times were not affected,

as expected. Figure 5.5 also shows the dependence of the CCDF of the simulated data on the parameters k_{23} and k_{31}, respectively, illustrating their pronounced effects on the "on" and "off" times distribution, respectively. These tests provide a valuable aid in understanding trends in our experimental data.

5.4 Results and Discussion

The initial results from the simulation show that the "on" times for the simulation are affected by the k_{23} rate and the "off" times are affected by both the k_{31} and the $k_{d,out}$ rates. It was also seen that when the rates were fixed, the data fit an exponential distribution, as expected for fixed rate transitions[62]. Since the experimental data are typically described by a more complicated distribution such as Weibull or lognormal distribution, this indicates a distribution in rates[18]. For example, in the SMFS data, the Weibull function has been used to describe the distribution of the "on" time durations due to the distributed probability of radical ion pair ISC in perylenediimide single molecules in PMMA and to describe heterogeneous kinetics of catalysis[38, 43]. This Weibull-distributed process is characterized by a time-dependent rate $k(t) = (A/\lambda)(t/\lambda)^{A-1}$, where A and λ are Weibull fit parameters.[64] (If $A = 1$, the time-independent rate $k = 1/\lambda$, characteristic of the single-exponential distribution, is recovered.) Since the majority of the data that were collected fit to a Weibull distribution, understanding the effects of that distribution was the focus.

To investigate how such time-dependent rates manifest into the CCDF so that

such rates can be successfully recovered from CCDF fits of the experimental data, we performed Monte Carlo simulations as follows. The model was simplified down to three states (1-3). Based on the model testing results, the transition rates k_{12}, k_{21}, and k_{23} were fixed at 2.9×10^4 s^{-1}, 7×10^7 s^{-1}, and 222 s^{-1}, respectively, to provide data that was similar to experimental data and provide plenty of "on" and "off" times for statistical analysis. The rate k_{21n} was fixed using the fluorescence quantum yield equation such that $k_{21}/(k_{21} + k_{21n} + k_{23}) = 0.82$, resulting in k_{21n} approximately equal to 1.5×10^7 s^{-1}. The Weibull rate $k(t)$ was applied to the k_{31} rate so that $k_{31} = (A * k_{31\text{orig}})(k_{31\text{orig}} * t)^{A-1}$, where $k_{31\text{orig}}$ is the original rate, which was varied from $0.025 - 2$ s^{-1}, t is the time the molecule has spent in the dark state, and A is the Weibull distribution parameter, which for our experiments varied from 1.2-1.5.[18] From these rates the predicted average "on" time can be calculated using $\tau_{on} = (k_{21} + k_{21n} + k_{23})/(k_{23} * k_{12})$, which is 13.15 seconds. The predicted average "off" time is calculated using $\tau_{off} = (1/k_{31\text{orig}}) * \Gamma(1 + 1/A)$, where Γ is the Gamma function. For the range of $k_{31\text{orig}}$ used in our simulations the predicted average "off" times range from $0.45 - 36.1$ seconds for $A = 1.5$ and $1.4 - 40$ for $A = 1$. Even at the high end, the sum of the predicted average "on" times and "off" time is lower than the 100 seconds limit, which should result in a sufficiently large data set to span the distribution.

Plots in Figure 5.6 show results from the simulated data for twelve sets of 100 time traces each for $A = 1.5$ and nine sets of 100 time traces for $A = 1$, where each set had a different $k_{31\text{orig}}$ value. As expected, the Weibull distribution produced the best fit, and the returned fit values were within error of the predicted

values. In particular, when using the Weibull rate $k(t)$ as a transition rate, the returned A values are very close to the expected value, and the fit of the λ vs $k_{31\text{orig}}$ values results in a linear relationship with a slope close to one. For example, when $k_{d1} = 0.3$ and A was set to 1, the fits of the simulated data return $A = 1.066 \pm 0.066$, which is within the error bars of the original value and $\lambda = 0.30 \pm 0.024$, which is exactly at the initial value. This was accurate for both values of A used in simulations. However, the accuracy in the returned A values decreased as the $k_{31\text{orig}}$ increased (Figure 5.6 right), which is likely due to the non-zero integration time (100 ms) dictated by our experimental settings and thus used in the simulation. When $k_{31\text{orig}}$ is large, the predicted "off" times become small, introducing rounding errors due to integration time. This skews the distribution and reduces accuracy in the fit values.

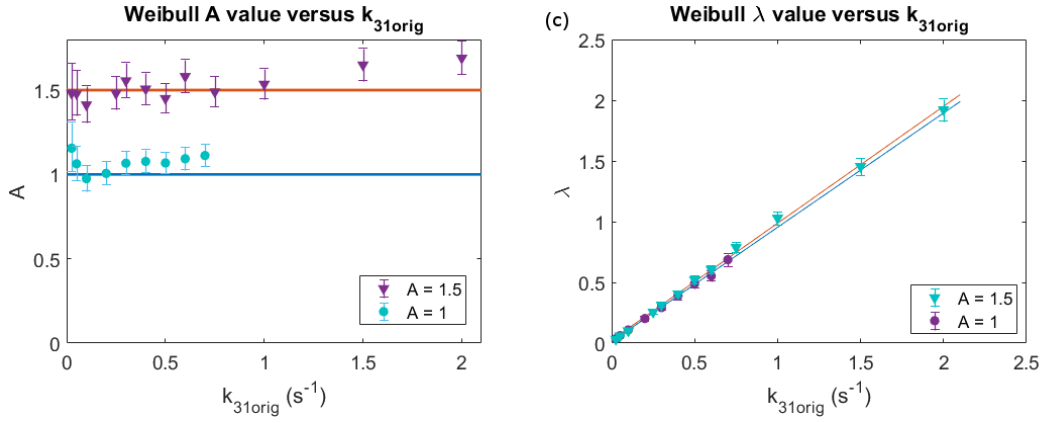

Figure 5.6: Indication that Our Model is Returning the Input Values. The plot in (a) shows the plot of the A fit parameter with $k_{d1,orig}$. Most of the data points are within error bars of the actual value of A used in the simulation. (b) The plot of the λ fit parameter with $k_{d1,orig}$ for both $A = 1$ and $A = 1.5$ data sets. Almost all the data points fall exactly on the line of the actual λ values, and those that do not, fall within error bars of the actual data.

5.5 Conclusions

Using a Monte Carlo simulation to model functionalized Pn has provided insight into the photophysics of these molecules. The four state model produces data very similar to the experimental data we collected (see Chapter 4) using rates that are close to the experimentally determined values, which indicates that this model is an accurate description of the physical processes. The model indicates that functionalized Pn goes through a two-step decay process, which involves an intermediate dark state, where the molecule does not fluoresce, but is still able to return to fluorescing. This agrees with the experimental data collected and with the photodegradation processes studied in this thesis. The simulation also related the Weibull distribution fits of SMFS data to time dependent transition rates. This is indicative of a distribution in activation energy required for transitioning into and out of the dark states. The simulation showed that the Weibull distribution rates could be recovered from the data, which provides insight into functionality of the fit parameters for experimental data. This simulation was successful in modeling functionalized Pn and providing insight into the photophysics of the molecules.

Chapter 6: Conclusion

Classes of tunable, solution processable, small molecular weight organic semiconductor materials are of interest for use in (opto)electronic devices. They have potential for use in applications including OLEDs, photovoltaics, and thin-film transistors. Molecules in the acene group, particularly functionalized derivatives, have been a benchmark organic material for (opto)electronic applications. These materials consist of a polyacene backbone with functional groups that affect solubility, molecular packing and molecular interaction. Within this family, functionalized Pn derivatives are of interest because of their high fluorescence and charge carrier mobility. However, one of the hurdles in organic device development is the low photostability of these materials. Understanding the environmental and molecular properties that affect the stability is key for future (opto)electronic device development.

Functionalized Pn has two prominent photodegradation pathways: oxygen-dependent endoperoxide formation and concentration dependent dimerization. For a better understanding of the photostability of functionalized Pn and the degradation pathways, the dependence of molecular structures, nanoscale morphology and local environment were probed using optical absorption, photoluminescence spectroscopy, single molecule fluorescence spectroscopy (SMFS), nuclear magnetic resonance spectroscopy (NMR) and Monte Carlo simulation. The combination of

these experimental and computational approaches investigated the affects of host material, molecular structure, temperature, molecular concentration, excitation wavelength and oxygen exposure had on the molecular photostability.

The effects of host material on photostability was seen in optical absorption, photoluminescence spectroscopy and SMFS. In solution, the higher polarity of the solvent encouraged higher decay. In film, the higher oxygen permeability had a strong correlation with faster decay rates and less photostable samples. This relationship held true with polymers PMMA, PS, and PVK, however it broke down when using PVDF. Despite having comparable oxygen permeability rates as PMMA, functionalized Pn in PVDF decayed roughly thirty times faster in high concentration films and twice as fast in low concentration SM films. Just as in solution, the higher polarity of PVDF encourages non-polar functionalized Pn into small aggregates, which are more likely to experience dimerization and EPO formation. The aggregation increases the probability that two molecules are close enough and have the correct orientation to form a dimer and the increased concentration speeds up the two step EPO formation process as the reactive oxygen have to diffuse a shorter distance before finding a molecule to bond with.

Although higher concentrations in SMFS increases the photodecay rate of functionalized Pn, the opposite effect was seen in solution and in higher concentration thin films. As the concentration increased for both sample types, the lifetimes of functionalized Pn increase with the increase of concentration. For the thin-film samples, the fluorescence actually increased before beginning to decay. The spacing at which this was occurring was close enough that the functionalized Pn

could interact with neighboring molecules which caused a fluorescence quenching. For example, at low intermolecular spacing, excimer formation and singlet fission become competitive pathways, which are non fluorescent. As photodegradation progressed through the sample, the number of molecules interacting with their nearest neighbor decreased, which caused an initial increase in fluorescence before the expected decrease.

The photostability was also dependent on the molecular structure, with larger side groups (NoDIPS and TCHS) providing better protection against photodegradation than smaller side groups like TIPS. The larger side groups provide a morphological barrier for both dimerization and EPO formation. This works in conjunction with the addition of fluorine to the outer aromatic rings of the Pn backbone. The fluorination changes the electron distribution of the π-bonds because they are so electronegative. This decreases the electron distribution at the bonding sites for both EPO formation and dimerization, which decreases the rate at which those reactions occur. This was supported by longer lifetimes for fluorinated derivatives in both SMFS and in solution.

The addition of acceptor molecules also decreased photostability. This changed the morphology of the sample which changed the orientation of functionalized Pn in the sample. Changes in orientation of the molecule change how well the host polymer and side groups can protect the molecule from EPO formation. In this case, the addition of acceptor molecules reduced the effectiveness of both interactions and the observed on-time was decreased.

In summary, the photostability of functionalized Pn is heavily dependent on

the environmental factors. Polar hosts with low oxygen permeability are more protective of functionalized Pn. Photodegradation is also mitigated by larger side groups and fluorination. Functionalized pentacene is also more stable at either very low concentrations or very high concentrations, but has the fastest degradation rates in samples where the concentration is high enough for easy product formation, but not high enough for Pn-Pn interactions, like singlet fission or exciton formation, which compete with the product formation processes.

Based on the characteristics of the photodegradation of functionalized Pn, EPO formation is the prevailing pathway for photodegradation. There is indication that a small population of dimers form based on the small decay of Pn-TCHS-F8 in PMMA in vacuum from Chapter 2 and the presence of a small NMR signal identified as dimer. However, the characteristics of decay and recover as seen in both SMFS experiments and in PL of films, indicates that the predominant degradation pathway is the two step EPO formation. This degradation process requires an intermediate "dark" state in which the optical fluorescence and absorption is inactive. However, this state is not permanent and the molecules can spontaneously recover back into an optically active state. The more permanent state of EPO formation can only be reversed through the addition of heat.

Computational efforts using the Monte Carlo method has modeled this process and has provided insight into the relationship between these states and the experimentally collected data. The model enables better understanding of relationships between the transition rates and the fit parameters obtained from the experimental CCDFs. In all samples studied, the blinking statistics observed could be described

in the framework of models relying on Weibull or lognormal distribution functions which correlate to distributed (rather than constant) transition rates.

The results of this study suggest that while there are many competing photodegradation pathways in functionalized Pn, the most prominent pathway is EPO formation. There are environmental and molecular design choices that can mitigate the effectiveness of oxygen and aid in the photostability of functionalized Pn. These findings inform us of the molecular design considerations and environmental conditions needed to prevent degradation of organic materials for the use in future (opto)electronic devices.

Bibliography

[1] *Modern NMR methodology.* Topics in current chemistry ; 335. Springer, Heidelberg, 2013.

[2] Rabih O. Al-Kaysi, Tai Sang Ahn, Astrid M. Müller, and Christopher J. Bardeen. The photophysical properties of chromophores at high (100 mm and above) concentrations in polymers and as neat solids. *Phys. Chem. Chem. Phys.*, 8(29):3453–3459, 2006.

[3] John E. Anthony. The larger acenes: Versatile organic semiconductors. *Angewandte Chemie International Edition*, 47(3):452–483, 2008.

[4] John E. Anthony, James S. Brooks, David L. Eaton, and Sean R. Parkin. Functionalized pentacene: improved electronic properties from control of solid-state order. *Journal of the American Chemical Society*, 123(38):9482–9483, 2001.

[5] Zorica Z. Baroš and Borivoj K. Adnađević. Weibull cumulative distribution function for modeling the isothermal kinetics of the titanium-oxo-alkoxy cluster growth. *Industrial & Engineering Chemistry Research*, 52(5):1836–1844, 2013.

[6] Eric D Bott, Erin A Riley, Bart Kahr, and Philip J Reid. Proton-transfer mechanism for dispersed decay kinetics of single molecules isolated in potassium hydrogen phthalate. *ACS Nano*, 3:2403–2411, 2009.

[7] Alan K. Burnham and Robert L. Braun. Global kinetic analysis of complex materials. *Energy & Fuels*, 13(1):1–22, 1998.

[8] Thomas Christ, Florian Kulzer, Patrice Bordat, and Thomas Basché. Watching the photo-oxidation of a single aromatic hydrocarbon molecule. *Angewandte Chemie International Edition*, 40(22):4192–4195, 2001.

[9] Kathryn A. Colby, Jonathan J. Burdett, Robert F. Frisbee, Lingyan Zhu, Robert J. Dillon, and Christopher J. Bardeen. Electronic energy migration on different time scales: Concentration dependence of the time-resolved anisotropy and fluorescence quenching of lumogen red in poly(methyl

methacrylate). *The Journal of Physical Chemistry A*, 114(10):3471–3482, 2010.

[10] P. Coppo and S. G. Yeates. Shining light on a pentacene derivative: The role of photoinduced cycloadditions. *Advanced Materials*, 17(24):3001–3005, 2005.

[11] Piero Cosseddu, Andrea Piras, and Annalisa Bonfiglio. Fully deformable organic thin-film transistors with moderate operation voltage. *IEEE Transactions on Electron Devices*, 58(10):3416–3421, 2011.

[12] Ying Diao, Kristina M. Lenn, Wen-Ya Lee, Martin A. Blood-Forsythe, Jie Xu, Yisha Mao, Yeongin Kim, Julia A. Reinspach, Steve Park, Alán Aspuru-Guzik, and et al. Understanding polymorphism in organic semiconductor thin films through nanoconfinement. *Journal of the American Chemical Society*, 136(49):17046–17057, 2014.

[13] Stephen R. Forrest. The path to ubiquitous and low-cost organic electronic appliances on plastic. *Nature*, 428(6986):911–918, 2004.

[14] Werner Fudickar and Torsten Linker. Why triple bonds protect acenes from oxidation and decomposition. *Journal of American Chemical Society*, 134:15071–15082, 2012.

[15] Gaurav Giri, Steve Park, Michael Vosgueritchian, Max Marcel Shulaker, and Zhenan Bao. High-mobility, aligned crystalline domains of tips-pentacene with metastable polymorphs through lateral confinement of crystal growth. *Advanced Materials*, 26(3):487–493, 2013.

[16] Christopher Grieco, Grayson S. Doucette, Kyle T. Munson, John R. Swartzfager, Jason M. Munro, John E. Anthony, Ismaila Dabo, and John B. Asbury. Vibrational probe of the origin of singlet exciton fission in tips-pentacene solutions. *The Journal of Chemical Physics*, 151(15):154701, 2019.

[17] Christopher Grieco, Grayson S. Doucette, Ryan D. Pensack, Marcia M. Payne, Adam Rimshaw, Gregory D. Scholes, John E. Anthony, and John B. Asbury. Dynamic exchange during triplet transport in nanocrystalline tips-pentacene films. *Journal of the American Chemical Society*, 138(49):16069–16080, 2016.

[18] Rebecca Grollman, Nicole Quist, Alexander Robertson, Jeremy Rath, Balaji Purushothaman, Michael M. Haley, John E. Anthony, and Oksana Ostroverkhova. Single-molecule level insight into nanoscale environment-dependent

photophysics in blends. *Journal of Physical Chemistry C*, 121:12483–12494, 2017.

[19] Rebecca R. Grollman, Whitney E. B. Shepherd, Alexander Robertson, Keshab R. Paudel, John E. Anthony, and Oksana Ostroverkhova. Photophysics of organic semiconductors: from ensemble to the single-molecule level. *Proc. of SPIE*, 2015.

[20] H. Harald Günther. *NMR spectroscopy : basic principles, concepts, and applications in chemistry*. Wiley-VCH, Weinheim, third completely revised and updated edition. edition, 2013.

[21] Tatsuo Hasegawa and Jun Takeya. Organic field-effect transistors using single crystals. *Science and Technology of Advanced Materials*, 10(2):024314, 2009.

[22] Dr Torsten Henning. Skeletal formula of the polymethyl methacrylate repeating unit (perspex, $(c_5o_2h_8)_n$), own work, drawn with bkchem. [Public Domain;Online; accessed 28-November-2021].

[23] Chelsea M. Hess, Erin A. Riley, and Philip J. Reid. Dielectric dependence of single-molecule photoluminescence intermittency: Nile red in poly(vinylidene fluoride). *Journal of Physical Chemistry B*, 118:8905–8913, 2014.

[24] Harald Hoppe and Niyazi Serdar Sariciftci. Organic solar cells: An overview. *Journal of Materials Research*, 19(7):1924–1945, 2004.

[25] Jay. Electronegativity and chemical shift.

[26] Justin C. Johnson. Open questions on the photophysics of ultrafast singlet fission. *Communications Chemistry*, 4(1), 2021.

[27] Andrew C. Jones, Nicholas M. Kearns, Jia-Jung Ho, Jessica T. Flach, and Martin T. Zanni. Impact of non-equilibrium molecular packings on singlet fission in microcrystals observed using 2d white-light microscopy. *Nature Chemistry*, 12(1):40–47, 2019.

[28] M. J. Kendrick, A. Neunzert, M. M. Payne, B. Purushothaman, B. D. Rose, J. E. Anthony, M. M. Haley, and O. Ostroverkhova. Formation of the donor-acceptor charge-transfer exciton and its contribution to charge photogeneration and recombination in small molecule bulk heterojunctions. *Journal of Physical Chemistry C*, 116:18108–18116, 2012.

[29] S. Kéna-Cohen and S. R. Forrest. Giant davydov splitting of the lower polariton branch in a polycrystalline tetracene microcavity. *Physical Review B*, 77(7), 2008.

[30] D. Kneppe, F. Talnack, B.K. Boroujeni, C. Teixeira da Rocha, M. Höppner, A. Tahn, S.C.B. Mannsfeld, F. Ellinger, K. Leo, H. Kleemann, and et al. Solution-processed pseudo-vertical organic transistors based on tips-pentacene. *Materials Today Energy*, 21:100697, 2021.

[31] Boleslaw Kozankiewicz and Michel Orrit. Single-molecule photophysics, from cryogenic to ambient conditions. *Chemical Society Review*, 43:1029–1043, 2014.

[32] LabEx. Organic electronics.

[33] A. Laudari and S. Guha. Polarization-induced transport in ferroelectric organic field-effect transistors. *Journal of Applied Physics*, 117(10):105501, 2015.

[34] Bin Liu, Vinod M. Menon, and Matthew Y. Sfeir. Ultrafast thermal modification of strong coupling in an organic microcavity. *APL Photonics*, 6(1):016103, 2021.

[35] Samuel J. Lord, Nicholas R. Conley, Hsiao lu D. Lee, Stefanie Y. Nishimura, Andrea K. Pomerantz, Katherine A. Willets, Zhikuan Lu, Hui Wang, Na Liu, Reichel Samuel, Ryan Weber, Alexander Semyonov, Meng He, Robert J. Twieg, and W. E. Moerner. Dcdhf fluorophores for single-molecule imaging in cells. *ChemPhysChem*, 10(1):55–65, 2009.

[36] Shinya Maenosono. Monte-carlo simulations of photoinduced fluorescence enhancement in semiconductor quantum dot arrays. *Chemical Physics Letters*, 405:182–186, 2005.

[37] Dipak K. Mandal. Chapter 3 - pericyclic reactions: Introduction, classification and the woodward–hoffmann rules. In Dipak K. Mandal, editor, *Pericyclic Chemistry*, pages 63–106. Elsevier, 2018.

[38] Masaaki Mitsui, Aki Unno, and Syun Azechi. Understanding photoinduced charge transfer dynamics of single perylenediimide dyes in a polymer matrix by bin-time dependence of their fluorescence blinking statistics. *Journal of Physical Chemistry C*, 120:15070–15081, 2016.

[39] W. E. Moerner and David P. Fromm. Methods of single-molecule fluorescence spectroscopy and microscopy. *Review of Scientific Instruments*, 74(8):3597–3619, 2003.

[40] Kyle T. Munson, Jianing Gan, Christopher Grieco, Grayson S. Doucette, John E. Anthony, and John B. Asbury. Ultrafast triplet pair separation and triplet trapping following singlet fission in amorphous pentacene films. *The Journal of Physical Chemistry C*, 124(43):23567–23578, 2020.

[41] Jenny Nelson. Organic photovoltaic films. *Materials Today*, 5(5):20–27, 2002.

[42] NEUROtiker. Structure of polyvinylidene fluoride, own work. [Public Domain; Online; accessed 28-November-2021].

[43] James D. Ng, Sunil P. Upadhyay, Angela N. Marquard, Katherine M. Lupo, Daniel A. Hinton, Nicolas A. Padilla, Desiree M. Bates, and Randall H. Goldsmith. Single-molecule investigation of initiation dynamics of an organometallic catalyst. *Journal of the American Chemical Society*, 138(11):3876–3883, 2016.

[44] Muhammad R. Niazi, Ruipeng Li, Er Qiang Li, Ahmad R. Kirmani, Maged Abdelsamie, Qingxiao Wang, Wenyang Pan, Marcia M. Payne, John E. Anthony, Detlef-M. Smilgies, and et al. Solution-printed organic semiconductor blends exhibiting transport properties on par with single crystals. *Nature Communications*, 6(1), 2015.

[45] Brian H. Northrop, K. N. Houk, and Ashok Maliakal. Photostability of pentacene and 6,13-disubstituted pentacene derivatives: A theoretical and experimental mechanistic study. *Photochemical & Photobiological Sciences*, 7(12):1463, 2008.

[46] O. Ostroverkhova, D. G. Cooke, F. A. Hegmann, J. E. Anthony, V. Podzorov, M. E. Gershenson, O. D. Jurchescu, and T. T. Palstra. Ultrafast carrier dynamics in pentacene, functionalized pentacene, tetracene, and rubrene single crystals. *Applied Physics Letters*, 88(16):162101, 2006.

[47] O. Ostroverkhova, D. G. Cooke, S. Shcherbyna, R. F. Egerton, F. A. Hegmann, R. R. Tykwinski, and J. E. Anthony. Bandlike transport in pentacene and functionalized pentacene thin films revealed by subpicosecond transient photoconductivity measurements. *Physical Review B*, 71(3), 2005.

[48] Oksana Ostroverkhova. Organic optoelectronic materials: Mechanisms and applications. *Chemical Reviews*, 116:13279 – 13412, 2016.

[49] Oksana Ostroverkhova. *Handbook of Organic Materials for electronic and photonic devices*. Woodhead Publishing is an imprint of Elsevier, 2019.

[50] Oksana Ostroverkhova and W. E. Moerner. Organic photorefractives: mechanisms, materials, and applications. *Chemical Reviews*, 104(7):3267–3314, 2004.

[51] Oksana Ostroverkhova, Svitlana Shcherbyna, David G. Cooke, Ray F. Egerton, Frank A. Hegmann, Rik R. Tykwinski, Sean R. Parkin, and John E. Anthony. Optical and transient photoconductive properties of pentacene and functionalized pentacene thin films: Dependence on film morphology. *Journal of Applied Physics*, 98(3):033701, 2005.

[52] Keshab Paudel, B. Johnson, A. Neunzert, Mattson Thieme, Balaji Purushothaman, M. Payne, J. Anthony, and Oksana Ostroverkhova. Small-molecule bulk heterojunctions: Distinguishing between effects of energy offsets and molecular packing on optoelectronic properties. *The Journal of Physical Chemistry C*, 117:24752–24760, 11 2013.

[53] Ryan D. Pensack, Christopher Grieco, Geoffrey E. Purdum, Samuel M. Mazza, Andrew J. Tilley, Evgeny E. Ostroumov, Dwight S. Seferos, Yueh-Lin Loo, John B. Asbury, John E. Anthony, and et al. Solution-processable, crystalline material for quantitative singlet fission. *Materials Horizons*, 4(5):915–923, 2017.

[54] Peter Peumans, Aharon Yakimov, and Stephen R. Forrest. Small molecular weight organic thin-film photodetectors and solar cells. *Journal of Applied Physics*, 93(7):3693–3723, 2003.

[55] Hubert Piwoński, Adam Sokołowski, and Jacek Waluk. In search for the best environment for single molecule studies: Photostability of single terrylenediimide molecules in various polymer matrices. *The Journal of Physical Chemistry Letters*, 6(13):2477–2482, 2015. PMID: 26266722.

[56] A. D. Platt, M. J. Kendrick, M. Loth, J. E. Anthony, and O. Ostroverkhova. Temperature dependence of exciton and charge carrier dynamics in organic thin films. *Physical Review B*, 84:235209, 2011.

[57] Andrew Platt, Jonathan Day, Sankar Subramanian, John Anthony, and Oksana Ostroverkhova. Optical, fluorescent, and (photo)conductive properties of high-performance functionalized pentacene and anthradithiophene derivatives. *The Journal of Physical Chemistry C*, 113:14006–14014, 08 2009.

[58] Ple210. Strukturformel polyvinylcarbazol, own work. [Public Domain;Online; accessed 30-November-2021].

[59] Daniel Polak, Rahul Jayaprakash, Thomas P. Lyons, Luis Á. Martínez-Martínez, Anastasia Leventis, Kealan J. Fallon, Harriet Coulthard, David G. Bossanyi, Kyriacos Georgiou, Anthony J. Petty, II, and et al. Manipulating molecules with strong coupling: Harvesting triplet excitons in organic exciton microcavities. *Chemical Science*, 11(2):343–354, 2020.

[60] Richard Puro, Jonathan D. B. Van Schenck, Reid Center, Emma K. Holland, J. E. Anthony, and O. Ostroverkhova. Exciton polariton-enhanced photodimerization of functionalized tetracene. *accepted*, 2021.

[61] Balaji Purushothaman, Sean R. Parkin, and John E. Anthony. Synthesis and stability of soluble hexacenes. *Organic Letters*, 12(9):2060–2063, 2010.

[62] Nicole Quist, Rebecca Grollman, Jeremy Rath, Alex Robertson, Michael Haley, John Anthony, and Oksana Ostroverkhova. Single molecule-level study of donor-acceptor interactions and nanoscale environment in blends. *Proc. of SPIE*, 10101-101010K, 2017.

[63] Nicole Quist, Mark Li, Michael M. Haley, Ryan Tollefsen, John Anthony, and Oksana Ostroverkhova. Effect of molecular side groups and local nanoenvironment on photodegradation and its reversibility. *Organic Photonic Materials and Devices XX*, 2018.

[64] E. A. Riley, C. M. Hess, P. J. Whitham, and P. J. Reid. Beyond power laws: A new approach for analyzing single molecule photolminescence intermittency. *The Journal of Chemical Physics*, 136:184508, 2012.

[65] Erin A. Riley, Chelsea M. Hess, Jan Rey Pioquinto, Werner Kaminsky, Bart Kahr, and Philip J. Reid. Proton transfer and photoluminescence intermittency of single emitters in dyed crystals. *The Journal of Physical Chemistry B*, 117(16):4313–4324, 2012.

[66] Srinibas Satapathy, Santosh Pawar, Pradeep Gupta, and Kbr Varma. Effect of annealing on phase transition in poly(vinylidene fluoride) films prepared using polar solvent. *Bulletin of Materials Science*, 34, 07 2011.

[67] L.B. Schein, D.S. Weiss, and Andrey Tyutnev. The charge carrier mobility's activation energies and pre-factor dependence on dopant concentration in molecularly doped polymers. *Chemical Physics*, 365(3):101–108, 2009.

[68] Thermo Fisher Scientific. *Physical Properties Chart*. Thermo Fisher Scientific. [accessed 28-November-2021].

[69] Sean E. Shaheen, David S. Ginley, and Ghassan E. Jabbour. Organic-based photovoltaics: Toward low-cost power generation. *MRS Bulletin*, 30(1):10–19, 2005.

[70] Sahar Sharifzadeh, Cathy Y. Wong, Hao Wu, Benjamin L. Cotts, Leeor Kronik, Naomi S. Ginsberg, and Jeffrey B. Neaton. Relating the physical structure and optoelectronic function of crystalline tips-pentacene. *Advanced Functional Materials*, 25(13):2038–2046, 2014.

[71] W. E. B. Shepherd, R. Grollman, A. Robertson, K. Paudel, R. Hallani, M. A. Loth, J. E. Anthony, and O. Ostroverkhova. Single-molecule imaging of organic semiconductors: Toward nanoscale insights into photophysics and molecular packing. *Chemical Physics Letters*, 629:29–35, 2015.

[72] Whitney E. B. Shepherd, Andrew D. Platt, David Hofer, Oksana Ostroverkhova, Marsha Loth, and John E. Anthony. Aggregate formation and its effect on (opto)electronic properties of guest-host organic semiconductors. *Applied Physics Letters*, 97:163303, 2010.

[73] Whitney E. B. Shepherd, Andrew D. Platt, Mark J. Kendrick, Marsha A. Loth, John E. Anthony, and Oksana Ostroverkhova. Energy transfer and exciplex formation and their impact on exciton and charge carrier dynamics in organic films. *Journal of Physical Chemistry Letters*, 2:362–366, 2011.

[74] Joseph Shinar. *Organic Light-Emitting Devices: A Survey*. Springer, 2004.

[75] Donald B. Siano. The log-normal distribution function. *Journal of Chemical Education*, 49(11):755, 1972.

[76] Michael Slootsky, Yifan Zhang, and Stephen R. Forrest. Temperature dependence of polariton lasing in a crystalline anthracene microcavity. *Physical Review B*, 86(4), 2012.

[77] Simil Thomas, Jack Ly, Lei Zhang, Alejandro L. Briseno, and Jean-Luc Bredas. Improving the stability of organic semiconductors: Distortion energy versus aromaticity in substituted bistetracene. *Chemistry of Materials*, 28(23):8504–8512, 2016.

[78] Brian J. Walker, Andrew J. Musser, David Beljonne, and Richard H. Friend. Singlet exciton fission in solution. *Nature Chemistry*, 5(12):1019–1024, 2013.

[79] Cathy Y. Wong, Benjamin L. Cotts, Hao Wu, and Naomi S. Ginsberg. Exciton dynamics reveal aggregates with intermolecular order at hidden interfaces in solution-cast organic semiconducting films. *Nature Communications*, 6(1), 2015.

[80] Natalie Z. Wong, Alana F. Ogata, and Kristin L. Wustholz. Dispersive electron-transfer kinetics from single molecules on TiO_2 nanoparticle films. *Journal of Physical Chemistry C*, 117:21075–21085, 2013.

[81] Kristin L. Wustholz, Eric D. Bott, Christine M. Isborn, Xiaosong Li, Bart Kahr, and Philip J. Reid. Dispersive kinetics from single molecules oriented in single crystals of potassium acid phthalate. *Journal of Physical Chemistry C*, 111:9146–9156, 2007.

[82] Kristin L. Wustholz, Eric D. Bott, Bart Kahr, and Philip J. Reid. Memory and spectral diffusion in single-molecule emission. *Journal of Physical Chemistry C*, 112(21):7877–7885, 2008.

[83] Yoshiro Yamashita. Organic semiconductors for organic field-effect transistors. *Science and Technology of Advanced Materials*, 10(2):024313, 2009.

[84] Le Yang, Maxim Tabachnyk, Sam L. Bayliss, Marcus L. Böhm, Katharina Broch, Neil C. Greenham, Richard H. Friend, and Bruno Ehrler. Solution-processable singlet fission photovoltaic devices. *Nano Letters*, 15(1):354–358, 2014.

[85] Yikrazuul. Repeating unit of ps polymer chain, own work. [Public Domain;Online; accessed 30-November-2021].

[86] Karl Ziemelis. Glowing developments. *Nature*, 399(6735):409–411, 1999.

[87] Rob Zondervan, Florian Kulzer, Mikhail A. Kol'chenk, and Michel Orrit. Photobleaching of rhodamine 6g in poly(vinyl alcohol) at the ensemble and single-molecule levels. *The Journal of Physical Chemistry A*, 108(10):1657–1665, 2004.

APPENDICES

Appendix A: Photoluminescence Spectroscopy Processing Program

In order to make it easier to check photoluminescence spectroscopy data as it is being taken, I wrote a small piece of software in Python that includes a graphical user interface (gui) to make it easy for non-programmers to use. The code was broken up into five files ("gui-build.py", "gui-plot.py", "IntegrateAllGUI.py", "plotInfo.py", and "processGUI.py"), but only the main file, "gui-build.py" is run from the command line using either

```
>> python gui-build.py
```

or

```
>> python3 gui-build.py
```

This opens the user interface that is seen in Figure A.1, and then interprets the user interactions and turns them into executable commands, which are run by this or the other four files. The flow of this program is explained below.

When the program first opens, the user is presented with the window in Figure A.1. The first thing the user needs to do is select the folder, or working directory, that contains the data that the user wants to process (Figure A.1 a). Once this is done, the full filename path is printed to the right of the select folder button (see fig A.2 (a)) and the folder is scanned for processed files. For a file to be considered processed, there must be two ".npy" (numpy) files in the working directory

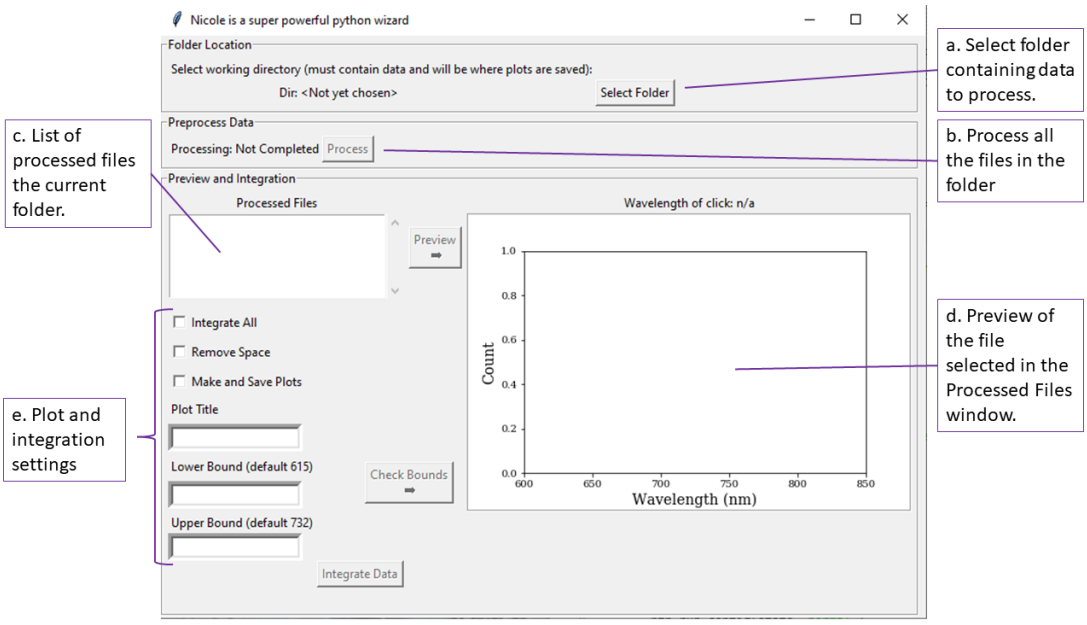

Figure A.1: Graphical User Interface: This is the user interface for the photoluminescence spectroscopy processing program. The folder containing the data to process can be selected using the "Select Folder" button (a). Then the "Process" button (b) is used to do the processing of the data. The preprocessed data in that folder is listed in the "Processed Files" box (c). Any of these files can be previewed on the plot (d) by pressing the "Preview" button. Integration setting can be changed using the settings underneath the file list (e). Once the user is ready, the data can be integrated using the "Integrate Data" button.

that contain its name: "filename_pros.npy" and "filename_time.npy". The list of already processed files is updated in the Processed Files box (Figure A.1(c)).

If the files have not been processed or there are new files that need to be processed in the folder, the button "Process" in the "Preprocess Data" section should be pressed to process the files (Figure A.1(b)). This takes the raw files from the spectrometer and converts it into the form of "filename_pros.npy" and "filename_time.npy". It does this by first finding complete file sets, which includes

two files titled “filename_sig.txt” and “filename_sig_dark.txt”, which is the full run of data and a reference dark spectra. It reads these files into python and formats it into two numpy arrays, one that contains a column of wavelength values followed by the consecutive spectra. The dark reference spectrum is subtracted from each of the spectra in the data array and then the data array is saved as “filename_pros.npy”.

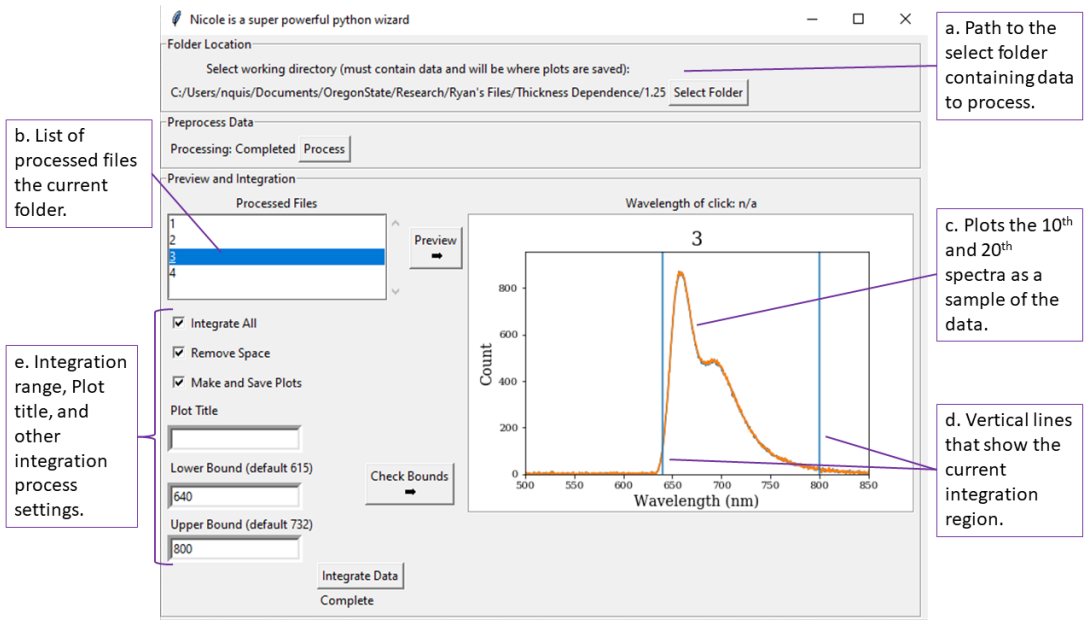

Figure A.2: Graphical User Interface in use: This is the user interface for the photoluminescence spectroscopy processing program while in use. (a) The path for the current working directory is displayed at the top. (b) The preprocessed data in that folder is listed in the “Processed Files” box, and currently file three is selected to preview. (c) The preview plot of file 3, which is the plot of the 10th and 20th spectra. (d) The vertial lines indicating the current lower bound and upper bound values entered in the respective boxes. (e) The integration settings, including the selected boundary values, that can be set before the data is integrated.

The time values, which is a row that runs across the top of the original

data is extracted and turned into it's own numpy array and then saved as "filename_time.npy". This process is done for all the files in the directory that do not already have "filename_pros.npy" and "filename_time.npy" files. The processed files list is then updated. Any files that don't have a corresponding dark reference spectra cannot be processed.

Once the pre-processing is done, the data can now be viewed and integrated. Any file listed in the Processed Files box can be selected and then the 10th and 20th spectrum can be viewed in the plotting window by clicking the "Preview" button. This allows the user to check that the data looks correct and it also allows the user to check the integration bounds. The default bounds of integration are 615 nm and 732 nm, but the bounds can be changed by entering the values in the "Lower Bounds" and "Upper Bounds" boxes. Once those contain values, the values will be displayed as vertical lines on the plot by using the "Check Bounds" button (see fig A.2 to see an example plot). Once the desired bounds are set, the data can be integrated using the "Integrate Data" button.

This is done by adding the values of the spectrum between the two wavelength values. This is done for all the spectra and then integrated values are saved with their corresponding values as "filenameInt<lower bound value>to<upper bound value>.npy" (example "TestInt615to732.npy"). If the laser was shuttered during the experiment to allow for recovery, the dark time will be removed if the "Remove Space" checkbox is checked.

If desired, all the files in the directory can be integrated all at the same time with the same parameters by selecting the "Integrate All" checkbox. Plots of the in-

tegrated data can also be created and the plots saved as “filenameInt<lower bound value>to<upper bound value>.png”, if the checkbox “Make and Save Plots” is checked (see Figure A.3) for an example plot. The plot title for both the display plot and the saved plot can be changed by entering the desired title in the “Plot Title” box. Once integration is complete the data is in a state to be used anyway that is needed.

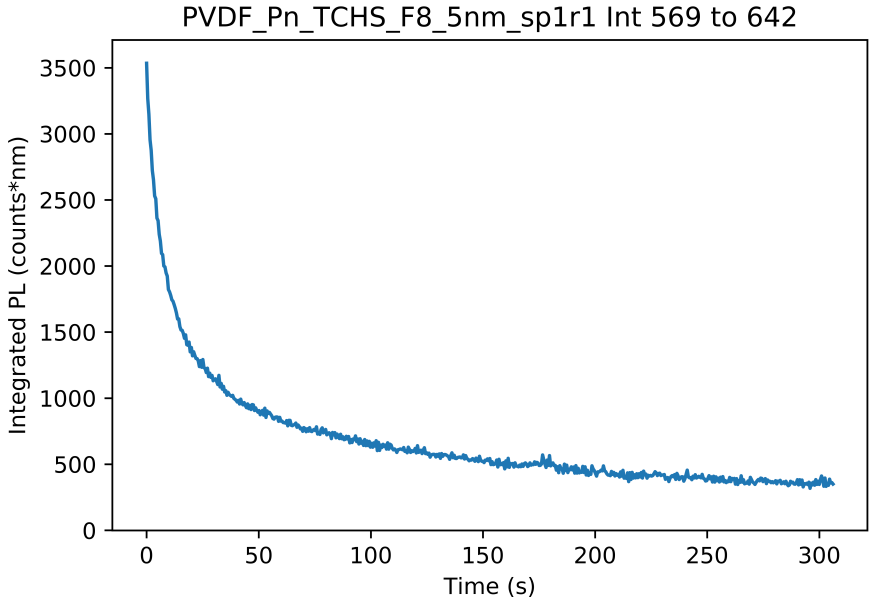

Figure A.3: Example of a plot produced by the Photoluminescence Spectroscopy Processing Program. This was a spot of Pn-TCHS-F8 in PVDF that was integrated from 569 to 642 nm.

Appendix B: Single Molecule Video Processing Program

This code processes the Single Molecule Fluorescence Spectroscopy video data. It starts by creating a composite image of all the frames added together and uses that to remove the background, find the distribution of pixel values and determine the threshold as either three times the standard deviation above the mean or the location of a jump in distribution. The threshold is then applied to the composite image and the image array is set to either a zero, if below the threshold, or a one, if above. A clustering process is used on the resulting array to group the pixels into fluorophores, with the limit that clusters are not larger than 5 pixels in any direction. A mask is created for each fluorophore and used to create the fluorescence time traces by applying the mask to every frame in the video.

The resulting time traces are displayed to the user, who sorts them. The sorted molecules are either fit to a single exponential or change-point detection is used to determine the step locations and heights. The exponential data and the step locations and heights is returned to the user.

```
# -*- coding: utf-8 -*-
"""
Created on Thu Aug  1 18:31:58 2019

@author: Hypatia
"""
```

```
7  import numpy as np
8  import matplotlib.pyplot as plt
9  import pandas as pd
10 import ruptures as rpt
11 from scipy import ndimage
12 from scipy.stats import mode
13 from sklearn.cluster import MeanShift
14 from sklearn.datasets.samples_generator import make_blobs
15 from mpl_toolkits.mplot3d import Axes3D
16 from scipy import ndimage, stats, optimize
17
18
19 histbins = 38
20 totMat_orig = np.zeros((512,512))
21 Inten = np.zeros((2,600))
22 Bkgnd = np.zeros((2,600))
23 x = np.zeros((2, histbins+1))
24 fl_name = r'C:\Users\nquis\Documents\OregonState\Research\Semi-SM\
       PMMA TIPS run-selected\slide1spot2x10.asc'
25 fl_dark = r'C:\Users\Hypatia\Documents\OregonState\Research\Semi-
       SM\TCHS in PVDF\PnTCHSF8 in PVDF July 2019\bkgrd2.asc'
26 fl_name2 = r'C:\Users\nquis\Documents\OregonState\Research\Semi-SM
       \PMMA TIPS run\slide1spot12x20.asc'
27
28 class SMprocessing:
29     vid_length = 600
30
```

```
31      def __init__(self, flnm, length):
32          self.fp = flnm
33          self.bkgd = np.zeros((5,length))
34          self.numTraces = 0
35          self.composite = np.zeros((512,512))
36          self.vid_length = 1*length
37          self.int = 0
38          self.cutoff = 0
39
40      def run_full(self):
41          print('starting')
42          self.CompositeImg()
43          print('Composite Image complete')
44          self.Threshhold()
45          print('Threshholding complete')
46          self.Traces()
47
48      def __repr__(self):
49          return 'class'
50
51  # The following three functions (gaussian, moments, fitgaussian)
      were found
52  # online and were edited to fit the the function of this class.
53      def gaussian(self, height, center_x, center_y, width_x,
      width_y):
54          """Returns a gaussian function with the given parameters
      """
```

```
55          width_x = float(width_x)
56          width_y = float(width_y)
57          return lambda x,y: height*np.exp(
58                      -(((center_x-x)/width_x)**2+((center_y-y)/
    width_y)**2)/2)
59
60
61      def moments(self, frame):
62          """Returns (height, x, y, width_x, width_y)
63          the gaussian parameters of a 2D distribution by
    calculating its
64          moments """
65          total = frame.sum()
66          X, Y = np.indices(frame.shape)
67          x = (X*frame).sum()/total
68          y = (Y*frame).sum()/total
69          col = frame[:, int(y)]
70          width_x = np.sqrt(np.abs((np.arange(col.size)-y)**2*col).
    sum()/col.sum())
71          row = frame[int(x), :]
72          width_y = np.sqrt(np.abs((np.arange(row.size)-x)**2*row).
    sum()/row.sum())
73          height = frame.max()
74          return height, x, y, width_x, width_y
75
76      def fitgaussian(self, frame, frame_num):
77          """Returns (height, x, y, width_x, width_y)
```

```
78          the gaussian parameters of a 2D distribution found by a
    fit"""
79          params = self.moments(frame)
80          errorfunction = lambda p: np.ravel(self.gaussian(*p)(*np.
    indices(frame.shape)) -
81                                       frame)
82          p, success = optimize.leastsq(errorfunction, params)
83          self.bkgd[:, frame_num] = p
84          return p
85
86      def Bkg_correction(self, frame, frame_num):
87          a = self.fitgaussian(frame, frame_num)
88          Xin, Yin = np.mgrid[0:len(frame[:,0]), 0:len(frame[0,:])]
89          pt = self.gaussian(self.bkgd[:,frame_num][0], self.bkgd[:,
    frame_num][1] ,self.bkgd[:,frame_num][2], self.bkgd[:,frame_num
    ][3], self.bkgd[:,frame_num][4])
90          mat = frame-pt(Xin, Yin)
91          frame_num += 1
92          return mat
93
94      def CompositeImg(self):
95          backgnd = np.zeros((512,512))
96          mdn = np.zeros((1,self.vid_length))
97          f = open(self.fp, 'r')
98          totMat = np.zeros((512,512))
99          totMat_tmp = np.zeros((512,512))
100         for j in range(self.vid_length):
```

```
101             i = 1
102             while i % 513 !=0:
103                 data = f.readline()
104                 data = data.split(',')[1:513]
105                 totMat_tmp[i-1,:] = np.array(list(map(int, data)))
106                 i+=1
107             if j%50 == 0:
108                 print("{0:.2%}".format(j/600))
109             self.bkgd[:,j] = [0,0,0,0,0]
110             val = self.Bkg_correction(totMat_tmp,j)
111             totMat+=val#(totMat_tmp - val)
112             mdn[0,j] = np.median(totMat_tmp)
113         plt.imshow(totMat, cmap='gray')
114         plt.show()
115         f.close()
116 
117         self.totMat = totMat
118 
119     def Threshhold(self, multi = 3, jump=5):
120         totMat2 = 0 *self.totMat
121         hist = np.histogram(self.totMat, histbins)
122         flat_array = np.ndarray.flatten(self.totMat)
123         sts = [np.mean(flat_array), np.median(flat_array), mode(
    flat_array)[0][0], np.std(flat_array)]
124         vstd = sts[2]+multi*sts[3]
125         i = 4
126         while self.cutoff == 0 and i < 50:
```

```
127             old = np.mean(hist[0][-(i-1):])
128             new = np.mean(hist[0][-i:])
129             if (new - old > multi*old) or new > jump:
130                 idx = 1*(histbins-i)+1
131                 self.cutoff = 1*hist[1][idx]
132             i+=1
133         totMat2[np.where(self.totMat[:,:]>self.cutoff)] = 1
134         self.hist = hist
135         self.stats = sts
136         self.pts, self.n_clusters, self.labels, self.masks =
    SMprocessing.Clustering(totMat2)
137
138     def Clustering(Mat):
139         pts2 = np.where(Mat==1)
140         pts = np.asarray(pts2).T
141
142         ms = MeanShift(bandwidth = 5)
143         ms.fit(pts)
144         labels = ms.labels_
145         cluster_centers = ms.cluster_centers_
146
147         labels_unique = np.unique(labels)
148         n_clusters_ = len(labels_unique)
149         print(n_clusters_)
150         msk_idex = []
151         for m in range(n_clusters_):
152             msk = np.zeros((512,512))
```

```
153             msk = np.where(msk==0, False, True)
154             tmp_idex = pts[np.where(labels==labels_unique[m])[0]]
155             for p in range(len(tmp_idex)):
156                 msk[tmp_idex[p][0],tmp_idex[p][1]] = True
157             msk_idex.append(msk)
158 
159         return pts, n_clusters_, labels, msk_idex
160 
161     def Traces(self):
162         backgnd = np.zeros((512,512))
163         Xin, Yin = np.mgrid[0:512, 0:512]
164         ave = np.zeros((1, self.vid_length))
165         trcs = np.zeros((len(self.masks)+1, self.vid_length))
166         f = open(self.fp, 'r')
167         totMat_tmp = np.zeros((512,512))
168         j = 0
169         for j in range(self.vid_length):
170             i = 1
171             while i % 513 !=0:
172                 data = f.readline()
173                 data = data.split(',')[1:513]
174                 totMat_tmp[i-1,:] = np.array(list(map(int, data)))
175                 i+=1
176             ave[0,j] = np.median(totMat_tmp)
177             pt = self.gaussian(self.bkgd[:,j][0], self.bkgd[:,j
    ][1] ,self.bkgd[:,j][2], self.bkgd[:,j][3], self.bkgd[:,j][4])
178             backgnd = 1*pt(Xin, Yin)
```

```
179             for q in range(len(self.masks)):
180                 trcs[q,j] = sum(totMat_tmp[self.masks[q]]-backgnd[
    self.masks[q]])
181         f.close()
182         self.traces = trcs
183         self.aveI = ave
184         self.traces = self.ChooseTraces()
185 
186     def ChooseTraces(self):
187         time = np.arange(0,600,1)/6
188         trces = []
189         info = np.array(['Trace Number', 'Trace Type', 'Max Count'
    , 'Min Count', 'Transistion Times', 'Off Levels', 'a', 'b', 'c'
    , 'R2', 'On Times'])
190         num = 1
191         for k in range(len(self.traces)):
192             blank = [' ', ' ', ' ', ' ', ' ', ' ', ' ', ' ', ' ',
    ' ', ' ']
193             plt.plot(time, self.traces[k,:])
194             plt.show()
195             val = input('Is this an Single Molecule (1), Decay (2)
    , Decay with Steps (3), or Noise (4)?')
196             if val in ['1', '2', '3']:
197                 trce = 1*self.traces[k,:]
198                 trces.append(trce)
199                 blank[0] = str(num)
200                 blank[2] = max(trce)
```

```
201                 blank[3] = min(trce)
202                 if val == '1':
203                     blank[1] = 'SM'
204                     num += 1
205                     steps = int(input('How many steps?').strip())
206                     blank[4:6] = SMprocessing.chng_pnt(trce, steps
    )
207                     blank[10] = SMprocessing.OnOffTimes(blank[4],
    blank[5])
208                 elif val == '2':
209                     trce[trce<0] = 0
210                     blank[1] = 'Decay'
211                     num += 1
212                     blank[6:10] = SMprocessing.Expo_fit(trce)
213                 elif val == '3':
214                     trce[trce<0] = 0.001
215                     blank[1] = 'Decay with Steps'
216                     num += 1
217                     blank[6:10] = SMprocessing.Expo_fit(trce)
218                     steps = int(input('How many steps?').strip())
219                     blank[4:6] = SMprocessing.chng_pnt(trce, steps
    )
220                     blank[10] = SMprocessing.OnOffTimes(blank[4],
    blank[5])
221                 info = np.vstack([info, blank])
222
223         self.info = info
```

```
224         return trces
225
226     def r_sqr(x, y, yfit):
227         ave = sum(y)/len(y)
228         top = sum((yfit-ave)**2)
229         bottom = sum((y-ave)**2)
230         rval = top/bottom
231         return rval
232
233     def Expo_fit(trace):
234         time = np.arange(0, 600, 1)/6
235         mn = min(trace)
236         mx = max(trace)
237         d, e = optimize.curve_fit(lambda t,a,b,c: a*np.exp(b*t)+c,
     time, trace, p0=(mx, -1, mn))
238         rsqr = SMprocessing.r_sqr(time, trace, d[0]*np.exp(d[1]*
    time)+d[2])
239         return list(map(str, [d[0], d[1], d[2], rsqr]))
240
241     def chng_pnt(trace, pts):
242         def heights(trace, points):
243             points.sort()
244             ave_heights = []
245             for i in range(len(points)-1):
246                 avH = sum(trace[points[i]:points[i+1]+1])/len(
    trace[points[i]:points[i+1]+1])
247                 ave_heights.append(avH)
```

```
248             str_heights = " ".join([str(x) for x in ave_heights])
249             return str_heights
250         algo = rpt.Binseg(model="l2").fit(trace)
251         result = algo.predict(n_bkps=pts)
252         plt.figure()
253         plt.plot(trace)
254         for i in range(len(result)):
255             plt.vlines(result[i], 0, max(trace))
256         plt.show()
257         good = input('Is this accurate result (yes (1)/no (2))?')
258         if good in ["2"]:
259             select = input('Do you want to rerun (1) or select
    points (2)?')
260             if select == '1':
261                 steps2 = int(input('How many steps?').strip())
262                 vals = SMprocessing.chng_pnt(trace, steps2)
263                 return vals
264             elif select == '2':
265                 list_steps = input('Which steps do you want to
    keep?').strip().split()
266                 list_steps = list(map(int,list_steps))
267                 keep_steps = [0]
268                 for i in range(len(list_steps)):
269                     try:
270                         step = result[list_steps[i]-1]
271                         keep_steps.append(step)
272                     except:
```

```
273                         print("Something went wrong")
274                 hts = heights(trace, keep_steps)
275                 result = 1*keep_steps
276         else:
277             result = [0]+result
278             hts = heights(trace, result)
279         result = [x/6 for x in result]
280         results_str = " ".join([str(x) for x in result])
281         return list(map(str, [results_str, hts]))
282 
283     def Color_spots(self):
284         plt.figure()
285         mat = 0*self.totMat
286         for i in range(len(self.labels)):
287             mat[self.pts[i][0], self.pts[i][1]] = self.labels[i]+1
288 
289         plt.imshow(mat, cmap='rainbow')
290 
291     def Play_video(self):
292         f = open(self.fp, 'r')
293         totMat_tmp = np.zeros((512,512))
294 
295         fig = plt.figure()
296         viewer = fig.add_subplot(111)
297         plt.ion() # Turns interactive mode on (probably
    unnecessary)
298         fig.show()
```

```
299
300         for j in range(self.vid_length):
301             i = 1
302             while i % 513 !=0:
303                 data = f.readline()
304                 data = data.split(',')[1:513]
305                 totMat_tmp[i-1,:] = np.array(list(map(int, data)))
306                 i+=1
307             val = self.Bkg_correction(totMat_tmp[100:380,40:300],j
    )
308             viewer.clear() # Clears the previous image
309             viewer.imshow(val, cmap='gray') # Loads the new image
310             plt.pause(.01) # Delay in seconds
311             fig.canvas.draw() # Draws the image to the screen
312
313
314     def OnOffTimes(times, levels):
315         Times = times.split(' ')
316         Levels = levels.split(' ')
317         Times = list(map(float, Times))
318         Levels = list(map(float, Levels))
319         lvl_sorted = 1*Levels
320         lvl_sorted.sort()
321
322         if Levels == lvl_sorted[::-1]:
323             ln = len(Times)-1
324             ons = Times[1:ln]
```

```
325         else:
326             print('Do by hand')
327             ons = []
328 
329         ons = [x/6 for x in ons]
330         ons = list(map(str, ons))
331         ons = ' '.join(ons)
332         return ons
333 
334 # %%
335 Try1 = SMprocessing(fl_name, 600)#, bkgd = fl_dark)
336 Try1.traces = SMprocessing.ChooseTraces(Try1.traces)
337 w = Try1.totMat
338 
339 plt.figure(1)
340 plt.imshow(Try1.totMat, cmap='gray')
341 
342 plt.figure(3)
343 plt.plot(Try1.hist[1][:38], Try1.hist[0])
344 plt.axvline(x=Try1.stats[2])
345 plt.axvline(x=(Try1.stats[2]+6*Try1.stats[3]))
346 
347 plt.show()
348 
349 # %%
350 import numpy as np
351 import matplotlib.pyplot as plt
```

```
352
353
354 def Construct_Trace(OnTimes, Levels):
355     ons = OnTimes[:]+" "
356     lvls = Levels[:]+" "
357     Times = []
358     Lvls = []
359     while " " in ons:
360         Times.append(int(ons[:ons.index(" ")]))
361         ons = ons[ons.index(" ")+1:]
362     while " " in lvls:
363         Lvls.append(float(lvls[:lvls.index(" ")]))
364         lvls = lvls[lvls.index(" ")+1:]
365     Lvls.append(0)
366     print(Times, Lvls)
367     plt.figure()
368     for i in range(len(Lvls)-1):
369         plt.hlines(Lvls[i], Times[i], Times[i+1], colors=['k'])
370         plt.vlines(Times[i+1], Lvls[i], Lvls[i+1], colors=['k'])
371     plt.show()
372     return(np.array(Lvls[:-1]), np.array(Times))
373
374 def Calc_ns(Levls, times):
375     lvls = Levls - Levls[-1]
376     ns = []
377     for i in range(len(lvls)-1):
378         val = lvls[i] - lvls[i+1]
```

```
379         ns.append(val*times[i+1])
380     return(np.array(ns))
```

Appendix C: Monte Carlo Simulation Program

I used the workload managing system Slurm to run the Python code on all the computers in the Physics Department computer lab (Weniger 412) in parallel on nights and weekends when the lab was not in use. The following Bash script (called bigrun.sh) submitted 100, or any number, jobs to the queue.

```
#!/bin/bash

for i in {1..100}
do
  sbatch --nice "/home/quistn/Documents/"‘
      ‘"Research/MonteCarlo/BRun2.sh" $i
done
```

This next Bash script (called BRun2.sh) included all the parameters for a given job and called the Python script to run.

```
#!/bin/bash

#SBATCH --workdir=FreshData/Weibull/DiffT/A1/k3103
#SBATCH --output=slurm-%j.out
#SBATCH --error=slurm-%j.err
#SBATCH --mail-type=end
#SBATCH --mail-user=quistn@oregonstate.edu

```

```
python "/home/quistn/Documents/Research/MonteCarlo"‘
     ‘"/SMMonteCarlofromPaper12.py" $1 > output$1.txt
```

This last file contained the Python code to simulate one fluorophore and return four files: NTimeTrace#.txt, which contained the time trace; NData#.txt, which contained the integrated N_{total}; OnTimes#.txt, which contained a list of the On times for that trace; and OffTimes#.txt, which contained the Off times for that trace;

```
from __future__ import division
import math
import random
import numpy as np
import matplotlib.pyplot as plt
import csv
from os import path
import sys

print("SMMonteCarlofromPaper12.py and weibul distribution on k31
   with A val of 1.5 # no exponetial but weibull rate on bottom
   and Crates (more accurate).")
        #and both exponetial"

## Export File Properties ##
num = sys.argv[1]
folder = "QYfour/Expo"
basic = "Documents/Research/MonteCarlo"
file1 = "NTimeTrace" + num + ".txt"
```

```
file2 = "NData" + num + ".txt"
file3 = "OnTimes" + num + ".txt"
file4 = "OffTimes" + num + ".txt"
file5 = "PBOnTimes" + num + ".txt"
Ttrace = file1 #path.join(basic, folder, file1)
Data = file2 #path.join(basic, folder, file2)
Ons = file3 #path.join(basic, folder, file3)
Offs = file4 #path.join(basic, folder, file4)
PBons = file5 #path.join(basic, folder, file5)


## Constants ##
k12 = 2.924e4                          #s^-1
    # alternative value used 1.1e4
k21 = 7e7                              #s^-1
    # alternative values used 9.1e8 and 1.00855e7
k23s = 222                             #s^-1
    # alternative values used 15, (1/20.8574), (0.5e-7)*k21,
   (1/164)*k21, 5e7, 1e6, and (0.18/0.82)*k21
k21n = ((18/82)*k21)-k23s           #s^-1
    # alternative values used 0.218*k21 and 35*k23
k31 = 0.3                           #s^-1
    # alternative value used 0.025
k3o = 0                            #s^-1
    # alternative value used 1e-1
G = 1
R = 1
```

```
T = 300                                 # kelvin
gam = 0
    # alternative value used 3
x = random.random()
dt = 1e-9                               #s
tfinal = 98.5                           #s
    # alternative value used 50, 98.5, and 30
t = 0                                   #s
state = 1
count = 0
rad = 0
intVal = 0.1                            #s
NumTraces = 1
out = np.zeros((NumTraces, 4))
k23 = 1.1861*k23s*((k23s*t)**0.1861)
quant = k21/(k21+k21n+k23) #0.8
triplen = 10
quant2 = k21n /(k21n+k23)
xtrans = 0

print("SMMonteCarloforPaper10.py")
print("k12 = ", k12, " k23s = ", k23s, " k21 = ", k21, " k21n = ",
    k21n, " k31 = ", k31, " k3o = ", k3o, " quant = ", quant, "
   gamma = ", gam)

## Photon Time Calculation ##
c = 3.0e8                               #m/s
```

```
wavelength = 633e-9                    #m
radius = 50e-6                         #m
power = 850e-6                         #J/s
h = 6.63e-34                           #Js
molecarea = 2.303*(22200)*(6.02214e23)  #m^2  #This is Pentacene
#photontime = (h*c/(power*wavelength))*
#               ((np.pi*radius**2)/molecarea)
photontime = 3.42e-5                   #s
numbofp = int(intVal/photontime)
#print (wavelength*power*10**-20)/(h*c*np.pi*radius**2)

time = np.arange(0, tfinal + 2*dt, intVal)
tof = np.zeros((len(time), 2))
#print len(tof)
#print len(t)

kij = math.exp(-G/(R*T))*math.exp(-gam*x)

def transition2(t, rad, dart):
    x = random.gauss(0,0.5)
    xtrans = 1*x
    k23 = k23s #1.5*k23s*((k23s*t)**0.5)
    k21n = ((18/82)*k21)-k23
    P21 = (k21+k23+k21n)*dt
    randnum2 = random.random()
    P23 = k23*dt*(math.exp(-gam*xtrans))
    quant = k21/(k21+k21n+k23)
```

```
96      quant2 = k21n/(k21n+k23)
97      randnumQ = random.random()
98      randnumQ2 = random.random()
99      if P21 > randnum2:
100         if quant > randnumQ:
101             state = 1
102             t+=dt
103             rad += 1
104         elif quant2 > randnumQ2:
105             state = 1
106             t+=triplen*dt
107         else:
108             state = 3
109             print( 3, t)
110             dart = 1*t
111             t+=dt
112     else:
113         state = 2
114         t += dt
115     #print "trans 2", state
116     return (t, rad, state, xtrans, dart)
117 
118 def transition3(t, count, xtrans, dart):
119     #if count > 100:
120         #count = 0
121     x = random.gauss(0, 0.5)
122     k31p = 1*k31*((k31*(t-dart))**0)
```

```
123     #or k31*math.exp(-gam*xtrans)
124     #or math.exp(-G/(R*T))*math.exp(-gam*x)
125     P3 = (k31p + k3o)*dt
126     P31 = k31p/(k31p+k3o)
127     P3o = k3o*dt#*math.exp(-gam*x)
128     randnum3 = random.random()
129     randnum3o = random.random()
130     randnum31 = random.random()
131     #or 300*P31*random.random()
132     #print t, "state 3", randnum31, P31
133     if P3 > randnum3:
134         if P31 > randnum31:
135             state = 1
136             t+= dt
137         else: # P3o > randnum3o:
138             state = 4
139             t+= dt
140     else:
141         state = 3
142         t+= dt
143     '''else:
144         state = 3
145         t+=photontime
146         count +=1'''
147 
148     #print "trans 3", state, t
149     return (t, state, count)
```

```
150
151 def TimeTrace(state, t, rad, count, dart):
152     #This finds the value from the time average
153     for i in range(0, len(time)):
154         while t < (i+1)*intVal:
155             if state == 1:
156                 P = k12*dt
157                 randnum = random.random()
158                 if P > randnum:
159                     state = 2
160                     t+=dt
161                 else:
162                     state = 1
163                     t+=dt
164             elif state == 2:
165                 (t, rad, state, xtrans, dart) = transition2(t, rad
    , dart)
166             elif state == 4:
167                 state = 4
168                 t = (i+1)*intVal
169             else:
170                 (t, state, count) = transition3(t, count, xtrans,
    dart)
171         #print state, i, rad
172         if rad > 0:
173             tof[i, 1] = rad
174             tof[i, 0] = i*intVal
```

```
175             rad = 0
176         else:
177             tof[i, 1] = 0
178             tof[i, 0] = i*intVal
179 
180     print( "loop")
181     return tof
182 
183 
184 ontimes = np.empty((0,1))
185 offtimes = np.empty((0,1))
186 pbontimes = np.empty((0,1))
187 data = np.empty((0,2))
188 Ptotal = 0
189 totaltrans = 0
190 numtrans = 0
191 oldtrans = 0
192 for j in range(0, NumTraces):
193     print( "j is", j)
194     st = 1
195     t = 0
196     rad = 0
197     count = 0
198     dart = 0
199     tof = TimeTrace(st, t, rad, count, dart)
200     offs = np.empty((0,1))
201     trans = 0
```

```
202
203     Threshold = (max(tof[:,1]))/2
204     print( Threshold)
205     for n in range(1, len(tof)):
206         if tof[n,1] < Threshold:
207             offs = np.append(offs, np.array([[tof[n,1]]]), axis =
    0)
208
209     if not offs.size or np.count_nonzero(offs) == 0:
210         mn = Threshold
211         std = 0
212     else:
213         mn = np.mean(offs)
214         std = np.std(offs)
215     Threshold = mn + 3*std
216     print(Threshold)
217
218     for n in range(1, len(tof)):
219         if (tof[n, 1] < Threshold and tof[n-1, 1] >= Threshold):
220             trans += 1
221         elif (tof[n, 1] >=Threshold and tof[n-1, 1] < Threshold):
222             trans += 1
223
224     #print tof
225     numtrans = 0
226     lasttime = 0
227     if trans > 1:
```

```
228         for i in range(1, len(tof)):
229             if (tof[i, 1] < Threshold
230                 and tof[i-1, 1] >= Threshold):
231                 #print "on"
232                 ontimes = np.append(ontimes, np.array([[(intVal*(i
    -lasttime))]]), axis = 0)
233                 lasttime = 1*i
234             elif (tof[i, 1] >= Threshold
235                   and tof[i-1, 1] < Threshold):
236                 #print "off"
237                 offtimes = np.append(offtimes, np.array([[(intVal
    *(i-lasttime))]]), axis = 0)
238                 lasttime = 1*i
239             '''if i == len(tof)-1:
240                 lasttime = 0'''
241     if trans == 1 and tof[0, 1] > Threshold:
242         for i in range(1, len(tof)):
243             if (tof[i, 1] < Threshold and tof[i-1, 1] >= Threshold
    ):
244                 pbontimes = np.append(pbontimes, np.array([[(
    intVal*(i-lasttime))]]), axis = 0)
245
246     numb = int(num)
247     if numb < 11:
248         with open(Ttrace, "w") as output:
249             writer=csv.writer(output,lineterminator='\n')
250             writer.writerows(tof)
```

```
251     totaltrans = len(ontimes) + len(offtimes)
252     numtrans = totaltrans - oldtrans
253     oldtrans = 1*totaltrans
254     Ptotal = sum(tof[:,1])
255     PBQY = quant/Ptotal
256 
257     data = np.append(data, np.array([[numtrans, Ptotal]]),
258                      axis = 0)
259     print j, data, offtimes
260     print("For data ", j, " the number of photons is ", Ptotal, "
        and the PBQY is ", PBQY)
261     #print ontime, offtime, ontime+offtime, tfinal
262 
263 
264 with open(Data, "w") as output:
265     writer = csv.writer(output, lineterminator='\n')
266     writer.writerows(data)
267 
268 with open(Ons, "w") as output:
269     writer = csv.writer(output, lineterminator='\n')
270     writer.writerows(ontimes)
271 
272 with open(Offs, "w") as output:
273     writer = csv.writer(output, lineterminator='\n')
274     writer.writerows(offtimes)
275 
276 with open(PBons, "w") as output:
```

```
277     writer = csv.writer(output, lineterminator='\n')
278     writer.writerows(pbontimes)
279
280 print "success!"
```